



CHAPTER 4

IONIC CONDUCTIVITY AND RELAXATION STUDIES OF THE CdI₂ DOPED Ag₂O-V₂O₅-B₂O₃ GLASS SYSTEM

4.1. Introduction

The interest in the electrical conductivity of ion conducting amorphous solid electrolytes has reflected a growing awareness since 1884 [1] by Warburg. The experimental results concerning the ionic conductivity of these materials have been collected and excellently reviewed [2-12]. The dc polarization or single frequency techniques of conductivity measurements were inappropriate to study the different phenomena occurring in solid state ionic conductors under an applied electric field. Ac fields are required for measuring bulk conductivities in order to prevent ion/electron charge transfer limitations or space charge building up which always happens at the electrodes of the ionic conductive materials tested under dc current flow. The use of impedance spectroscopy is truly the beginning of noticeable progress in the study of conduction and interface phenomena and is now widely used for experimental investigations [13,14]. In a solid electrolyte cell, the situation is much more complicated since there are various factors which contribute towards electrical impedance [15,16]. The current in these electrolytes is due to the several processes like ion movement through the bulk of the electrolyte, electrode-electrolyte interface impedance, charge transport across the interface, the resulting double layer capacitance etc. All these electrical and electrochemical parameters are the functions of applied frequency and their responses are quite different in the different frequency ranges due to their widely

different relaxation times. At very low frequencies, electrode polarization becomes important while ionic migration losses become significant at higher frequencies. With recent advances in electrochemistry, rigorous analysis of the ac response of an electrolyte or electrochemical cell has been done. Complex impedance (Z^*), complex admittance (Y^*), complex permittivity (ϵ^*) and complex modulus (M^*) are the four basic functions for the analysis of ac data [17] and they are related to each other as

- Complex Impedance, $Z^* = R_p - 1/j\omega C_p = Z' - j Z''$
- Complex Admittance, $Y^* = 1/Z^* = Y' + j Y''$
- Complex Permittivity, $\epsilon^* = 1/j\omega C_0 Z^* = \epsilon' - j \epsilon''$
- Complex Modulus, $M^* = j\omega C_0 Z^* = M' + j M''$

All these formalisms are derived from the same experimental data and each type of representation has its own advantages at particular circumstances.

Impedance spectroscopy was first applied by Baurale 1969 [18,19] to analyze the response of zirconia solid electrolyte cells to sinusoidal perturbations. Since then, this technique has been used for characterizing a wide range of materials which include polymers, oxides, glasses, halides etc. This technique involves applying an ac signal of low amplitude across the solid electrolyte cell. The output signal which is also a sine wave is compared with the input signal to determine impedance modulus and phase shift. If the voltage function applied is given by

$$V_{(t)} = V_m \exp(j\omega t) \quad (4.1)$$

Then the current function will be given by

$$I_{(t)} = I_m \exp(j\omega t + \phi) \quad (4.2)$$

The impedance $Z_{(\omega)}$ has both magnitude $|Z|$ and phase angle ϕ and can be expressed in both polar and cartesian form

$$Z_{(\omega)} = |Z| \exp(-j\phi) \quad (4.3)$$

$$= |Z| (\cos \phi - j \sin \phi) = Z' - j Z'' \quad (4.4)$$

where $|Z| = \sqrt{Z'^2 + Z''^2}$ and $\phi = \arctan(Z''/Z')$, Z' and Z'' are the real and imaginary part of the impedance. The data is computed and displayed in the complex plane in the form of real and imaginary component as an implicit function of frequency and is called the complex impedance plot. It is from the resulting structure of impedance versus frequency response that one derives information about the electrical properties of the full electrode-electrolyte system.

A small signal ac measurement on such a cell shows that the impedance is usually frequency dependent and the cell can be represented by a network of resistances and capacitances, the so called equivalent circuit. A pure resistance R has a frequency independent impedance $Z=R$, and this corresponds to a vector ending at the point R on the real axis as shown in Fig.1(a). For a pure capacitance, C , the impedance $Z= (j2\pi fC)^{-1}$ is dependent on the inverse of frequency f . In the complex impedance plane, we get a point on the imaginary axis for each measured frequency and the points, if taken at infinitely many frequencies, form a straight line coinciding on the imaginary axis, Fig.4.1 (b). A parallel combination of resistance R and capacitance C corresponds to a semicircle in the complex impedance plane intersecting the real axis at the origin and at R Fig.4.1 (c). If a resistance R and a capacitance C are connected in series, the impedance is represented by a line parallel to the imaginary axis intersecting on the real axis at R Fig.4.1 (d).

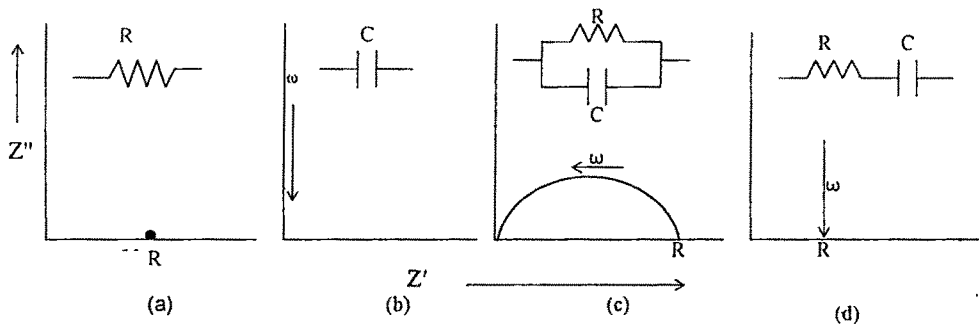


Fig.4.1 Complex Impedance plot for some elementary circuits.

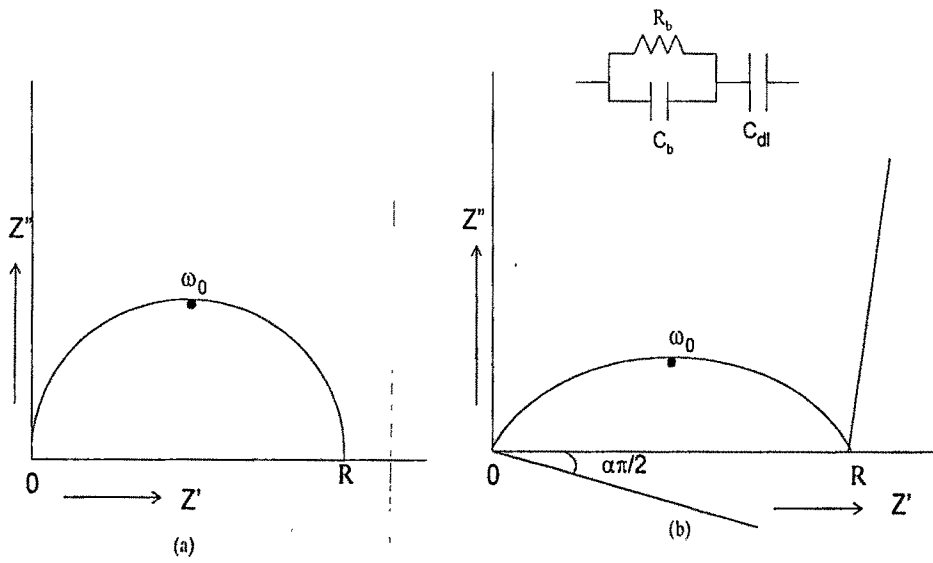


Fig. 4.2. Geometric response for an (a) ideal circuit (b) distributed elements

A systematic study of complex impedance on silver based super ion conducting glasses was first made by Grant et.al., [20,21] for $\text{Ag}_7\text{I}_4\text{AsO}_4$. After that ac conductivity studies on many silver iodide doped systems $\text{AgI-Ag}_2\text{B}_4\text{O}_7$ [22], $\text{AgI-Ag}_2\text{MoO}_4$ [23], AgI-AgPO_3 [24], $\text{AgI-Ag}_2\text{O-B}_2\text{O}_3$ [25], $\text{AgI-Ag}_2\text{O-V}_2\text{O}_5$ [26], $\text{AgI-Ag}_2\text{O-P}_2\text{O}_5\text{-MoO}_3$ [27], $\text{AgI-Ag}_2\text{O-B}_2\text{O}_3\text{-V}_2\text{O}_5$ [28] etc. have been studied widely and the experimental results support the fact that AgI introduced in the glassy network, is responsible for the high ionic conductivity. The relaxation effect in these systems is due to the motion of the mobile species, Ag^+ ions, rather than by the rotation of the dipoles and is termed as conductivity relaxation. The studies on $\text{PbI}_2\text{-AgPO}_3$ [29], $\text{CuI-Ag}_2\text{O-V}_2\text{O}_5$ [30], $\text{CuI-Ag}_2\text{O-B}_2\text{O}_3$ [31], $\text{PbI}_2\text{-Ag}_2\text{O-V}_2\text{O}_5$ [32] etc. explain the feasibility of obtaining the Ag^+ ion conducting systems with appreciably high conductivity. In the present study, it was confirmed earlier by the characterization studies that even if CdI_2 is doped in the $\text{Ag}_2\text{O-V}_2\text{O}_5\text{-B}_2\text{O}_3$ system, AgI clusters are formed due to the exchange reaction between CdI_2 and Ag_2O and the Ag^+ ions from these AgI clusters formed will act as mobile species. Hence, this system will behave as AgI doped glass. In this chapter, we discuss the results obtained from the ac measurements of the system $\text{CdI}_2\text{-Ag}_2\text{O-V}_2\text{O}_5\text{-B}_2\text{O}_3$ over a range of frequency, composition and temperature, including dc conductivities.

4.2. Complex Impedance Analysis

Ionic conductivity process can be visualized as a series process involving consecutive hops of an ion over potential energy barriers along the direction of the electric field [33]. This can be modeled as a parallel RC circuit and the impedance of the circuit is

$$Z^*(\omega) = R - (j \omega C)^{-1} = Z' - j Z'' \quad (4.5)$$

The complex admittance.

$$Y^* = (Z^*)^{-1} = R^{-1} + j \omega C \quad (4.6)$$

$$Z' = \frac{R}{1 + \omega^2 R^2 C^2} \quad (4.7)$$

and

$$Z'' = \frac{\omega R^2 C}{1 + \omega^2 R^2 C^2} \quad (4.8)$$

Eliminating ω from Eqns.4.7 and 4.8 and rearranging them, it follows that

$$\left(Z' - \frac{R}{2} \right)^2 + Z''^2 = \frac{R^2}{4} \quad (4.9)$$

This is the equation of a circle with radius $R/2$ and centre at $(R/2, 0)$ (Fig 4.2a). The coordinates on the top of the arc are $(R/2, R/2)$, and the complex impedance plot will be a perfect semicircle with its centre on the real axis. Thus, the frequency ω_0 is given as;

$$\omega_0 = \frac{1}{RC} = \frac{1}{\tau_0} \quad (4.10)$$

where $\tau_0 (=RC)$ is the relaxation time for the circuit and is given by the inverse of the frequency at the top of the semicircle. A wide range of materials so reported [34] have shown a depressed semicircle in the impedance spectrum. In order to explain the depression of the semicircle, a new circuit element called constant phase element (CPE) has been introduced [35]. For this case, the real and imaginary parts of impedance are given by

$$Z' = \frac{R(1 + \omega\tau_0)^{-\alpha} \sin(\alpha\pi/2)}{1 + 2(\omega\tau_0)^{1-\alpha} \sin(\alpha\pi/2) + (\omega\tau_0)^{2(1-\alpha)}} \quad (4.11)$$

$$Z'' = \frac{R(\omega\tau_0)^{-\alpha} \cos(\alpha\pi/2)}{1 + 2(\omega\tau_0)^{1-\alpha} \sin(\alpha\pi/2) + (\omega\tau_0)^{2(1-\alpha)}} \quad (4.12)$$

$$\left(Z' - \frac{R}{2}\right)^2 + \left(Z'' - \frac{R \tan(\alpha\pi/2)}{2}\right)^2 = r^2 \quad (4.13)$$

$$r^2 = \left(\frac{R}{2}\right)^2 + \left(\frac{R}{2}\right)^2 (\tan(\alpha\pi/2))^2 \quad (4.14)$$

This is the equation of a circle with centre at $[R/2, R \tan(\alpha\pi/2)/2]$ with radius r . Thus, the impedance response of the above circuit or of a practical solid electrolyte would be an arc depressed below the real axis by an angle $\alpha\pi/2$ and intersecting it at R and 0 (Fig. 4.2b). The co-ordinates at the top of the arc are $R/2$ and $R/2[(\cos \alpha\pi/2)/(1+\sin \alpha\pi/2)]$.

In the present investigation, complex impedance measurements were carried out to determine the electrical conductivity and the ac behavior of the present glasses over a range of temperature and frequencies. Figs.4.3 and 4.4 show the complex impedance plot obtained for the glass system $x\text{CdI}_2-(100-x) [2\text{Ag}_2\text{O}-(0.7\text{V}_2\text{O}_5-0.3\text{B}_2\text{O}_3)]$ with $x=5$ and 10 mole% of CdI_2 composition at different temperatures. Such shapes are typical for super ionic solids exhibiting lattice disorder [36]. From the above figs., it can be seen that with the increase in temperature, the intercept of the straight line on the real axis shifts towards the origin i.e., the bulk resistance of the sample decreases with increase of temperature and thus conductivity increases. Fig.4.5 shows the impedance plot for different mole% of CdI_2 compositions. It is found that the resistance value decreases with the addition of CdI_2 in the system as seen from the shifting of straight line towards the origin. At higher dopant concentration the angle between the straight line and real axis decreases as due to the electrode polarization.

Fig.4.6 shows the impedance plot obtained for the system $20\text{CdI}_2-80[x\text{Ag}_2\text{O}-y(0.7\text{V}_2\text{O}_5-0.3\text{B}_2\text{O}_3)]$ with different x/y ratios (in second series). It can be seen from the figure that the system with x/y ratio 1.75 has a lower side intercept on the real axis

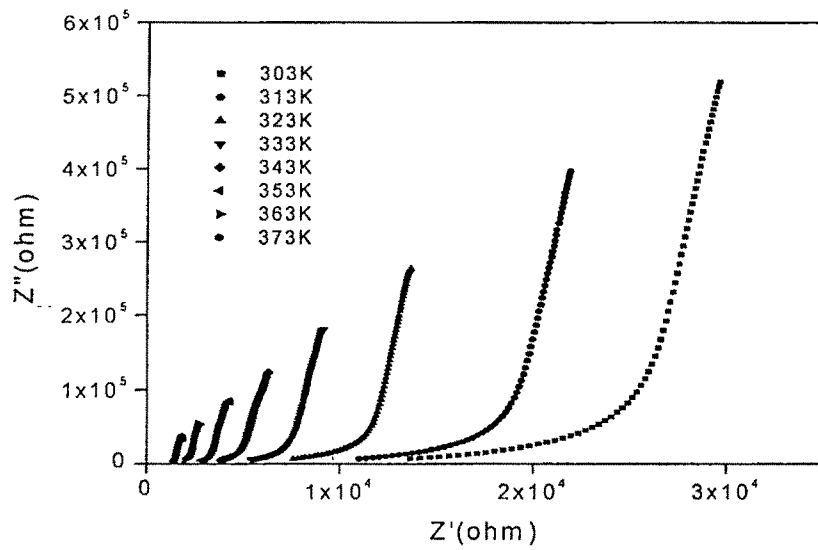


Fig.4.3 Complex impedance plot for the system $x\text{CdI}_2-(100-x)$ $[2\text{Ag}_2\text{O}-(0.7\text{V}_2\text{O}_5-0.3\text{B}_2\text{O}_3)]$ with $x=5$ mole% of CdI_2 .

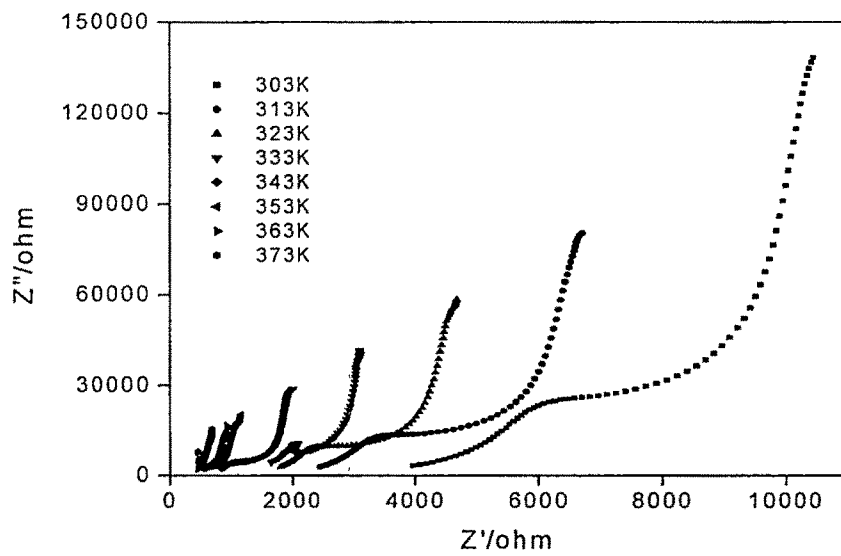


Fig.4.4. Complex impedance plot for the 10 mole% of CdI_2 doped system

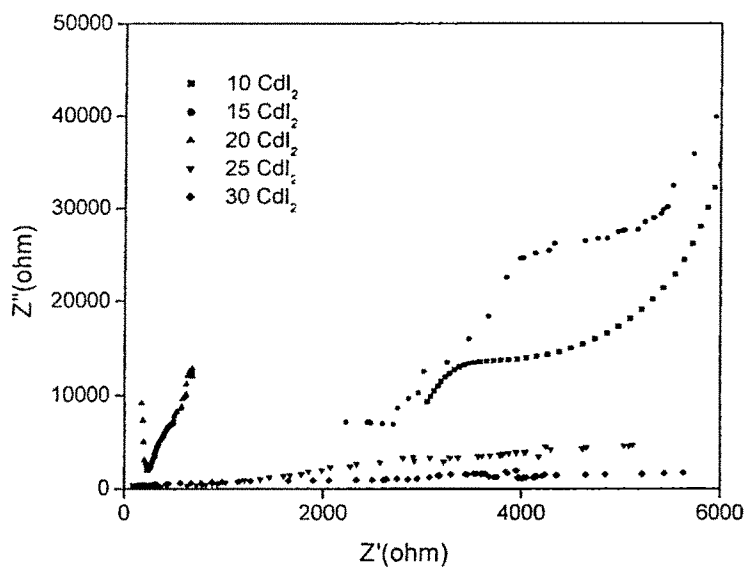


Fig.4.5. Impedance plot for different mole% of CdI_2 compositions of the system $xCdI_2-(100-x) [2Ag_2O-(0.7V_2O_5-0.3B_2O_3)]$

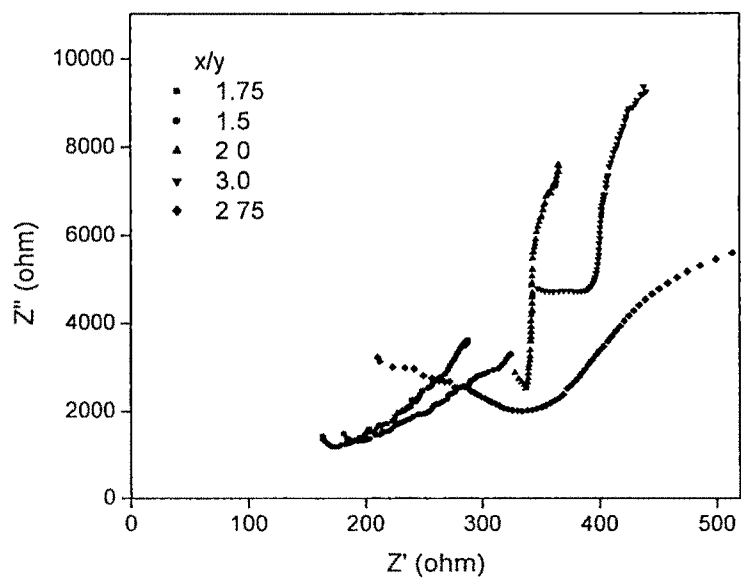


Fig.4.6 Impedance plot for different x/y ratio for the system $20CdI_2- 80[xAg_2O-y(0.7V_2O_5-0.3B_2O_3)]$

and is regarded as the best conducting system in the second series. Fig.4.7 shows the impedance plot obtained for the system with x/y ratio 1.25 at different temperatures. The figure shows that the real axis intercept of the impedance plot is shifted towards the origin with increase of temperature, i.e., the resistance value decreases with increase of temperature.

Similar behavior of the impedance spectrum at different temperatures is obtained for the third series, $20\text{CdI}_2\text{-}53.4\text{Ag}_2\text{O}\text{-}26.6[\text{x}\text{B}_2\text{O}_3\text{-(}1\text{-x)}\text{V}_2\text{O}_5]$ where $x=0.2$ and is shown in Fig.4.8. The figure shows a continuous decrease in the value of resistance with the increase of temperature. In this series, the amount of CdI_2 and Ag_2O are constant and one glass former is replaced by another. There is no continuous change in the value of resistance in this series as shown in Fig. 4.9 and the system with $x=0.8$ has a lower side intercept on the impedance spectrum and is regarded as the best conducting system in this series.

Fig.4.10 shows the impedance plot for the composition containing 20 mole% of CdI_2 doped system of the series $\text{x}\text{CdI}_2\text{-(}100\text{-x)} [2\text{Ag}_2\text{O}\text{-(}0.7\text{V}_2\text{O}_5\text{-}0.3\text{B}_2\text{O}_3)]$. It is observed to have a low frequency spike and a small portion of the semicircle. A depressed semicircle is obtained by the extrapolation of this plot. The depressed semicircle at the high frequency region arises from the bulk relaxation and the low frequency spike from the interfacial effects. With the increase of temperature, the size of the depressed semicircle decreases as expected and the real axis intercept of the plot shifts towards the origin. The high frequency semicircle in the impedance plot is characteristic of a parallel combination of a capacitor and a resistor respectively which are the bulk capacitance C_b and the bulk resistance R_b of the material [20,37]. The low

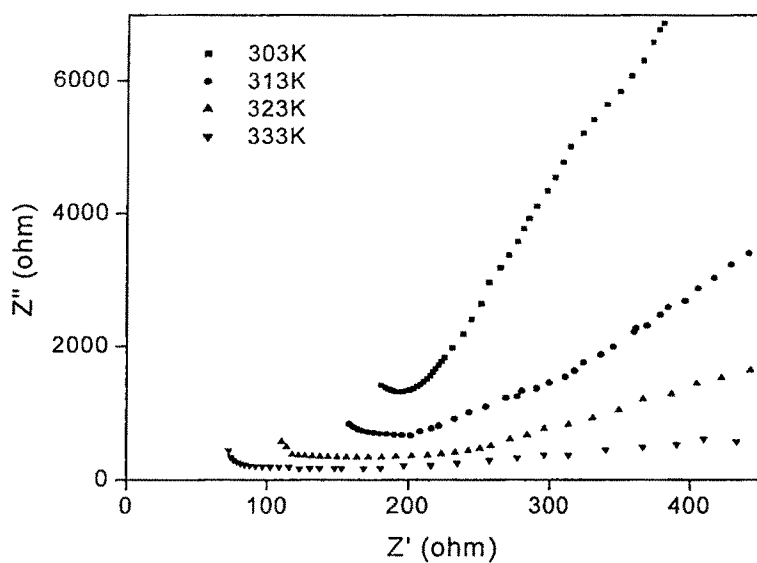


Fig.4.7 Complex impedance plot for $20\text{CdI}_2\text{-}80[\text{xAg}_2\text{O-y}(0.7\text{V}_2\text{O}_5\text{-}0.3\text{B}_2\text{O}_3)]$ with x/y ratio=1.5.

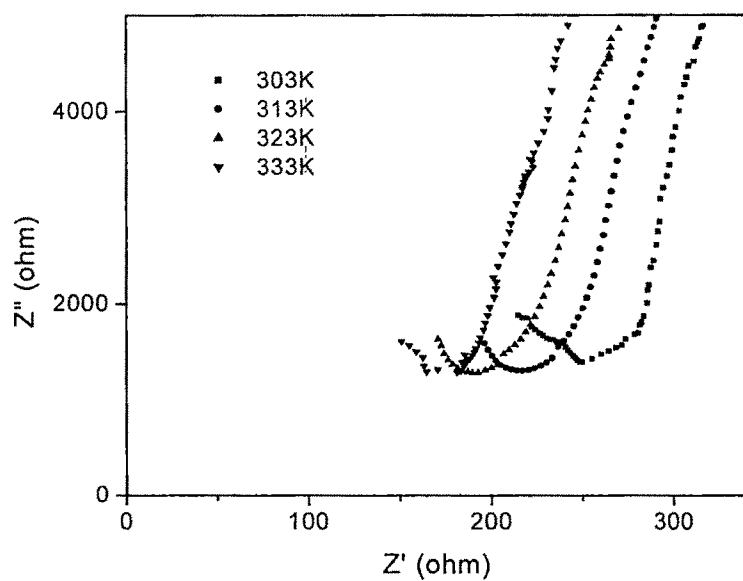


Fig.4.8 Impedance spectrum for the system $20\text{CdI}_2\text{-}53.4\text{Ag}_2\text{O}\text{-}26.6$ $[\text{xB}_2\text{O}_3\text{-(}1\text{-x)}\text{V}_2\text{O}_5]$ where $\text{x}=0.4$ at different temperatures

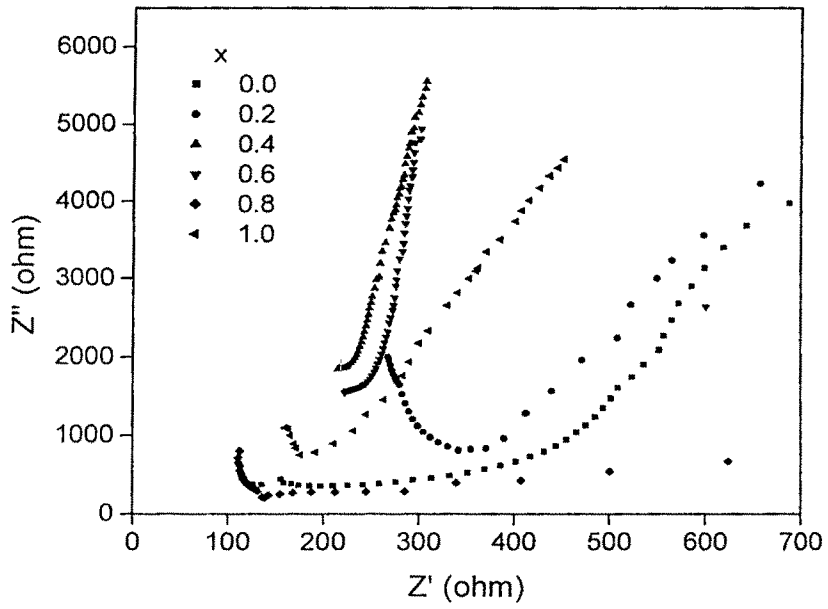


Fig.4.9 Impedance plot for the system $20\text{CdI}_2\text{-}53.4\text{Ag}_2\text{O-}26.6$ $[\text{xB}_2\text{O}_3\text{-(}1\text{-x) V}_2\text{O}_5]$ for different x values.

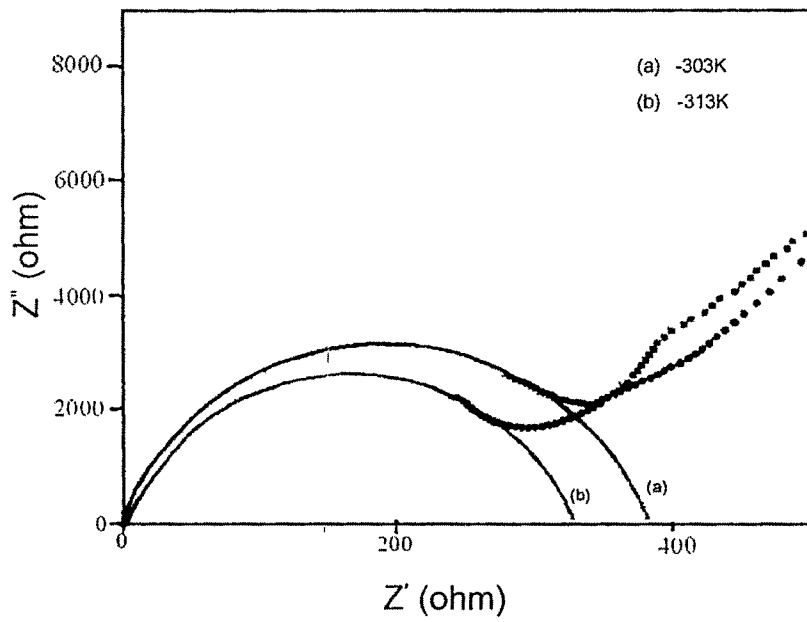


Fig.4.10. Complex impedance plot for the 20 mole% of CdI_2 doped system.

frequency straight line in the impedance plot is characteristics of a double layer capacitance C_{dl} at the electrode-electrolyte interface. The glasses are isotropic materials and have negligible grain boundary resistance R_{gb} and no capacitance, C_{gb} [37]. It was also reported that the grain size does not affect the bulk conductivity of the super ion conducting glassy materials [38]. So the observed impedance spectrum can be worked out by assuming the following equivalent circuit, a parallel combination of C and R followed by a double layer capacitance C_{dl} in series. The appropriate physical model (equivalent circuit) is shown in the Fig. 4.2(b). The semicircles obtained in the impedance plots have their centers below the real axis of the complex plot. The straight line connecting the origin of the complex plane to the centre of the semicircle formed an angle of about 20° with the real axis. Such distortion is probably due to the existence of asymmetry between the electrode/ electrolyte interface. This can also be seen from the inclination of the low frequency straight line in the impedance plot. The depressed semicircle obtained by the extrapolation of the impedance plot indicates that the relaxation time τ is not a single value but it is distributed around a mean value [35]. These observations suggest the presence of constant phase element (CPE), because the properties of the glassy materials are themselves distributed. The CPE at the electrode-electrolyte interface represents the effects of double layer capacitance C_{dl} and other effects [14,23,38].

The dc conductivity of the sample has been found out from the bulk resistance (R) obtained from the impedance plot together with its dimensions

$$\sigma = \left(\frac{l}{AR} \right) \quad (4.15)$$

where l is the thickness of the sample and A is the area. DC conductivity has also been obtained from the frequency independent plateau region of the conductivity spectra (discussed in the next section).

Fig.4.11 shows the plot of $\log \sigma$ versus $10^3/T$ for various compositions of the system $x\text{CdI}_2-(100-x) [2\text{Ag}_2\text{O}-(0.7\text{V}_2\text{O}_5-0.3\text{B}_2\text{O}_3)]$ where $x=5, 10, 15, 20, 25, 30$ mole% of CdI_2 . The temperature variation of conductivity is found to obey the Arrhenius behavior of the form

$$\sigma = \sigma_0 \exp(-E_a / kT) \quad (4.16)$$

where σ_0 is the pre-exponential factor, k is the Boltzmann constant, T is the absolute temperature and E_a is the activation energy for conduction whose value is equal to the energy required to overcome the electrostatic force and the energy barriers during the jump. The pre-exponential factor σ_0 depends on the concentration of the mobile ions n , the cation vibration frequency ν , and the mean jump distance d , given by

$$\sigma_0 \propto n\nu d^2 \quad (4.17)$$

It is clear from Table 4.1 that the value of σ_0 is found to increase with the increase in the concentration of the dopant salt. The increase in conductivity with the dopant salt is mainly due to the increase in the mobile ion concentration. From the slope of the plots, the activation energy E_a has been calculated. Table 4.1 shows that the room temperature conductivity values increase with increase in the CdI_2 content and reach a maximum value, 7.8×10^{-4} S/cm for 30 mole% of CdI_2 doped system, whereas the activation energy decreases with the CdI_2 content and the highest conducting composition has an activation energy of 0.33 eV. Fig.4.12 shows the variation of dc conductivity and activation energy

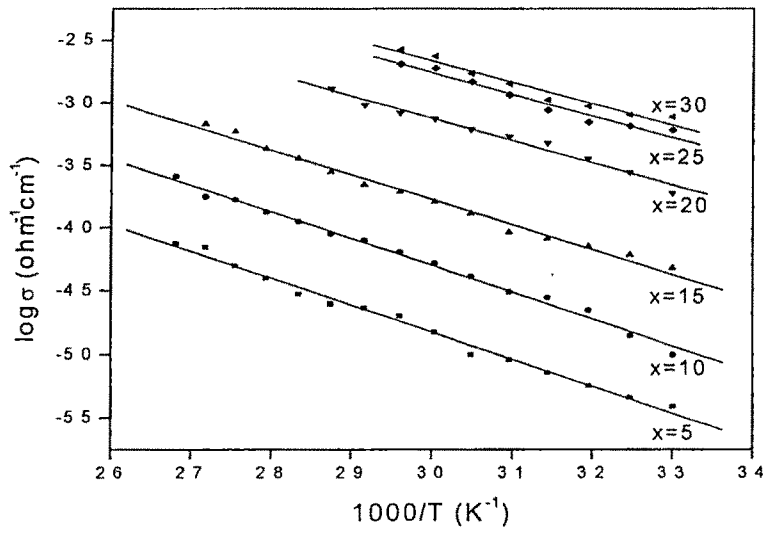


Fig.4.11. Arrhenius plot for $x\text{CdI}_2-(100-x)[2\text{Ag}_2\text{O}-(0.7\text{V}_2\text{O}_5-0.3\text{B}_2\text{O}_3)]$ System, where $x=5, 10, 15, 20, 25, 30$.

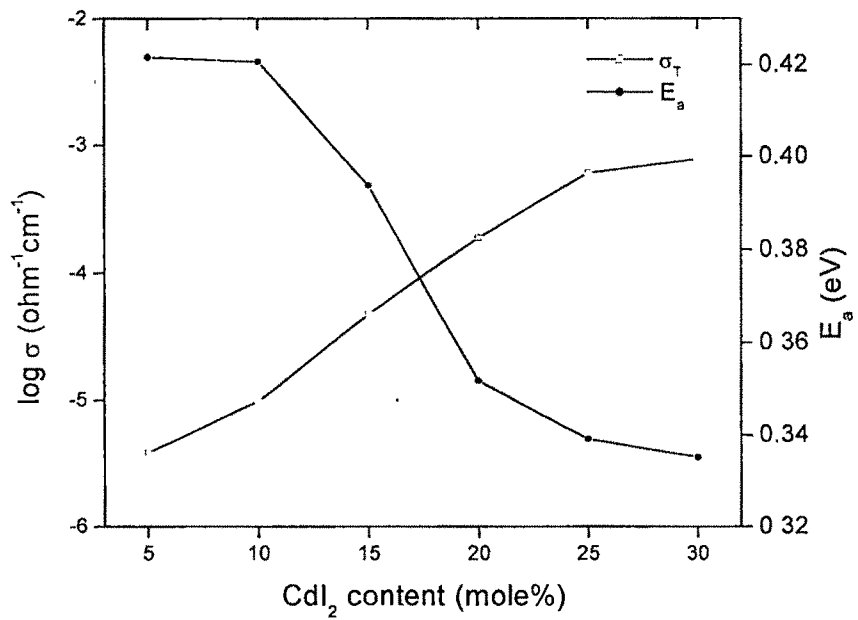


Fig.4.12. The dc conductivity and activation energy plot for $x\text{CdI}_2-(100-x)[2\text{Ag}_2\text{O}-(0.7\text{V}_2\text{O}_5-0.3\text{B}_2\text{O}_3)]$ where $x=5, 10, 15, 20, 25, 30$.

Table 4.1

Mole percentage of CdI₂, Conductivity at room temperature σ_{RT} , activation energy E_a and pre-exponential factor σ_0 for the system $x\text{CdI}_2\text{-(100-x)[2Ag}_2\text{O-(0.7V}_2\text{O}_5\text{-0.3B}_2\text{O}_3\text{)]}$

CdI ₂	$\sigma_{RT}(\text{ohm}^{-1}\text{cm}^{-1})$	E_a (eV)	σ_0
05	3.9×10^{-6}	0.421	35.55
10	9.9×10^{-6}	0.420	115.22
15	4.8×10^{-5}	0.393	150.61
20	1.9×10^{-4}	0.351	156.57
25	6.1×10^{-4}	0.339	231.95
30	7.8×10^{-4}	0.335	250.60

Table 4.2

Composition of the glasses studied according to different x/y ratio between 1 and 3, room temperature conductivity σ_{RT} , activation energy E_a and pre-exponential factor σ_0 , for the system $20\text{CdI}_2\text{-80}[x\text{Ag}_2\text{O-y(0.7V}_2\text{O}_5\text{-0.3B}_2\text{O}_3\text{)]}$.

x/y ratio	Conductivity σ_{RT} (Ohm ⁻¹ cm ⁻¹)	Activation energy (E_a) eV	Pre-exponential factor σ_0
1.00	1.5717×10^{-6}	0.404	7.532
1.25	1.1352×10^{-5}	0.363	11.39
1.50	4.0855×10^{-4}	0.298	36.618
1.75	5.2597×10^{-4}	0.288	32.441
2.00	1.9000×10^{-4}	0.351	156.57
2.25	1.6621×10^{-5}	0.363	16.676
2.50	1.3851×10^{-4}	0.332	49.778
2.75	2.4171×10^{-4}	0.313	36.334
3.00	2.9670×10^{-4}	0.308	40.260

against the dopant content CdI_2 at room temperature. This increase of conductivity is in accordance with the conductivity expression,

$$\sigma = n e \mu \quad (4.18)$$

where n is the number of charge carriers, e is the charge and μ is the mobility. In this series, the formation of AgI clusters is expected to increase with increase in CdI_2 and the mobility of these ions may also increase because of the increase in molar volume, so an increase in the conductivity is obtained.

In the second series, the amount of dopant content CdI_2 is fixed at 20 mole% and the glass modifier (x) to glass former (y) ratio is changed between $1 \leq x/y \leq 3$ in steps of 0.25. Fig.4.13 shows the Arrhenius plot for the system $20\text{CdI}_2-80[x\text{Ag}_2\text{O}-y(0.7\text{V}_2\text{O}_5-0.3\text{B}_2\text{O}_3)]$ with different x/y ratios between 1 and 3. Fig.4.14 shows the dc conductivity and activation energy versus x/y ratio of the glass system studied. With increasing addition of Ag_2O to this system, the ionic conductivity increases and attains a maximum value, 5.74×10^{-4} S/cm for the x/y ratio 1.75 at room temperature and decreases continuously until $x/y = 2.25$ and thereafter increases from x/y ratio 2.25 to 3. The non-linear nature shown by the conductivity versus x/y plot for the present system gives the idea that glass modifier Ag_2O content affects the ionic conductivity and for the x/y ratio 1.75 and 3 the ionic conductivity shows a maximum. The obtained non-linear behavior is the evidence to the existence of inhomogeneous ionic clusters due to structural effects produced from different x/y ratios [39]. Following different reasons may be possible for non-linear behavior in this glass system.

The addition of metal oxide Ag_2O to the glass formers involves incorporation of oxygen into the macromolecular chain formed by the network formers V_2O_5 and B_2O_3 ,

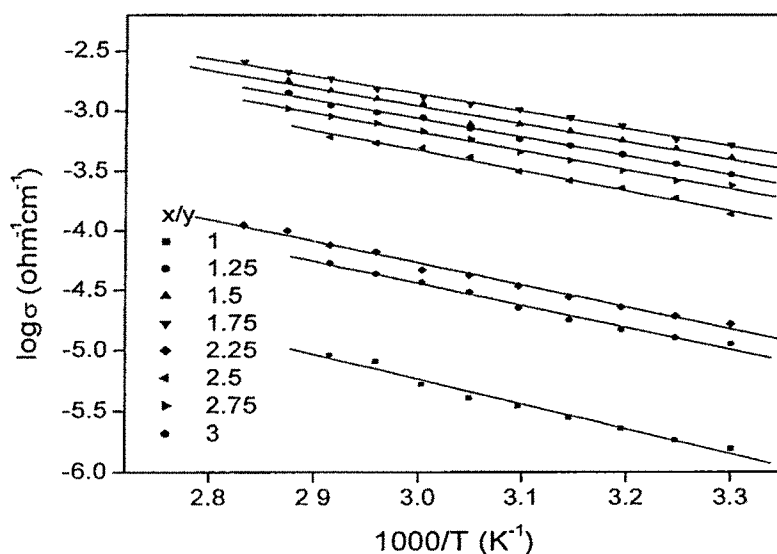


Fig. 4.13. Arrhenius plot for the system $20\text{CdI}_2\text{-}80[\text{xAg}_2\text{O-y}(0.7\text{V}_2\text{O}_5\text{-}0.3\text{B}_2\text{O}_3)]$ with different x/y ratios between 1 and 3.

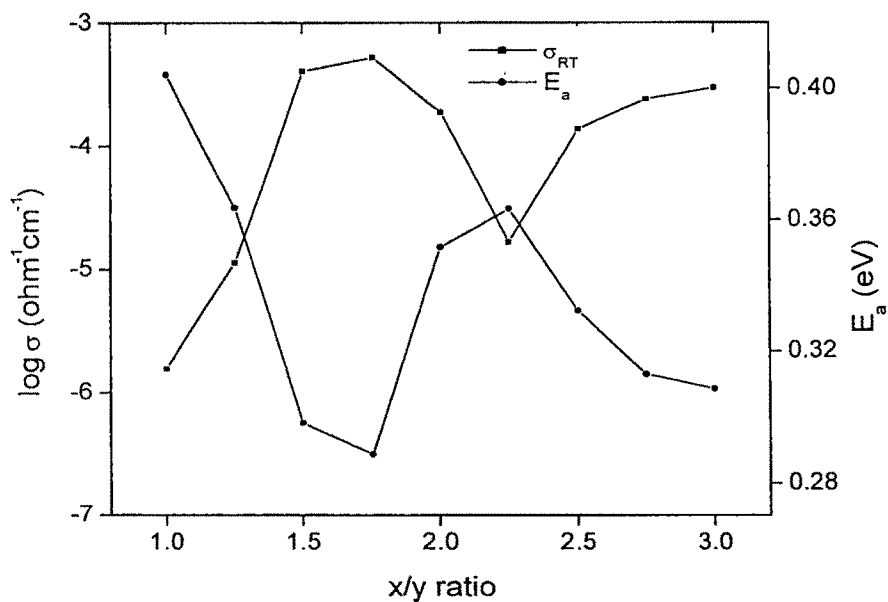


Fig.4.14. The dc conductivity and activation energy plot for $20\text{CdI}_2\text{-}80[\text{xAg}_2\text{O-y}(0.7\text{V}_2\text{O}_5\text{-}0.3\text{B}_2\text{O}_3)]$ with different x/y ratios between 1 and 3.

thereby introducing ionic bonds in the glass system. As the modifier to former content increases, greater numbers of oxygen bridges are broken. The increasing non-bridging oxygen in the system decreases the length of the macromolecular chains. So the increasing addition of modifier breaks the bond and facilitates easy migration of the conducting ions. After a particular value of x/y the conductivity decreases due to the increased randomness in the glassy matrix. The existence of the random structure in glass may be responsible for the non-linear behavior of conductivity with respect to x/y [40].

In the present system, the AgI clusters formed (as evident from the x-ray analysis), due to the exchange reaction between CdI_2 and Ag_2O . So the charge carriers may increase with Ag_2O content to a certain extent and after that its amount is practically constant since the amount of CdI_2 is fixed. With these conditions we expect no continuous change in conductivity with x/y ratio. The observed two maxima in these systems might be due to the effect of Ag_2O in the glass structure. The probable explanation for this is that at these two compositions with $x/y=1.75$ and 3, the glassy matrix is such that it might have created open channels for the mobile ions to migrate [40]. This causes an enhancement in ionic mobility and in turn conductivity. The double maxima in conductivity with the ratio of modifier to former in the glasses is obtained for other systems $AgI-Ag_2O-B_2O_3-MoO_3$ [41], $AgI-Ag_2O-WO_3-MoO_3$ [39] etc. Table 4.2 shows the room temperature conductivity values and the activation energy obtained for the different x/y ratio compositions.

In the third series, where the amount of dopant and modifier is constant and the amount of B_2O_3 content is varied with x from 0 to 1 in steps of 0.2 to study the effect of mixed former in the system, $20CdI_2-53.4Ag_2O-26.6[xB_2O_3-(1-x)V_2O_5]$. Fig.4.15 shows the $\log \sigma$ versus $10^3/T$ plot for the series for different amount of B_2O_3 content gives an

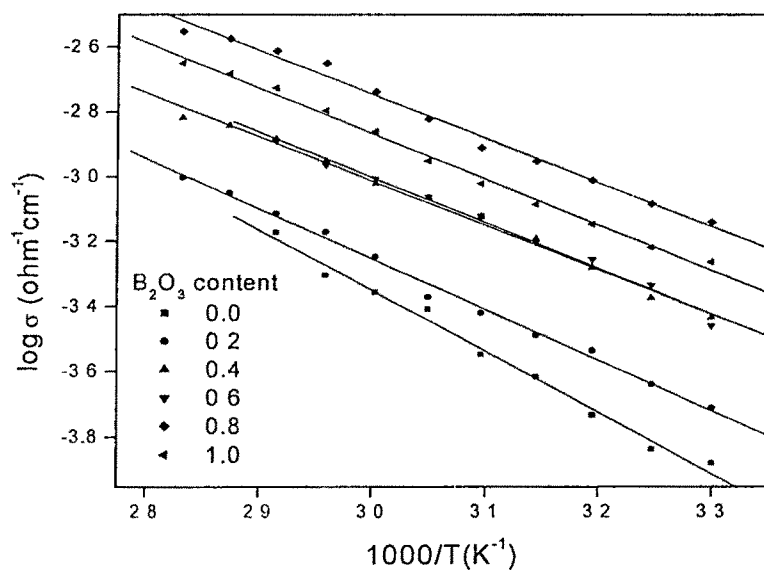


Fig. 4.15. Arrhenius plot for the system $20\text{CdI}_2-53.4\text{Ag}_2\text{O}-26.6[x\text{B}_2\text{O}_3-(1-x)\text{V}_2\text{O}_5]$ with different x values.

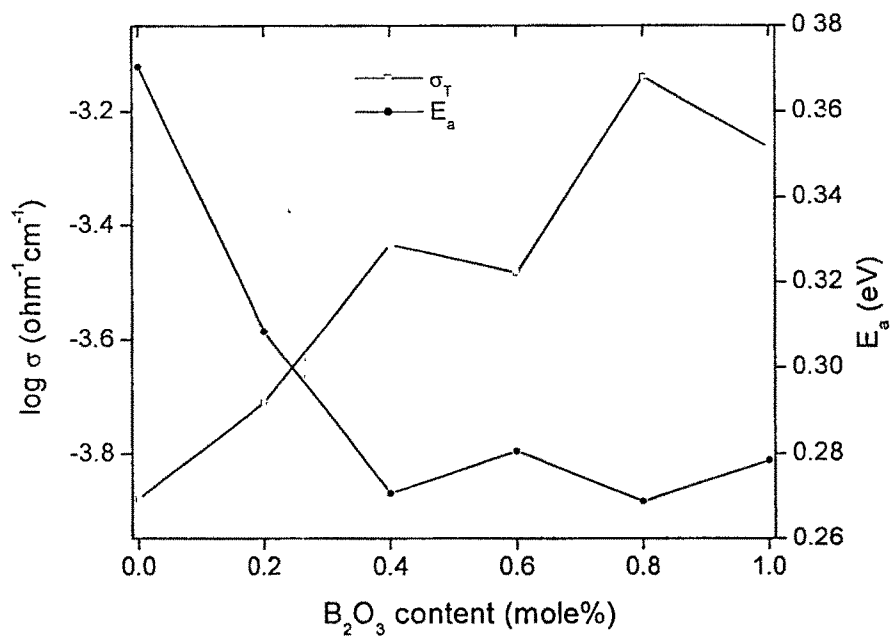


Fig.4.16. The dc conductivity and activation energy plot for $20\text{CdI}_2-53.4\text{Ag}_2\text{O}-26.6[x\text{B}_2\text{O}_3-(1-x)\text{V}_2\text{O}_5]$ with different x values

Arrhenius nature. The plot of conductivity and activation energy against B_2O_3 content is of non-linear nature (Fig.4.16). The conductivity increases from 1.324×10^{-4} to 3.69×10^{-4} S/cm as the fraction of B_2O_3 (x) content increases from 0 to 0.4. There after the conductivity decreases to 3.2869×10^{-4} S/cm for $x=0.6$, then an increased value 7.2576×10^{-4} S/cm is obtained for $x=0.8$. The dual maxima observed for $x=0.4$ and 0.8 indicates that there is no linear increase or decrease of conductivity as the amount of B_2O_3 varies. As is seen, there is no change in the order of magnitude in conductivity at room temperature for all compositions indicating that the overall change is not so well defined. If more than one anion is present in the system, then according to weak electrolyte model, the conductivity goes through a maximum when one anion is subtracted by another [46]. Conductivity is a non-linear function of B_2O_3 content, which might be the effect of the structure of glass on conductivity. The variation in conductivity has been explained according to the conductivity expression, $\sigma = n e \mu$. In this series, the carrier concentration n is fixed because the amount of AgI formed between CdI_2 and Ag_2O is constant in all the samples of the series. Thus the charge carriers are practically constant, as is the mobility. Under these conditions we expect no continuous change in conductivity with change in the B_2O_3 content. The existence of two maxima in conductivity has been reported for other oxide glasses [50,54,55] and also for sulphide glasses [56]. The room temperature dc conductivity values and activation energies obtained for the system $20CdI_2-53.4Ag_2O-26.6[xB_2O_3-(1-x)V_2O_5]$ with different x values are given in Table 4.3. In the ternary glasses i.e., AgI- Ag_2O - B_2O_3 [25], and AgI- Ag_2O - V_2O_5 [26], it is seen that with the increase in the mole% of AgI, the conductivity increases and activation energy decreases. In the first series of the present study, with the increase of the dopant amount CdI_2 the

Table 4.3

Room temperature conductivity σ_{RT} , activation energy E_a and pre-exponential factor σ_0 for the system $20\text{CdI}_2\text{-}53.4\text{Ag}_2\text{O-}26.6[\text{x}\text{B}_2\text{O}_3\text{-(1-x)}\text{V}_2\text{O}_5]$ with different x values.

x	Conductivity σ_{RT} ($\text{Ohm}^{-1}\text{cm}^{-1}$)	Activation energy (E_a) eV	Pre-exponential factor σ_0 .
0	1.324×10^{-4}	0.370	177.59
0.2	1.949×10^{-4}	0.308	25.72
0.4	3.686×10^{-4}	0.270	12.01
0.6	3.286×10^{-4}	0.280	16.76
0.8	7.257×10^{-4}	0.268	20.38
1.0	5.466×10^{-4}	0.278	22.02

Table 4.4

DC Conductivity, Frequency dependent conductivity parameters A , n and the hopping rate ω_p for the system (mole%) $5\text{CdI}_2\text{-}63.4\text{Ag}_2\text{O-}22.12\text{V}_2\text{O}_5\text{-}9.48\text{B}_2\text{O}_3$.

Temperature (K)	DC conductivity σ_0 ($\text{ohm}^{-1}\text{cm}^{-1}$)	A ($\text{ohm}^{-1}\text{cm}^{-1}\text{rad}^{-n}$)	n	ω_p (s^{-1})
303	3.91×10^{-6}	1.37×10^{-11}	0.8937	1.62×10^6
313	5.71×10^{-6}	1.57×10^{-11}	0.8812	2.04×10^6
323	9.15×10^{-6}	2.09×10^{-11}	0.8669	3.21×10^6
333	1.50×10^{-6}	3.37×10^{-11}	0.8484	4.53×10^6
343	2.30×10^{-5}	4.47×10^{-11}	0.8343	6.99×10^6
353	3.0×10^{-5}	5.39×10^{-11}	0.8309	8.21×10^6
363	5.0×10^{-5}	8.28×10^{-11}	0.8264	9.88×10^6

conductivity increases and the activation energy decreases. On the other hand, in the third series where the mole% of CdI_2 and Ag_2O are fixed and such a variation is not observed.

The observed results on electrical conductivity and Ag^+ ion concentration variations are qualitatively discussed using the diffusion path model proposed by Minami [10]. This model suggests that the Ag^+ ions interact with two type of anions present in the glass. The interaction potential of the I^- ion is wide and shallow and that of the O^- ion is deep and narrow (Fig.1.6, Chapter 1). The Ag^+ ions in the shallow iodide potential are more mobile than Ag^+ ions in deep oxide potentials. The carrier concentration depends on the number of Ag^+ ions located in the iodide potential. The increase in the AgI content with the addition of CdI_2 increases the number of Ag^+ ions in the shallow iodide potentials and simultaneously decreases the number of Ag^+ ions in the oxyanion potentials. Thus the increase in the AgI content increases the period of shallow potentials, which forms a favorable path for ion transport with low activation energy, known as diffusion path. This is also evident from the linear decrease of activation energy with the CdI_2 content as explained in the first series. In the second series, with the addition of Ag_2O , the formation of AgI is increasing to a certain level since the amount of CdI_2 is constant, so a non-linear dependence of conductivity is obtained with x/y ratio. In the third series, such an increase in conductivity is not seen because the amount of dopant (CdI_2) and the modifier (Ag_2O) are kept constant.

4.3. Frequency dependent conductivity

The subject of the frequency dependence of ac conductivity of solid electrolyte materials has received a considerable amount of attention both experimentally and theoretically. The theoretical interpretation of the power law dependence of ac conductivity shown by a large number of materials was first proposed by Pollak and Geballe [47] in terms of a distribution of hopping probabilities between sites distributed randomly in space and energy in a disordered solid [48] and a large number of succeeding developments are seen from the literature [49-52]. In solid electrolytes, the frequency dependence of electrical conductivity has been largely interpreted as being the consequence of distributions of relaxation times [53] and the possibility of non-exponential relaxation processes has also been considered [54]. Jonscher has suggested that the dispersion is a universal property of dielectric materials [53]. It has been substantially underpinned by the microscopic theories of Ngai [54] and Dissado and Hill [55] who have shown that dispersion is an inevitable consequence of many body interactions between the conducting species. In recent theories [56,57], the hopping phenomena considered in connection with many particle coulomb interactions, the motion of the charge carriers are greatly influenced by the relaxation of its neighborhood. In a disordered material, a number of energetically favorable sites are available for the mobile charge carriers. These regions may be associated with oppositely (negatively) charged atoms at fixed positions in the glass forming matrix. In equilibrium, all the charge carriers occupy positions corresponding with the lowest energy. If a charge carrier performs a discontinuous jump from its original site, the screening charge which is supplied by other charges in its environment, faces a non-equilibrium situation. The

environment relaxes relatively slowly compared to the short jump time of the charge carrier. Before the relaxation is complete, there is an enhanced probability that the charge will jump back to its original position causing a correlated forward backward hopping sequence. If the backward hop does not take place before the screening charge relaxation is complete, then the jump is successful and diffusion occurs. Thus, at low frequencies only the successful jumps contribute to the conductivity yielding a dc value, whereas at higher frequencies, unsuccessful hops cause a dispersive conductivity i.e., transition from constant low frequency conductivity to a power law behavior.

Frequency dependent conductivity spectra obtained for the presently studied glass system $x\text{CdI}_2-(100-x) [2\text{Ag}_2\text{O}-(0.7\text{V}_2\text{O}_5-0.3\text{B}_2\text{O}_3)]$ with $x=5$ and 10 mole% of CdI_2 doped composition at different temperatures is shown in Figs. 4.17 and 4.18. The conductivity is found to be increasing with increase of temperature. The obtained spectra can be divided into two different regions: a frequency independent plateau region corresponding to dc conductivity at low frequencies and a high frequency dispersion region. Fig.4.19 shows the conductivity versus frequency plot for the system $x\text{CdI}_2-(100-x) [2\text{Ag}_2\text{O}-(0.7\text{V}_2\text{O}_5-0.3\text{B}_2\text{O}_3)]$ at room temperature with $x=5, 10, 15, 20, 25, 30$. As the mole % of CdI_2 increases, conductivity shows a gradual enhancement. The gradual increase in conductivity observed for 25 mole% of CdI_2 system could be attributed to the electrode effects that are usually seen in highly conducting samples [58]. For $x=5$ and 10 mole% CdI_2 the low frequency dispersion is not observed due to the high resistivity of the sample. For $x=25$ and 30 mole % doped CdI_2 systems, the plot shows the low frequency

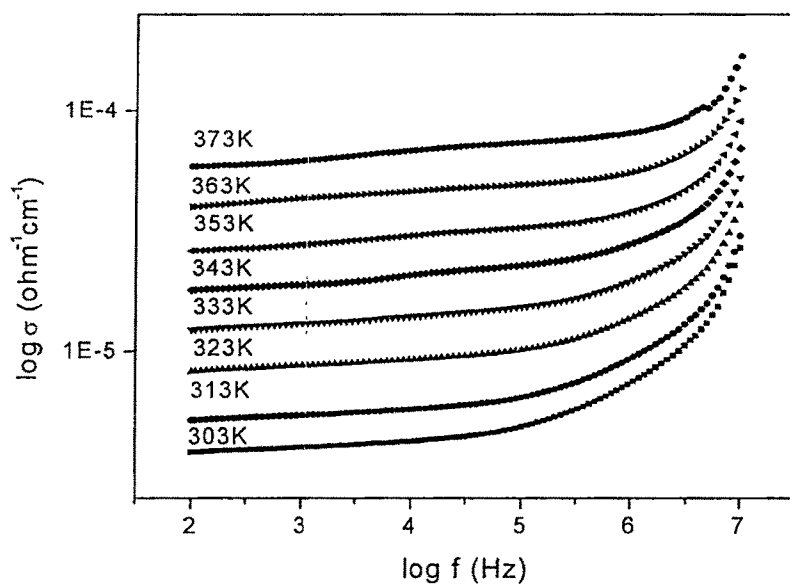


Fig.4.17. Conductivity versus frequency plot for 5 mole% of CdI_2 doped system at different temperatures

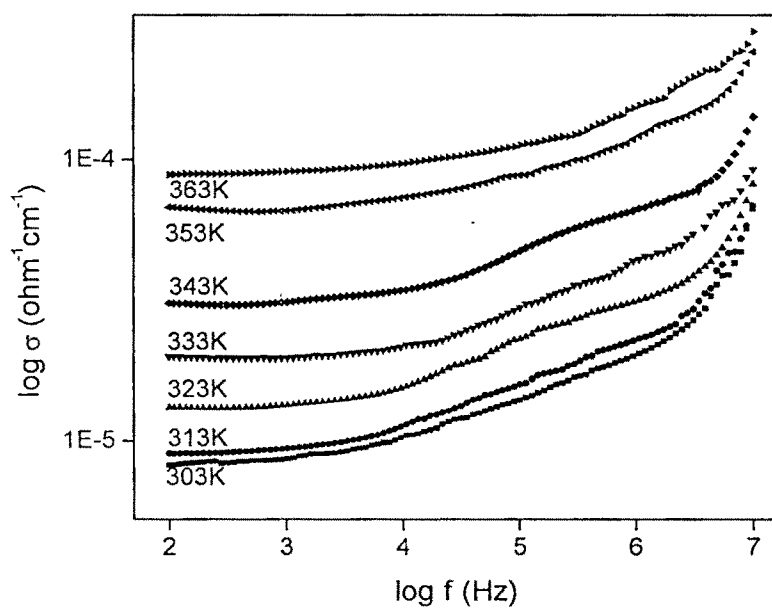


Fig.4.18. Conductivity versus frequency plot for 10 mole% of CdI_2 doped system at different temperatures

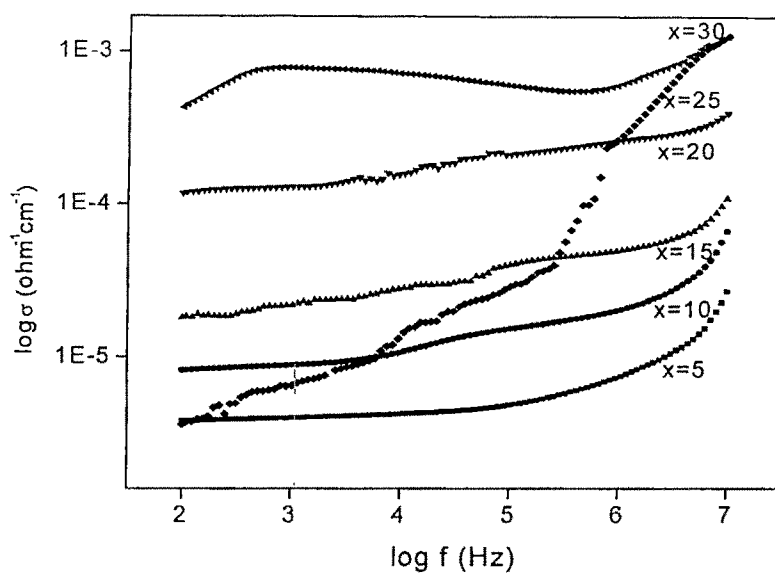


Fig.4.19. Conductivity versus frequency plot for $x\text{CdI}_2-(100-x) [2\text{Ag}_2\text{O}-(0.7\text{V}_2\text{O}_5-0.3\text{B}_2\text{O}_3)]$ system at room temperature.

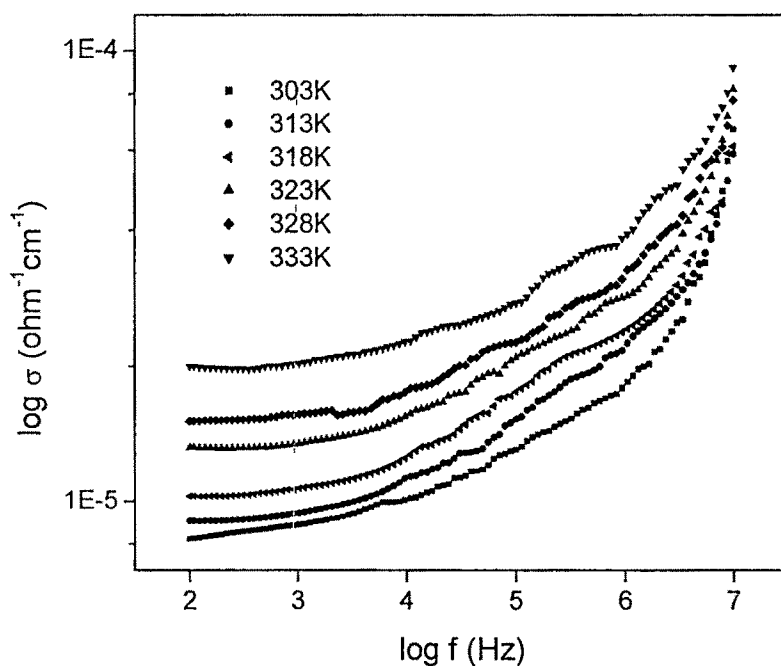


Fig.4.20. Conductivity versus frequency plot for the system $20\text{CdI}_2-80[x\text{Ag}_2\text{O}-y(0.7\text{V}_2\text{O}_5-0.3\text{B}_2\text{O}_3)]$ with $x/y = 1.25$.

dispersion due to electrode polarization. Similar features have also been observed for the conductivity spectra of the samples of other two series.

The conductivity spectra for the system (in the second series) $20\text{CdI}_2\text{-}80[\text{xAg}_2\text{O-y}(0.7\text{V}_2\text{O}_5\text{-}0.3\text{B}_2\text{O}_3)]$ with x/y ratio 1.25 at different temperatures are shown in Fig.4.20, which shows that the conductivity of the system increases with increase in temperature and the dispersion region obtained at higher frequencies are shifted to still higher range with temperature as expected for this kind of systems. The conductivity spectra for different x/y values of the compositions at room temperature are shown in Fig.4.21. The samples with x/y ratio 1, 1.5, 1.75, 2.25 and 2.75 show low frequency dispersion (electrode polarization) at room temperature and it may be due to surface roughness at the electrode-electrolyte interface. The conductivity is found to increase non-linearly with the increase in the modifier to former ratio of the system and a maximum is obtained for the system with x/y ratio 1.75.

Fig.4.22 shows the conductivity spectra obtained for the third series with $x=0.8$ mole% of B_2O_3 of the system $20\text{CdI}_2\text{-}53.4\text{Ag}_2\text{O}\text{-}26.6[\text{xB}_2\text{O}_3\text{-}(1\text{-x})\text{V}_2\text{O}_5]$ for the frequency range from 1Hz-1MHz. Here also, the conductivity is found to increase and the low frequency dispersion increases with increase in temperature. Conductivity spectra for varying concentration of B_2O_3 content are shown in Fig. 4.23 at room temperature. The spectrum shows the low frequency dispersion for the sample at room temperature and is more prominent for $x=0.0, 0.2$ and 0.4% B_2O_3 for the presently studied system. The spectra show a non-linear increase in conductivity when one of the glass former content is replaced by another and a maximum is obtained for 0.8 mole% B_2O_3 system in the present series. These types of systems show three regions in conductivity spectrum and are

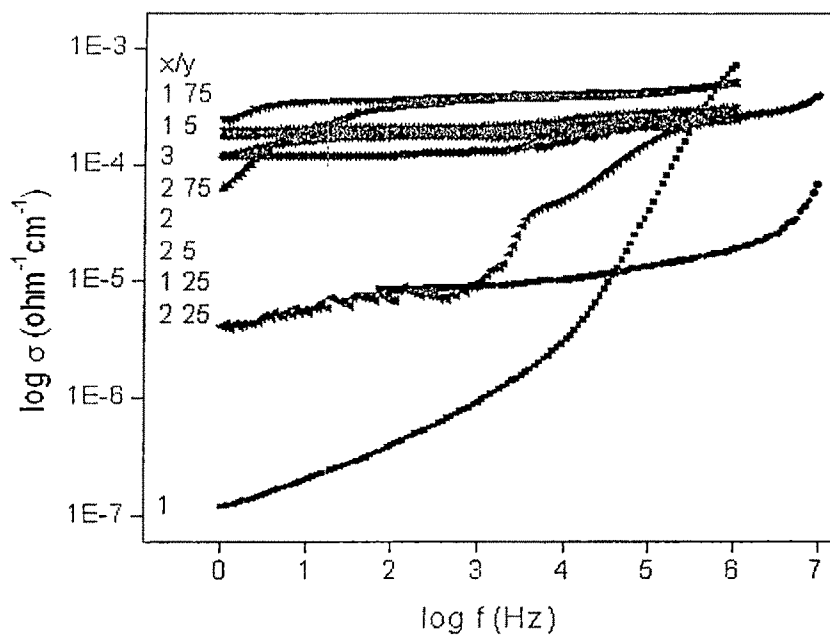


Fig.4.21 Conductivity versus frequency plot for the system $20\text{CdI}_2\text{-}80 [x\text{Ag}_2\text{O-}y(0.7\text{V}_2\text{O}_5\text{-}0.3\text{B}_2\text{O}_3)]$ for different x/y ratios.

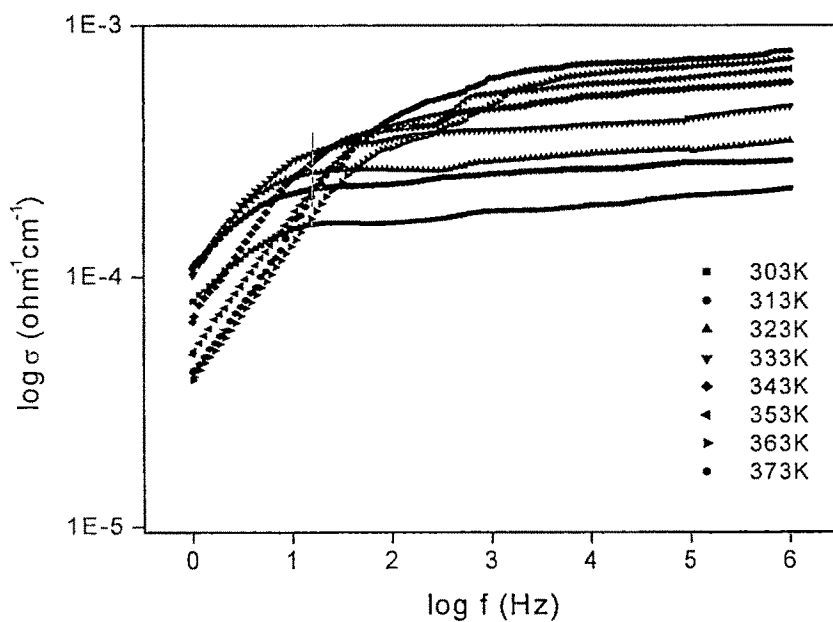


Fig.4.22. Conductivity spectra for the system $20\text{CdI}_2\text{-}53.4\text{Ag}_2\text{O-}[x\text{B}_2\text{O}_3\text{-}(1-x)\text{V}_2\text{O}_5]$ for $x=0.8$.

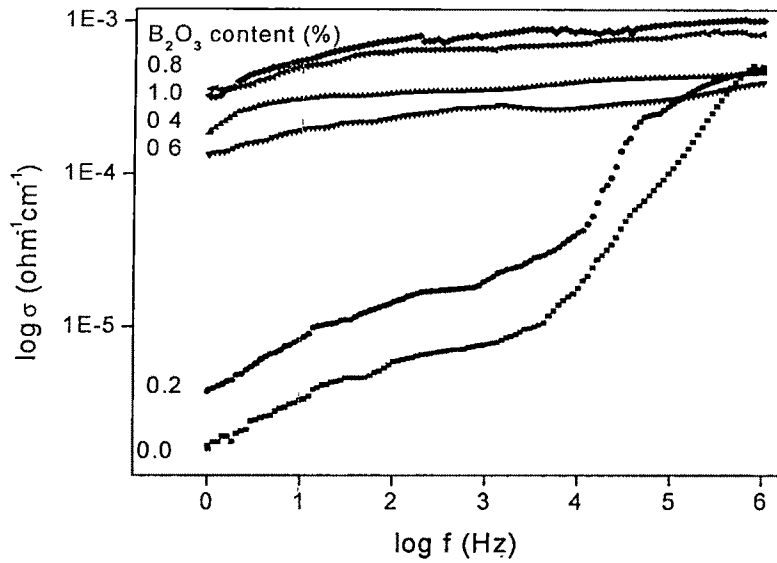


Fig.4.23. Conductivity spectra obtained for varying concentration of B_2O_3 content for $20\text{CdI}_2\text{-}53.4\text{Ag}_2\text{O}\text{-}[x\text{B}_2\text{O}_3\text{-(}1-x\text{) V}_2\text{O}_5]$ system.

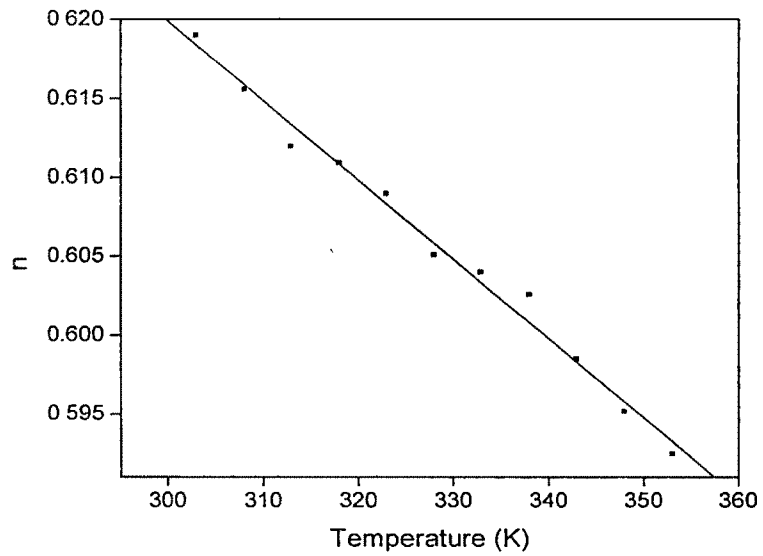


Fig.4.24. Variation of the parameter n with temperature for 20 mole% of CdI_2 doped system.

associated with different phenomena; (1) The low frequency dispersion at higher temperatures arises due to the electrode polarization (2) The high frequency dispersions at low temperatures and (3) The frequency independent plateau region corresponds to dc conductivity.

The power law variation observed in these systems (Figs. 4.17 and 4.18) has been widely investigated and the strong dispersion at low temperature in the high frequency region is attributed to many body effects [59]. The high frequency dispersion is predominant at lower temperatures and with increase in temperature it shifts towards the high frequency region, i.e., with increases in temperature the bulk relaxation of the material shifts to higher frequencies. Finally, the high frequency dispersion region almost disappears at higher temperatures, since the jump frequency of the charge carriers increases with temperature as discussed by Ingram [60]. The variation of conductivity with frequency has been analyzed using the power law exponent

$$\sigma_{(\omega)} = \sigma_0 + A\omega^n \quad (4.19)$$

where $\sigma_{(\omega)}$ is the conductivity at a particular frequency, σ_0 is the dc conductivity at zero frequency, A and n are weakly temperature dependent parameters. This power law of ac behavior is observed in a wide range of systems, Jonscher called it Universal behavior, since Eqn.4.19 is accepted universally for finding the sample conductivity, hopping rate, frequency dependence of conductivity etc.

The value of σ_0 and the parameter A and n for 5 mole% CdI₂ are obtained from the non-linear curve fitting of the conductivity plot and is given in Table 4.4 at different temperatures and for different compositions of all the three series at room temperature are shown in the Table 4.5 to 4.7. The value of the parameter A is found to increase with

Table 4.5

Values of the dc conductivity, frequency dependent conductivity parameters A, n and the hopping rate ω_p for the system $x\text{CdI}_2-(100-x) [2\text{Ag}_2\text{O}-(0.7\text{V}_2\text{O}_5-0.3\text{B}_2\text{O}_3]$ at room temperature for different CdI_2 amount.

x	dc conductivity $\sigma_0(\text{ohm}^{-1}\text{cm}^{-1})$	A $(\text{ohm}^{-1}\text{cm}^{-1}\text{rad}^{-n})$	n	ω_p (s^{-1})
05	3.9×10^{-6}	1.37×10^{-11}	0.8937	1.62×10^6
10	9.9×10^{-6}	6.95×10^{-10}	0.686	1.134×10^6
15	4.8×10^{-5}	1.280×10^{-8}	0.527	6.051×10^6
20	1.9×10^{-4}	9.63×10^{-8}	0.621	2.023×10^5
25	6.1×10^{-4}	1.649×10^{-9}	0.652	3.467×10^8
30	7.8×10^{-1}	9.12×10^{-11}	0.761	1.285×10^9

Table 4.6

Values of the dc conductivity, frequency dependent conductivity parameters A, n and the hopping rate ω_p for the system $20\text{CdI}_2-80[x\text{Ag}_2\text{O}-y(0.7\text{V}_2\text{O}_5-0.3\text{B}_2\text{O}_3)]$ at room temperature for different x/y ratios.

x/y	dc conductivity $\sigma_0(\text{ohm}^{-1}\text{cm}^{-1})$	A $(\text{ohm}^{-1}\text{cm}^{-1}\text{rad}^{-n})$	n	ω_p (s^{-1})
1.0	1.5717×10^{-6}	2.46×10^{-9}	0.657	1.867×10^4
1.25	1.1352×10^{-5}	4.929×10^{-9}	0.642	1.726×10^5
1.50	4.0855×10^{-4}	3.605×10^{-7}	0.556	3.114×10^5
1.75	5.2597×10^{-4}	9.941×10^{-7}	0.440	1.548×10^6
2.0	1.9000×10^{-4}	9.63×10^{-8}	0.621	2.023×10^5
2.25	1.6621×10^{-5}	1.924×10^{-9}	0.732	2.385×10^5
2.5	1.3851×10^{-4}	3.137×10^{-9}	0.591	7.326×10^7
2.75	2.4171×10^{-4}	3.808×10^{-7}	0.493	4.838×10^5
3.0	2.9670×10^{-4}	7.58×10^{-8}	0.561	2.535×10^6

Table 4.7

Values of the dc conductivity, frequency dependent conductivity parameters A , n and the hopping rate ω_p for the system $20\text{CdI}_2\text{-}53.4\text{Ag}_2\text{O-}26.6[\text{xB}_2\text{O}_3\text{-(1-x)V}_2\text{O}_5]$ at room temperature for different amount of B_2O_3 .

x	dc conductivity σ_0 ($\text{ohm}^{-1}\text{cm}^{-1}$)	A ($\text{ohm}^{-1}\text{cm}^{-1}\text{rad}^{-n}$)	n	ω_p (s^{-1})
0	1.324×10^{-4}	1.008×10^{-6}	0.532	9.54×10^4
0.2	1.949×10^{-4}	2.321×10^{-6}	0.461	1.49×10^4
0.4	3.686×10^{-4}	6.54×10^{-7}	0.587	4.85×10^6
0.6	3.286×10^{-4}	5.02×10^{-7}	0.531	2.01×10^5
0.8	7.257×10^{-4}	6.406×10^{-6}	0.428	6.30×10^4
1.0	5.4660×10^{-4}	4.1×10^{-6}	0.458	4.36×10^4

Table 4.8

Frequency dependent conductivity results for the composition;
 $5\text{CdI}_2\text{-}63.4\text{Ag}_2\text{O-}22.12\text{V}_2\text{O}_5\text{-}9.48\text{B}_2\text{O}_3$.

Frequency (Hz)	Frequency dependent conductivity at room temperature (S/cm)	Frequency dependent activation energy (E_a^*) eV	Activation energy Obtained from dc conductivity (E_a) eV
100	3.869×10^{-6}	0.38	0.42
1000	4.049×10^{-6}	0.38	
10000	4.309×10^{-6}	0.39	
100000	4.914×10^{-6}	0.38	
1000000	7.556×10^{-6}	0.33	
10000000	2.687×10^{-5}	0.26	

temperature and the n value decreases. Fig 4.24 shows the variation of n with temperature. In most of the systems it was evident that the n value decreases with temperature and then level off in the neighborhood of 0.5 [61]. Jonscher [62] has shown that a non-zero n in the dispersive region of conductivity is due to the energy stored in the short range collective motion of ions. A higher n implies that larger energy is stored in such collective motions. The values of the frequency exponent n in the range 0.5-0.6 seem to be universally observed in all types of ionically conducting glasses [52,63,64] and can be compared with the n value obtained for most of the presently studied glasses. Some models have been proposed in the literature [65] that can account for some aspects of this behavior but all suffer from some drawbacks. In the jump diffusion model of Funke [66], the frequency exponent is determined by the fractional mismatch between a neighboring ion position after a central ion hop and a local potential minimum before the hop and suggested a universal value of n to be 0.5-0.6. The Coulomb interacting lattice gas model [57,67] predicts a limiting value of n as 0.75 where as Diffusion Controlled Relaxation model [52] predicts $n=0.5$. All these models predict that the ac conductivity should be thermally activated with activation energy less than that for dc conductivity.

The conductivity variations at various frequencies are shown in Fig.4.25 in the form of Arrhenius plots for the composition containing 5 mole% of CdI_2 system. It is interesting to note that Arrhenius relation is obeyed over the temperature range at different frequencies. The activation energy values (E_a^*) obtained from the frequency dependent Arrhenius plots also agree well with that calculated from the conductivity plot during the impedance analysis. This feature is consistent with Jonschers analysis of ac conduction [18, 68]. Table 4.8 contains the results of frequency dependent conductivity, frequency

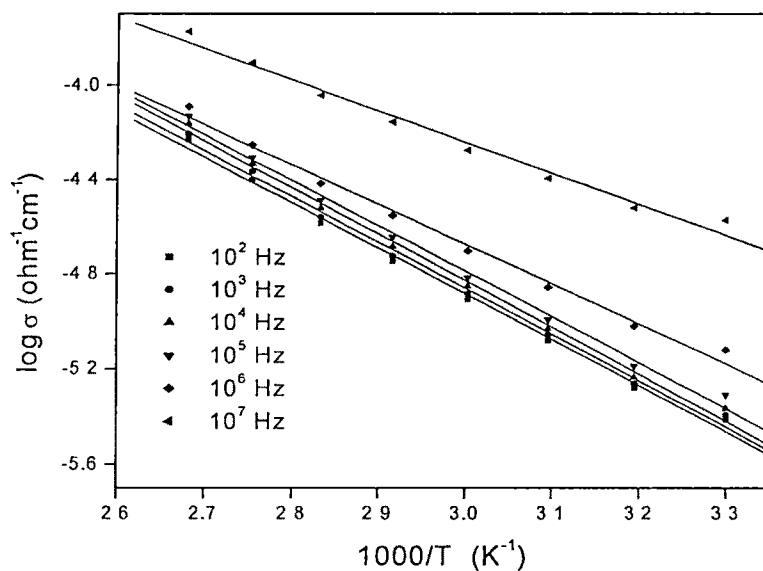


Fig.4.25. Conductivity variations at various frequencies for the compositions containing 5 mole% of CdI₂

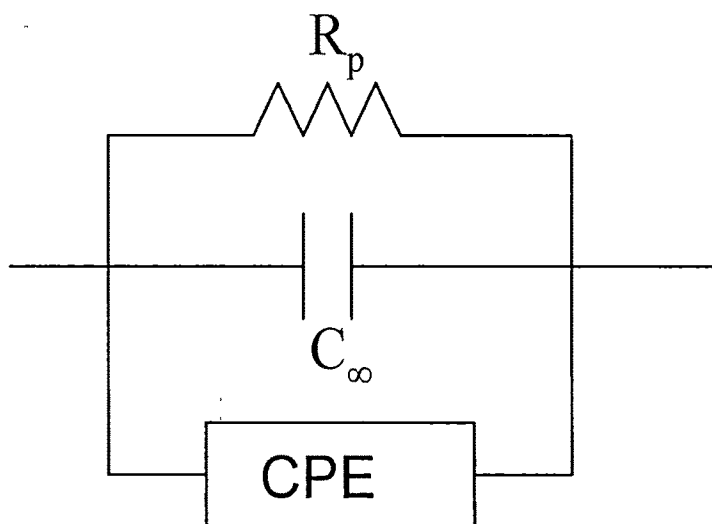


Fig.4.26. Equivalent circuit model for a dispersive conductor.

dependent activation energy and the activation energy for silver ion migration obtained from the impedance analysis at room temperature.

In the presently investigated systems, the concentration of mobile ions in all the systems is large so that the average distance between Ag^+ ions is small. The interaction among the mobile cations in these systems leads to a distribution of relaxation time. Bruce et. al., [69] proposed an equivalent circuit, a parallel combination of R_p , C_∞ and a CPE element as shown in the Fig.4.26 to model the electrical properties of this type of intrinsically dispersive conductor. The admittance of the CPE is defined as (Macdonald, 1984)

$$Y_{CPE} = A_0(j\omega)^n \quad (4.20)$$

$$Y_{CPE} = A\omega^n + jB\omega^n \quad (4.21)$$

when $n=0$, $A_0=1/R$ and for $n=1$, $A_0=C$. The total admittance of the above circuit is

$$Y^*(\omega) = \frac{1}{R_p} + A\omega^n + j(B\omega^n + \omega C_\infty) \quad (4.22)$$

The real and imaginary part of admittance correspond respectively with the conductivity $\sigma_{(\omega)}$, the product of angular frequency ω and the capacitance $C_{(\omega)}$ of the equivalent circuit, therefore

$$\sigma_{(\omega)} = \frac{1}{R_p} + A\omega^n \quad (4.23)$$

$$C_{(\omega)} = C_\infty + B\omega^{n-1} \quad (4.24)$$

The parameters A and B are related by

$$B = A \tan(n\pi/2) \quad (4.25)$$

In these systems, the concentration of mobile ions is independent of temperature but the hopping frequency of the mobile ions depends on the temperature. Almond and West [70, 71] suggested a simple way to calculate the hopping frequency from Eqn.4.19, by knowing the value of A, n, σ_0 and the frequency, where $\sigma_{(\omega)} = 2\sigma_0$. Making use of Jonschers empirical expression, Eqn.4.19 can be written as [53, 72]

$$\sigma_{(\omega)} \propto \omega \left[\left(\frac{\omega}{\omega_p} \right)^{n_1-1} + \left(\frac{\omega}{\omega_p} \right)^{n_2-1} \right] \quad (4.26)$$

where n_1 and n_2 are empirical constants of the material and ω_p is the hopping frequency. For materials, which show a frequency independent region of conductivity $n_1=0$ and $n_2=n$, i.e.,

$$\sigma_{(\omega)} \propto \left(\omega_p + \omega_p^{1-n} \omega^n \right) \quad (4.27)$$

$$\sigma_{(\omega)} = K\omega_p + K\omega_p^{1-n} \omega^n \quad (4.28)$$

where K is a constant, which depends on the concentration of the mobile charge carriers and by comparing Eqns. 4.19 and 4.28, the hopping rate is given by

$$\omega_p = \left[\frac{\sigma_0}{A} \right]^{1/n} \quad (4.29)$$

Table 4.4 shows the value of ω_p estimated using the above equation. From Figs. 4.17 and 4.18 we can see that the frequency ω_p shifts to higher frequencies with increase of temperature. because the hopping frequency is assumed to be thermally activated and is represented by

$$\omega_p = \omega_0 \exp\left(-\frac{E_m}{kT}\right) \quad (4.30)$$

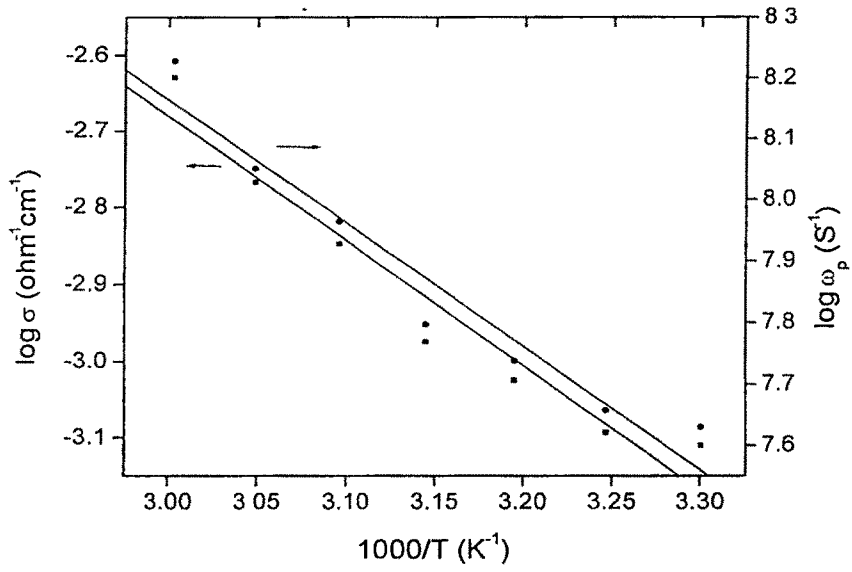


Fig.4.27. Temperature dependence of the ω_p plot for 30 mole% of CdI_2 doped system

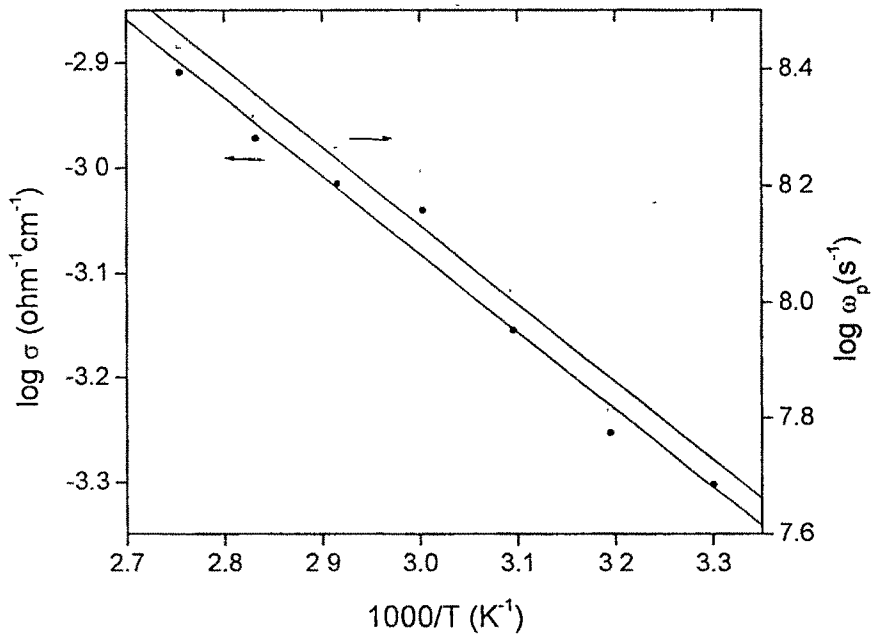


Fig. 4.28. The ω_p against $1000/T$ plot for the system with x/y ratio 1.75.

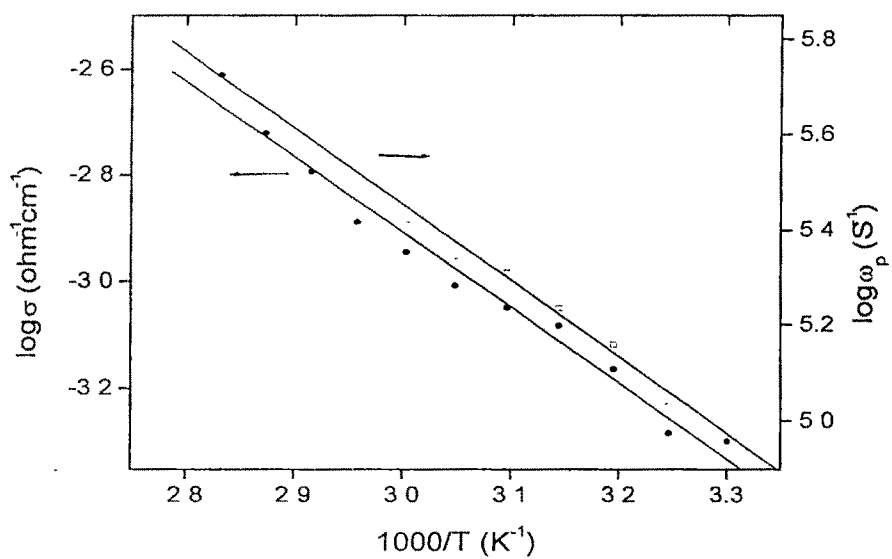


Fig.4.29. The ω_p against $1000/T$ plot for the system with $x=0.8$ of the system $20\text{CdI}_2-53.4\text{Ag}_2\text{O}-26.6[x\text{B}_2\text{O}_3-(1-x)\text{V}_2\text{O}_5]$.

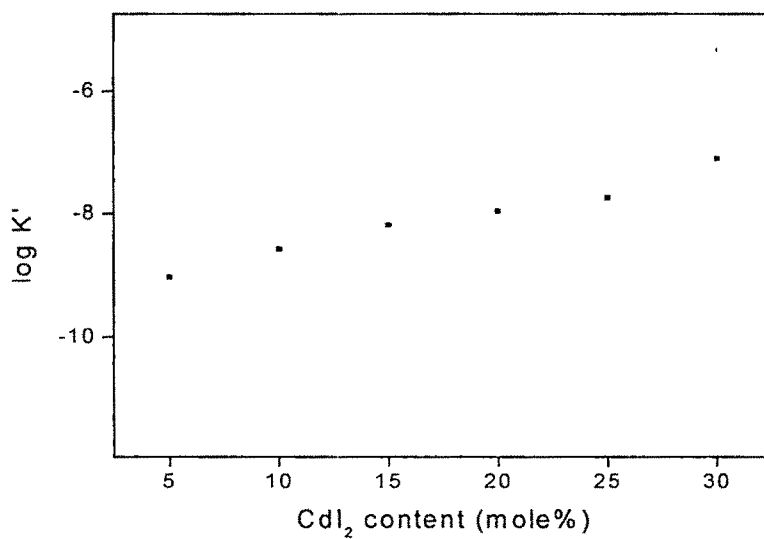


Fig.4.30. Mobile ion concentration factor K' versus CdI_2 content

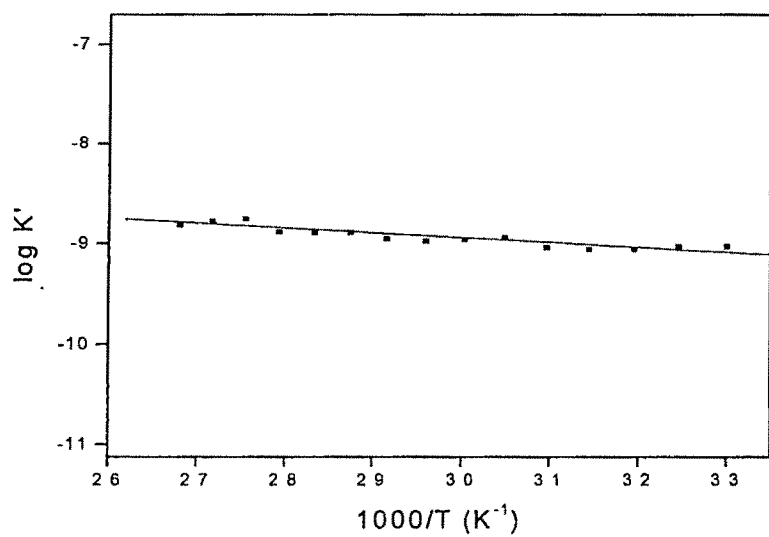


Fig.4.31. Mobile ion concentration versus inverse of temperature plot for 5 mole % of CdI₂ doped system.

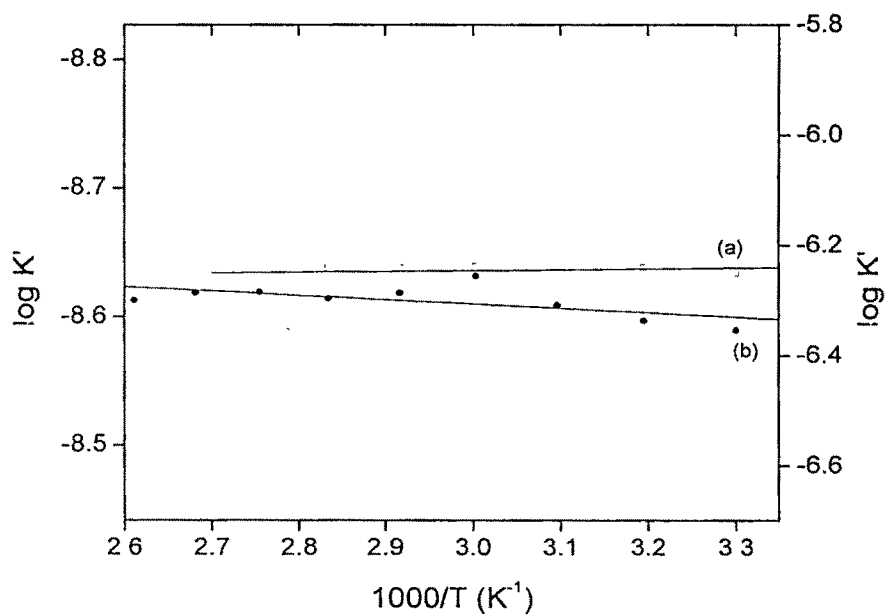


Fig.4.32 (a) and (b) shows the K versus inverse of temperature for x/y ratio 1.25 (second series) and x=0.6 B₂O₃ (third series)

where ω_0 is the effective attempt frequency and E_m is the free energy of migration of the mobile ions. Temperature dependence of ω_p for $x=30$ mole% of CdI_2 doped system calculated using Eqn. 4.29 follows the Arrhenius nature and is shown in Fig.4.27. Fig.4.28 shows the ω_p against $1000/T$ plot for the system with x/y ratio 1.75 (second series). Fig.4.29 shows the ω_p plot for 0.8 B_2O_3 content for the system $20CdI_2-53.4Ag_2O-26.6[xB_2O_3-(1-x) V_2O_5]$. The free energy of migration, E_m obtained from the slope of $\log\omega_p$ plot and the activation energy obtained from the conductivity plot are comparable.

From Eqn.4.28, it is seen that dc conductivity depends on mobile ion concentration factor K and hopping rate. Temperature dependence of mobile ion concentration factor K has been calculated by the method of Almond et.al, [73]

$$K = \frac{\sigma_0 T}{\omega_p} \quad (4.31)$$

Figs. 4.30 and 4.31 show the plot of K versus CdI_2 content and inverse of temperature. The mobile ion concentration factor K is found to increase with CdI_2 concentration and is found to be independent of temperature. This shows that the increase in the mobile ion concentration is attributed to the increase in the conductivity with the increase in the CdI_2 content. In the presently studied systems, mobile ion concentration factor K is not thermally activated and the variation of conductivity arises due to the temperature dependence of the hopping rate of mobile ions. Figs.4.32 (a) and (b) show the independence of temperature of K for the modifier to former ratio 1.25 (in second series) and the $x=0.6$ B_2O_3 content system (third series).

The dc conductivity of most of the ionic conductors is determined by the expression obtained from the theory of random walk [74, 71]

$$\sigma_0 = K\omega_p = \left(\frac{Ne^2 a^2}{kT} \right) \gamma c(1-c)\omega_p \quad (4.32)$$

where γ is a geometrical factor, c is the concentration of mobile ions on N equivalent lattice sites per unit volume, a is the hopping distance, e is the electronic charge, k is the Boltzmann's constant, T is the absolute temperature and ω_p is the hopping rate of mobile ions. From the equation, it is seen that dc conductivity depends on carrier concentration and hopping rate. In super ionic conductors, carrier concentration is not thermally activated and variation of conductivity arises mainly due to the temperature dependence of hopping rate of the mobile species [32]. As the hopping rate is increasing with temperature, the conductivity should increase as is observed in the present glass system.

4.4. Dielectric Analysis

In the present work, complex permittivity of the system is calculated using the impedance data

$$\varepsilon^* = \frac{1}{j\omega C_0 Z^*} = \varepsilon' - j\varepsilon'' \quad (4.33)$$

where Z^* is the complex impedance, $C_0 = \varepsilon_0 A/t$, t is the thickness of the sample, A is the effective area of the electrodes, ε_0 is the permittivity of free space (8.854×10^{-12} F/cm), $j = \sqrt{-1}$ and $\omega = 2\pi f$, the angular frequency of the applied field, ε' and ε'' represent the dielectric constant and dielectric loss respectively. The familiar Debye equation for complex permittivity,

$$\varepsilon_p^* = \varepsilon_\infty + \frac{\varepsilon_0 - \varepsilon_\infty}{1 + j\omega\tau} \quad (4.34)$$

where ε_0 and ε_∞ are the low and high frequency dielectric constants, substitution and separation of real and imaginary parts give the equally familiar expressions for the dielectric constant, ε' and dielectric loss ε'' .

$$\varepsilon' = \varepsilon_\infty + \frac{\varepsilon_0 - \varepsilon_\infty}{1 + \omega^2\tau^2} \quad (4.35)$$

$$\varepsilon'' = \frac{(\varepsilon_0 - \varepsilon_\infty)\omega\tau}{1 + \omega^2\tau^2} \quad (4.36)$$

The dielectric constant ε' and dielectric loss ε'' of complex permittivity are plotted against each other according to the method of Cole-Cole, an arc is obtained. The centre of the circle of which the arc is a part lies on the abscissa axis and is the condition for single

relaxation time. This is often referred to as “Debye behavior” since the behavior is now accurately described by the Debye Equations 4.35 and 4.36. But for many systems, the centre of the circle of which the arc is a part lies below the real axis makes an angle $\alpha\pi/2$.

The dielectric response obtained from a wide range of materials departs significantly from the ideal Debye behavior and shows the dispersion and distribution of relaxation times which is dominated by hopping charge carriers [34]. In many materials, the Debye loss peak is found to overlap at low frequencies with either dc conduction or low frequency dispersion process to give a resultant response which departs significantly from a pure Debye response [34,75]. Experimental evidence [34,75] shows that the Universal dielectric response has a fractional power law dependence on frequency

$$\epsilon_{(\omega)}^* = A(i\omega)^{n-1} \quad (4.37)$$

with $0 < n < 1$, where A is a constant. The Kramers-Kronig transformation of the above equation is independent of frequency and the ratio

$$\frac{\epsilon_{(\omega)}''}{\epsilon_{(\omega)}'} = \cot(n\pi/2) = \text{constant} \quad (4.38)$$

which is a general property of the so called Universal dielectric response in complete contrast with the Debye behavior for which the ratio is equal to $\omega\tau$ [54]. A detailed survey of the dielectric properties of wide range of solids has been given by Jonscher [34]. Dielectric relaxation studies on different systems $\text{Ag}_2\text{O}-\text{B}_2\text{O}_3-\text{P}_2\text{O}_5$ [75], $\text{BaHPW}_{12}\text{O}_{40} \cdot 7\text{H}_2\text{O}$ [77], $\text{B}_2\text{O}_3-\text{Li}_2\text{O}-\text{Li}_2\text{Cl}_2$ [78] etc have been studied.

Fig.4.33 shows the Cole-Cole plot, i.e.. the imaginary part ϵ'' versus real part ϵ' of dielectric permittivity obtained for 5 mole% of CdI_2 doped glass system $x\text{CdI}_2-(100-x)$

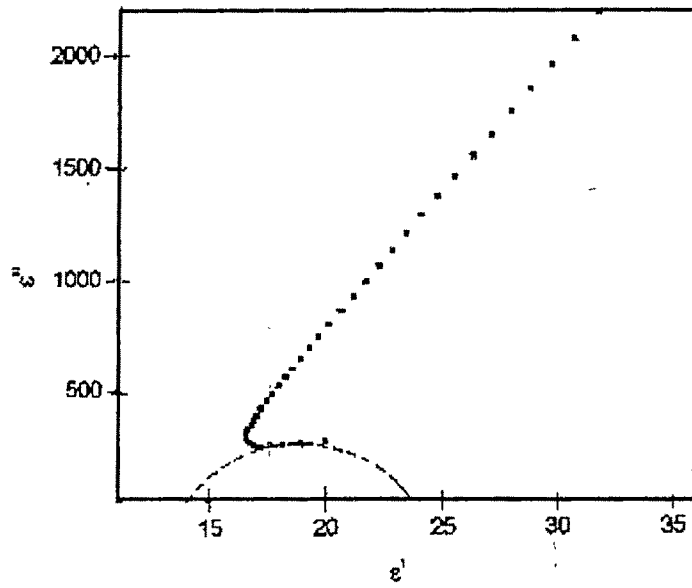


Fig.4.33. Cole-Cole plot obtained for the 5 mole% of CdI₂ doped system at room temperature.

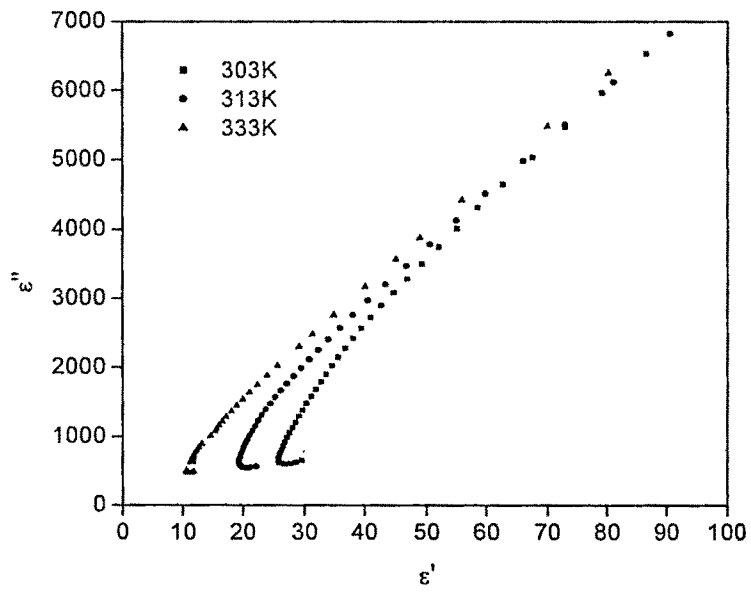


Fig.4.34 Cole- Cole plot obtained for the system with x/y ratio 1.25 at three different temperatures.

[2Ag₂O - (0.7 V₂O₅ - 0.3 B₂O₃)] at room temperature. A depressed semicircle has been extrapolated from this plot. Similar behavior is obtained for all the glass samples studied. A typical Cole-Cole plot for x/y ratio 1.25 at different temperatures is shown in Fig 4.34. In most of the cases, the conductivity loss $\sigma_0 / \omega \epsilon_0$ has been subtracted out from ϵ_p^* in order to give a good picture of dielectric relaxation [79]. In the presently studied systems where many relaxations are present and a depressed semicircle is obtained with its centre below the abscissa and is due to the distribution of relaxation time, instead of the Debye behavior, which shows a single relaxation time. The most classical equation used for this behavior for the complex dielectric constant is thus

$$\epsilon_p^* = \epsilon_\infty + \frac{\epsilon_s - \epsilon_\infty}{1 + (j\omega\tau)^{1-\alpha}} \quad (4.39)$$

where α is an empirical parameter, whose values lie between 0 and 1, which may vary with temperature but not with frequency. When α is zero, there is only one relaxation time and the Eqn. 4.39 becomes identical with the Debye equation, 4.34. Similar behavior is obtained for other systems [77, 79, 80].

The variation of dielectric constant ϵ' with frequency at different temperatures for 5 mole% of CdI₂ doped systems has been shown in fig.4.35. The ϵ' is found to decrease with frequency and tend to saturate at higher frequencies which is found to be more or less temperature independent employed in the present investigation. This is because as temperature increases the jump frequency of the mobile ion becomes large and comparable with the frequency of the applied field [81]. The high value of dielectric constant in the low frequency region is attributed to the interfacial ionic polarizations due to localized Ag⁺ ion motion within the vanadoborate network [82]. Similar features of

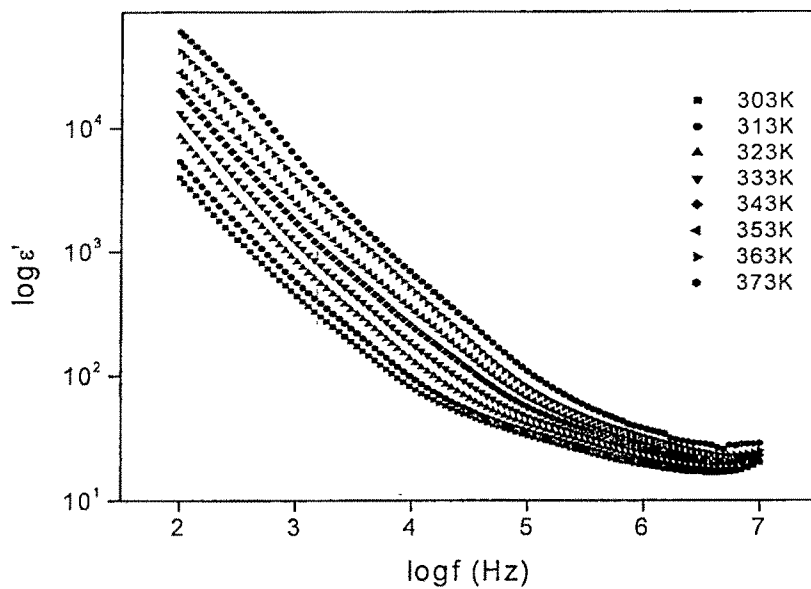


Fig.4.35. Dielectric constant versus frequency at different temperatures for 5 mole% of CdI_2 doped system.

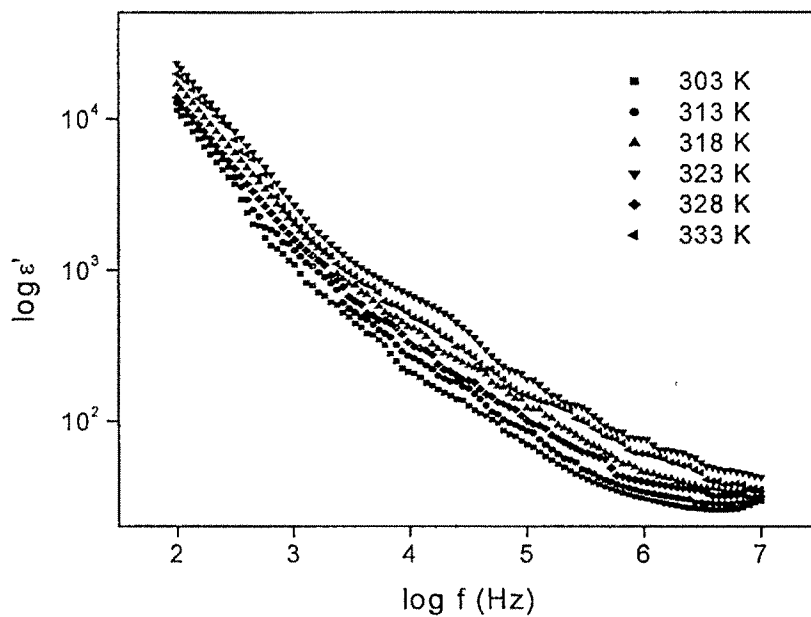


Fig.4.36. Frequency dependent dielectric constant for the system with x/y ratio 1.25 at different temperatures.

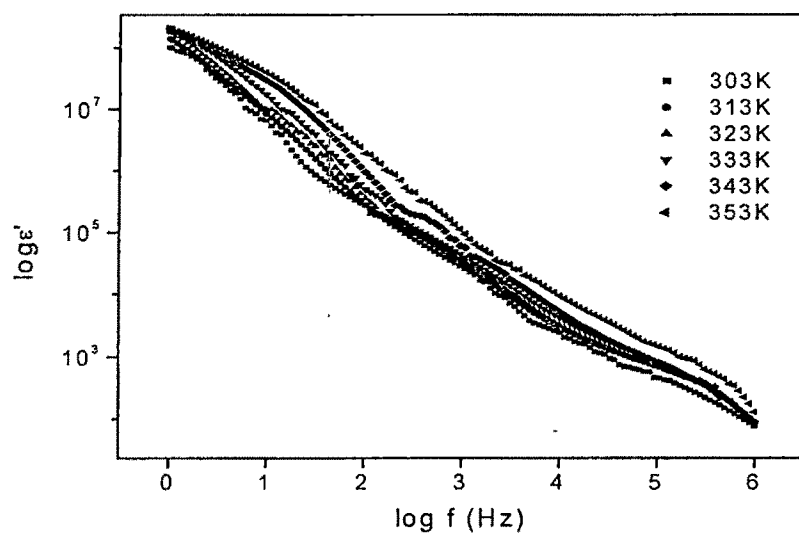


Fig.4.37. Frequency dependent dielectric constant for the system with $x=0.6$ B_2O_3 at different temperatures

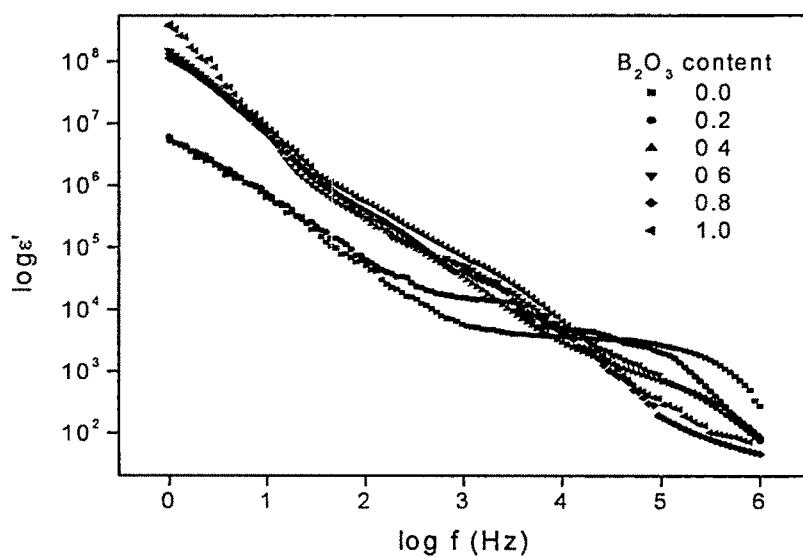


Fig.4.38. Frequency dependent dielectric constant for different mole% B_2O_3 in the system $20CdI_2-53.4Ag_2O-26.6[xB_2O_3-(1-x)V_2O_5]$.

dielectric dispersion spectrum shown by all the other samples. Fig. 4.36 shows the variation of dielectric constant ϵ' versus frequency for x/y ratio 1.25 (in the second series) at different temperatures. The dielectric constant value is found to decrease with the frequency. Fig.4.37 shows the dielectric spectrum obtained for the system with 0.6 mole% of B_2O_3 content (third series). The frequency dependent dielectric constant for different B_2O_3 in the system $20CdI_2-53.4Ag_2O-26.6[xB_2O_3-(1-x)V_2O_5]$ at room temperature are shown in fig.4.38. It is found that for all these samples the dielectric constant decreases with increase of frequency and it saturates at higher frequencies. As the temperature is increased a similar variation with an increase in the ϵ' value results. This is the usual behavior noted for any dielectric. These are in conformity with the observation made by earlier workers [81-84]. The values of ϵ' are observed to be fairly high in all these systems. Such high values are attributed to the high ionic conductivity in the material. Most of the solid electrolytes have been reported to possess high value of dielectric constant [85-88].

The experimental results obtained in the present system for dielectric permittivity can be explained on the Stevels model on dielectric relaxation in glasses [33]. In glasses, the dielectric relaxation and dispersion could be accounted for by the lack of translational invariance of the free energy barriers impeding the ionic motion in the glassy sub lattice. But the case is different in ionic crystals, where the free energy barriers are regularly spaced and of uniform height. The present glass system is expected to be disordered on a molecular level, so we can expect a variation in the free energy barriers from site to site in the glassy vanado-borate lattice. The conduction of silver ions in the glass system can be visualized as a series of jumps along the lattice sites. At lower frequencies, the mobile Ag^+

ions can jump easily out of the sites with low free energy barriers in the electric field direction but tend to pile up at sites with high free energy barriers. This leads to a net polarization of the ionic medium and hence a contribution of $(\epsilon_0 - \epsilon_\infty)$ in Eqn. (4.34) at lower frequencies is responsible for ϵ' obtained in Fig.4.35. Thus, the variation of ϵ' at lower frequencies is due to the long range diffusion of Ag^+ ions involving series of jumps over barriers of varying heights. At higher frequencies, the periodic reversal of the field takes place so rapidly that there are no excess ionic jumps in the field direction. The polarization due to charge pile up at high free energy barrier sites disappears and the contribution of mobile ions to dielectric ϵ' falls to ϵ_∞ and an increase in conductivity is expected as seen in the present system.

Fig.4.39 shows the imaginary part of permittivity ϵ'' as a function of frequency at various temperatures for the system $x\text{CdI}_2-(100-x) [2\text{Ag}_2\text{O}-(0.7\text{V}_2\text{O}_5-0.3\text{B}_2\text{O}_3)]$ with $x=5$ mole%. Fig.4.40 shows the imaginary part of permittivity plot for different x/y ratio values of the system $20\text{CdI}_2-80[x\text{Ag}_2\text{O}-y(0.7\text{V}_2\text{O}_5-0.3\text{B}_2\text{O}_3)]$ at room temperature. Fig.4.41 shows the ϵ'' plot for different B_2O_3 content systems at room temperature $20\text{CdI}_2-53.4\text{Ag}_2\text{O}-26.6[x\text{B}_2\text{O}_3-(1-x)\text{V}_2\text{O}_5]$. All of them found to have a $1/\omega$ dependence with frequency. The dielectric loss, ϵ'' will not show a peak unless the dc conductance is subtracted, which could be possible only for low conducting materials. The dielectric loss obtained is found to increase with increase in temperature. Similar behavior is reported for other Ag^+ ion conducting glasses [81-83]. The observed variation in ϵ' and ϵ'' with frequency could also be attributed to the formation of a space charge region at the electrode electrolyte interface, which is familiarly known as the $\omega^{(n-1)}$ variation or the

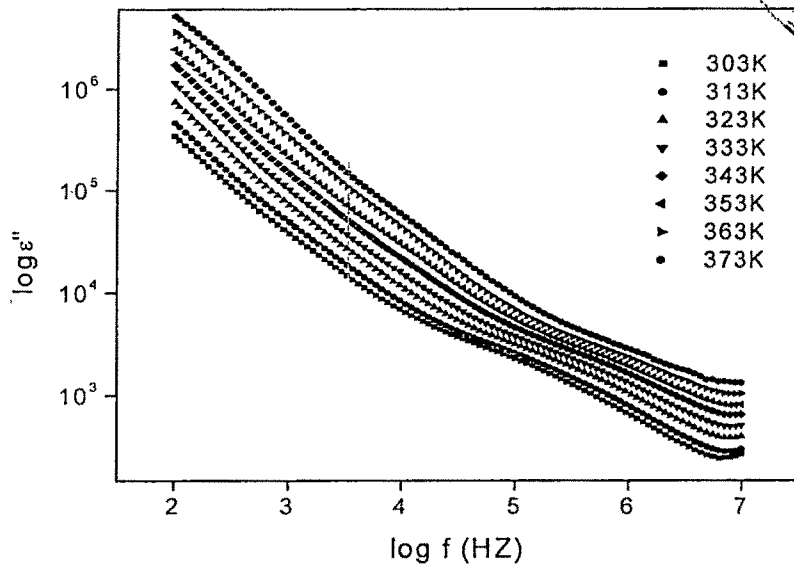
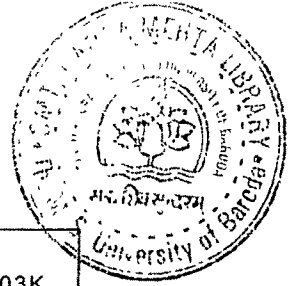


Fig.4.39 Frequency dependence of the imaginary part of permittivity for $x=5$ mole% of CdI_2 doped system.

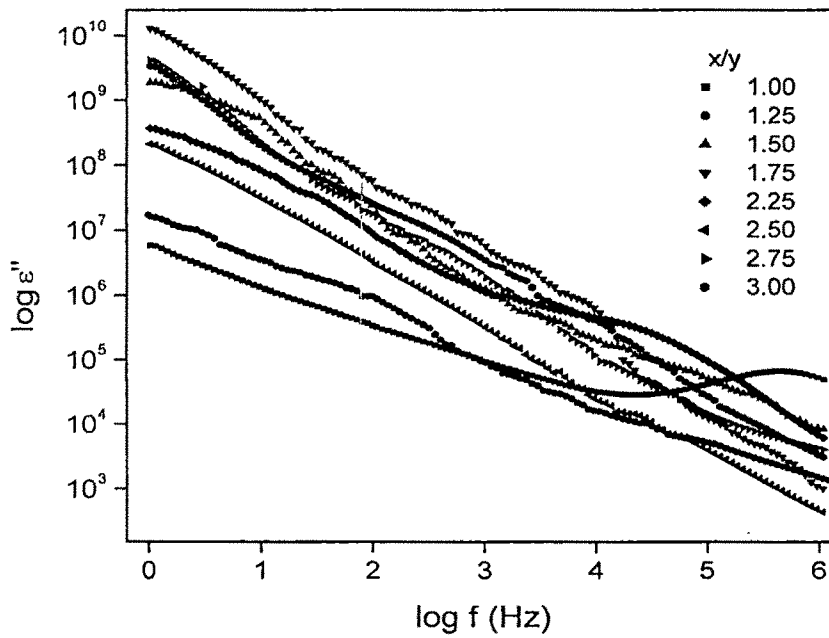


Fig.4.40. The plot of dielectric loss versus frequency at different x/y ratios.

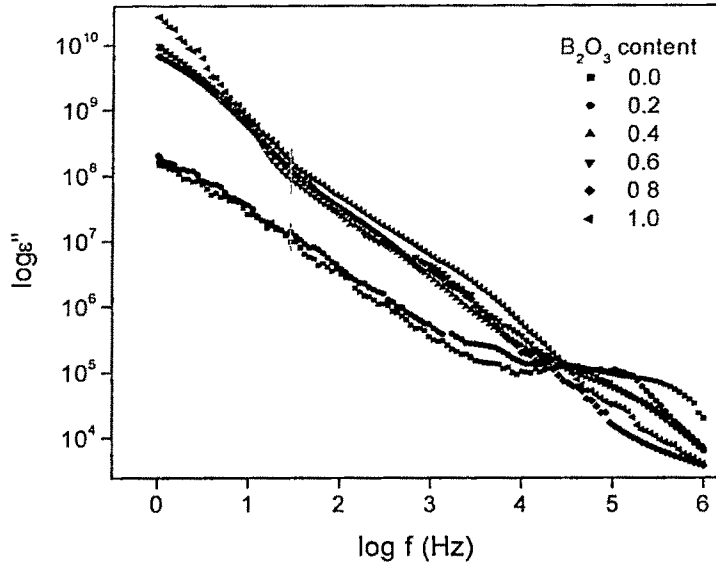


Fig.4.41. Dielectric loss plot for different B_2O_3 content in the system $20CdI_2-53.4Ag_2O-26.6[xB_2O_3-(1-x)V_2O_5]$ at room temperature.

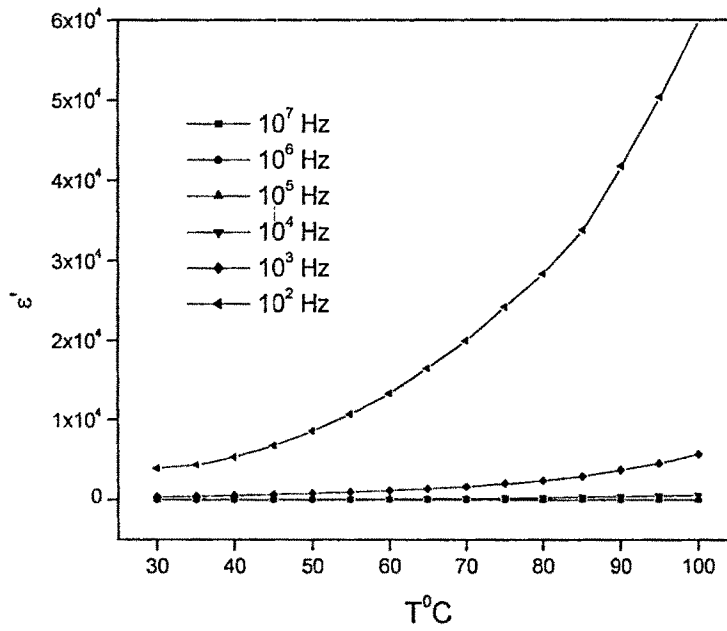


Fig.4.42 (a). Temperature dependence of the real part of permittivity for $5CdI_2$ system at several values of frequencies.

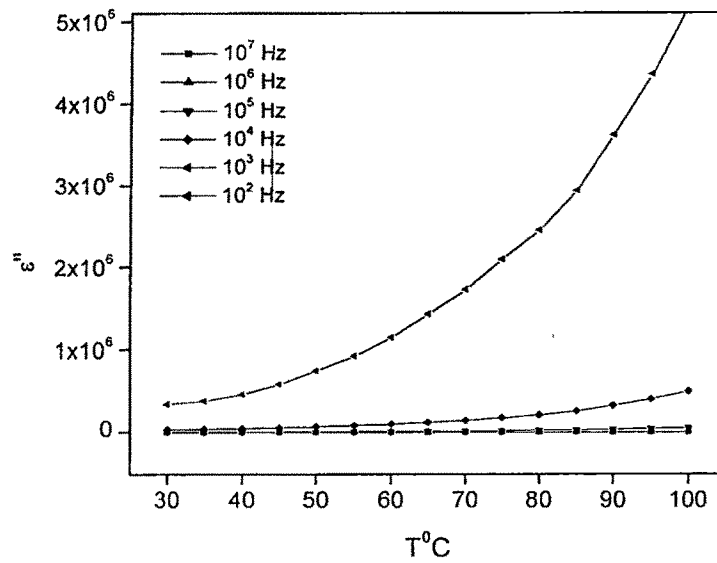


Fig.4.42(b). Temperature dependence of the imaginary part of permittivity for several values of frequencies.

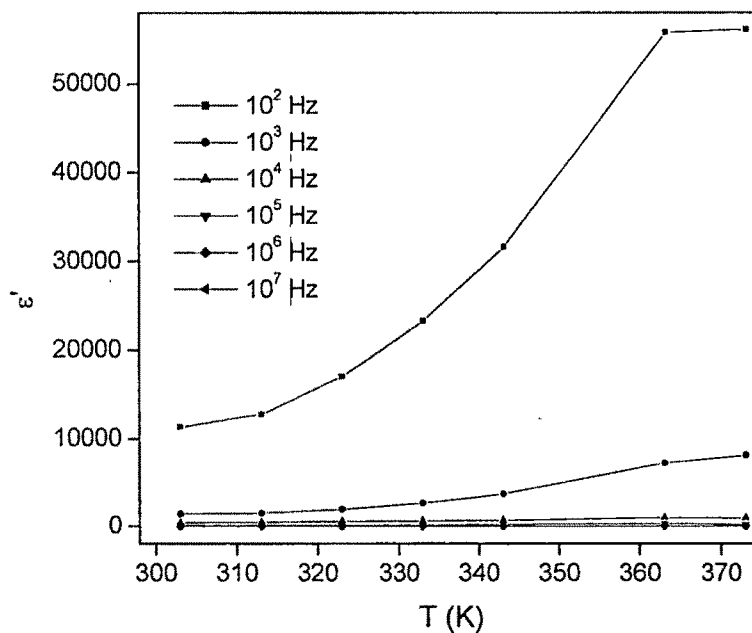


Fig.4.43 (a). Temperature dependence of the real part of permittivity for different frequencies of the system with $x/y=1.25$.

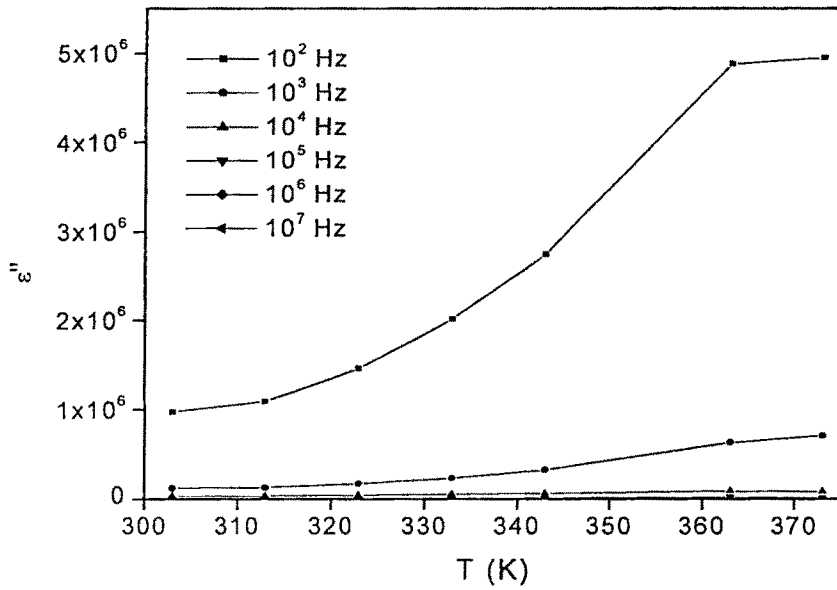


Fig.4.43 (b). Temperature dependence of the imaginary part of permittivity for different frequencies of the system with $x/y=1.25$.

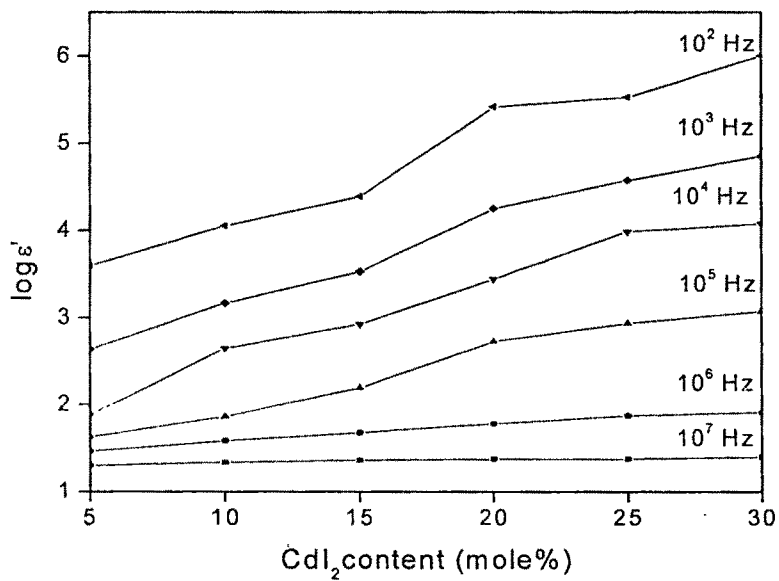


Fig.4.44. Dielectric constant versus mole % of CdI₂ content in the series, $x\text{CdI}_2-(100-x)[2\text{Ag}_2\text{O}-(0.7\text{V}_2\text{O}_5-0.3\text{B}_2\text{O}_3)]$, at different frequencies.

non- Debye type behavior, where the space charge regions with respect to frequency is explained in terms of ion diffusion [89,35].

Figs.4.42 (a) and (b) show the temperature dependence of the real and imaginary part of permittivity for several values of frequencies within the interval of 10^2 Hz to 10^7 Hz for 5 mole% of CdI_2 in the system $x\text{CdI}_2-(100-x) [2\text{Ag}_2\text{O}-(0.7\text{V}_2\text{O}_5-0.3\text{B}_2\text{O}_3)]$. At low frequencies from 100 Hz-10 KHz both ϵ' and ϵ'' rise with increase in temperature. For frequencies higher than 10 KHz the increase in ϵ' and ϵ'' are very less pronounced compared to low frequencies. At low frequencies, with the increase in temperature, the mobile ions are free to hop themselves parallel to the applied field, which lead to the rise in the permittivity. For higher frequencies, in the temperature interval where our experiments have been done, the charge carriers (i.e., Ag^+ ions) are not sufficiently free to follow the changing electric field and therefore the ϵ' and ϵ'' quantities remain nearly constant. Fig.4.43 shows the similar behavior for the system $20\text{CdI}_2-80[x\text{Ag}_2\text{O}-y(0.7\text{V}_2\text{O}_5-0.3\text{B}_2\text{O}_3)]$ with x/y ratio 1.25 for different frequency values. Similar temperature dependence of dielectric constant and dielectric loss is obtained for $\text{BaHPW}_{12}\text{O}_{40}\cdot 7\text{H}_2\text{O}$ [77].

Fig.4.44 shows the plot of logarithm of the dielectric constant (ϵ') versus mole % of CdI_2 content in the $x\text{CdI}_2-(100-x)[2\text{Ag}_2\text{O}-(0.7\text{V}_2\text{O}_5-0.3 \text{B}_2\text{O}_3)]$, series of glass system at different frequencies. At low frequencies from 10^2 Hz to 10^5 Hz, the dielectric constant increases with increase in the mole % of CdI_2 which is due to the long range ionic motion of the mobile charge carriers, the Ag^+ ions in the present system with in the lattice sites of the glass. At 10^6 Hz to 10^7 Hz, the measured value of dielectric constant is almost composition independent due to the contribution of the high frequency dielectric constant

ϵ_{∞} as discussed above. The dielectric constant is found to be increasing with increase in the CdI_2 content which is due to the fact that the mobile ion concentration is also increasing, which leads to the increasing conductivity and hence the dielectric constant. Similar behavior has also been reported for $\text{Ag}_2\text{O}-\text{B}_2\text{O}_3-\text{P}_2\text{O}_5$ glass [90].

Fig. 4.45 shows the ϵ' and ϵ'' value obtained for the glass system $20\text{CdI}_2-80[x\text{Ag}_2\text{O}-y(0.7\text{V}_2\text{O}_5-0.3\text{B}_2\text{O}_3)]$ at room temperature at 1Hz frequency. The ϵ' and ϵ'' values show a non-linear behavior with x/y ratios with a maximum value at x/y at 1.5. Fig.4.46 shows the variation of ϵ' and ϵ'' values against B_2O_3 content for the system $20\text{CdI}_2-53.4\text{Ag}_2\text{O}-26.6[x\text{B}_2\text{O}_3-(1-x)\text{V}_2\text{O}_5]$. Both the plots show a non-linear behavior. The high dielectric loss for these materials satisfies the characteristic features of all high ionic conducting materials. The high value of dielectric constant is considered to be a contribution mainly due to high ionic conductivity and much less due to the electronic conductivity [87]. The dielectric loss observed in these materials is nearly two orders of magnitude higher compared to dielectric constant.

The dielectric loss angle of a system can be explained as the ratio of the energy dissipated per radian in the material to the energy stored at the peak of the polarization. This parameter is usually described by the so called loss tangent, $\tan \delta$.

$$\tan \delta = \frac{\epsilon''(\omega)}{\epsilon'(\omega)} \quad (4.40)$$

Fig.4.47 shows a plot of $\tan \delta$ versus $\log f$ at different temperatures for 5 mole% of CdI_2 doped system $x\text{CdI}_2-(100-x)[2\text{Ag}_2\text{O}-(0.7\text{V}_2\text{O}_5-0.3\text{B}_2\text{O}_3)]$. From the figure the value of $\tan \delta$ shows a constant value independent of temperature at low frequencies and afterwards rapidly decreasing at higher frequencies and seems to be flattened around 10^7 Hz and

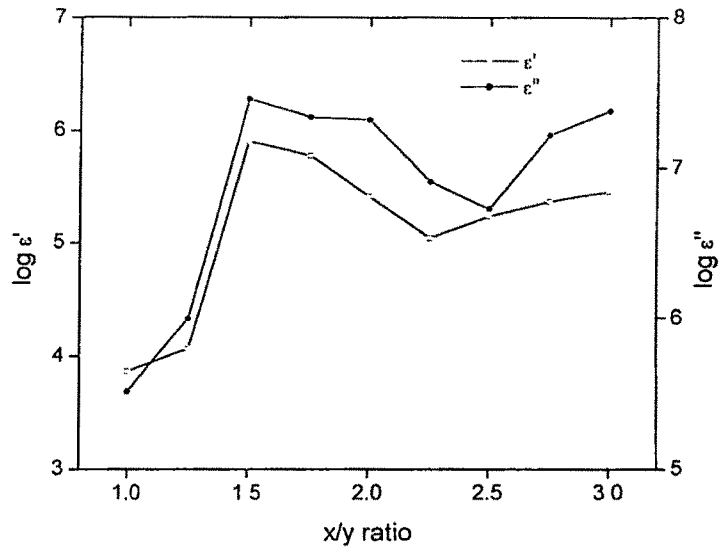


Fig.4.45. Real and Imaginary part of complex permittivity versus x/y ratio at 1Hz frequency.

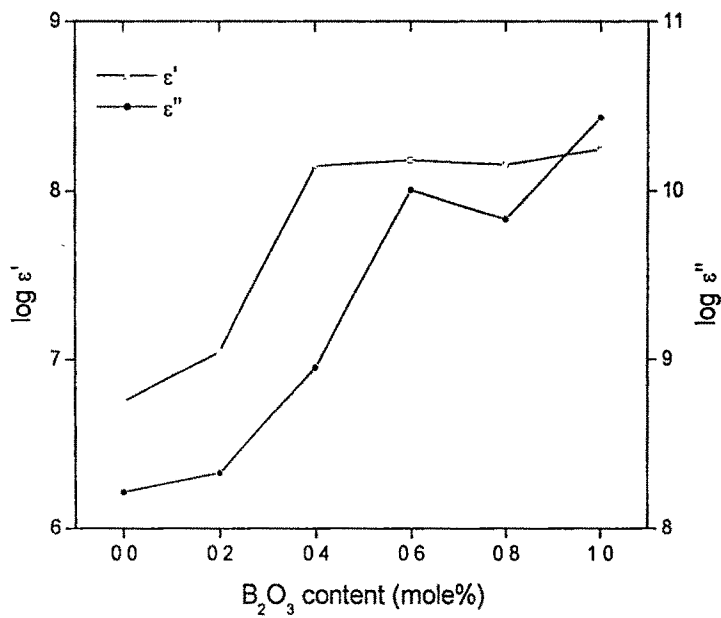


Fig.4.46. Real and Imaginary part of complex permittivity versus B₂O₃ content at 1Hz frequency.

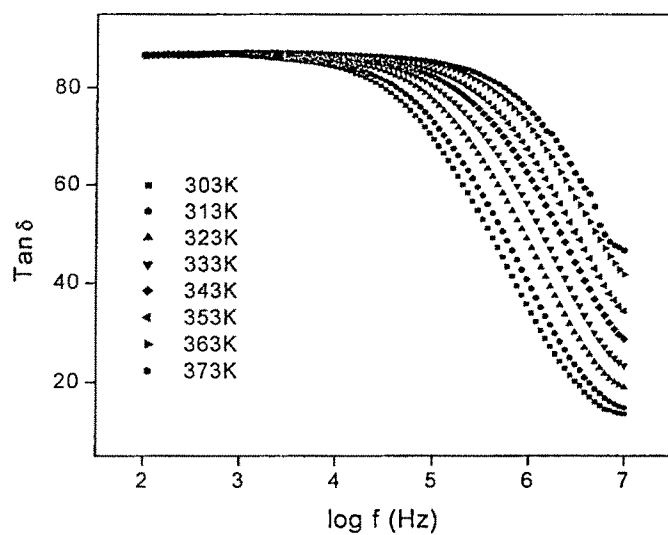


Fig.4.47 Tan δ versus frequency at different temperatures for 5 mole% of CdI₂ doped system.

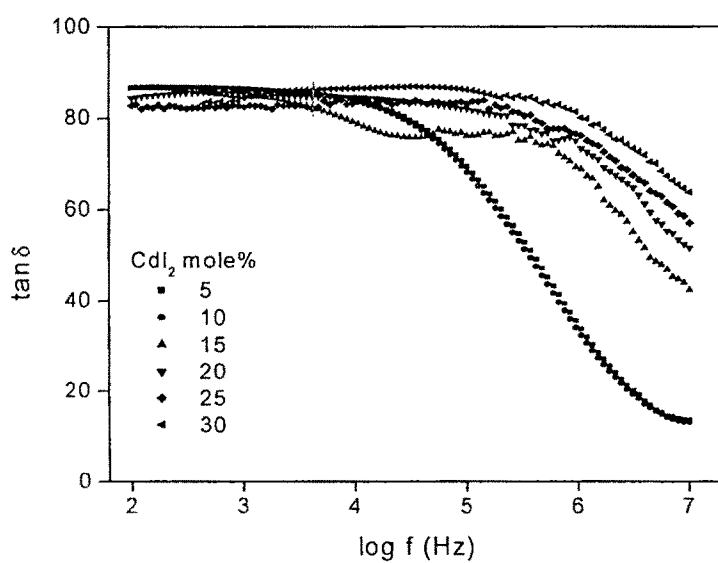


Fig.4.48. Tan δ versus frequency at different amount of CdI₂ doped glass system at room temperature

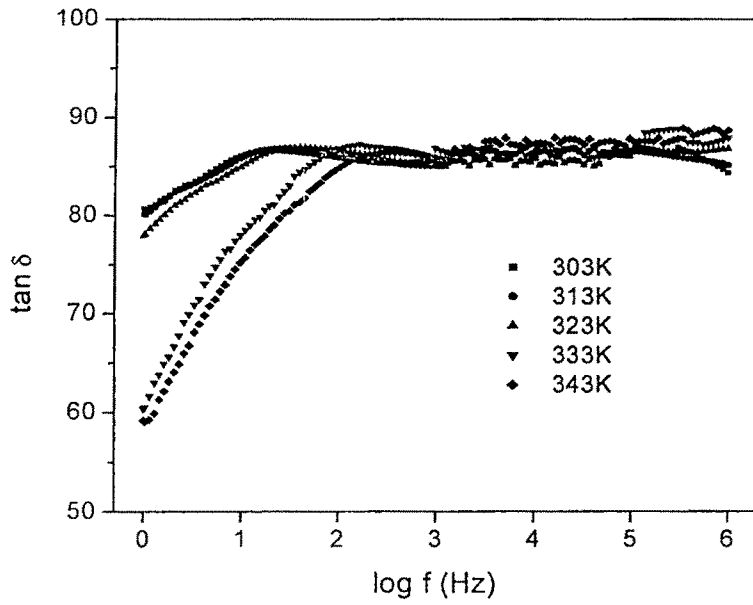


Fig.4.49 $\tan \delta$ versus frequency at different temperatures for the glass system with x/y ratio 2.75.

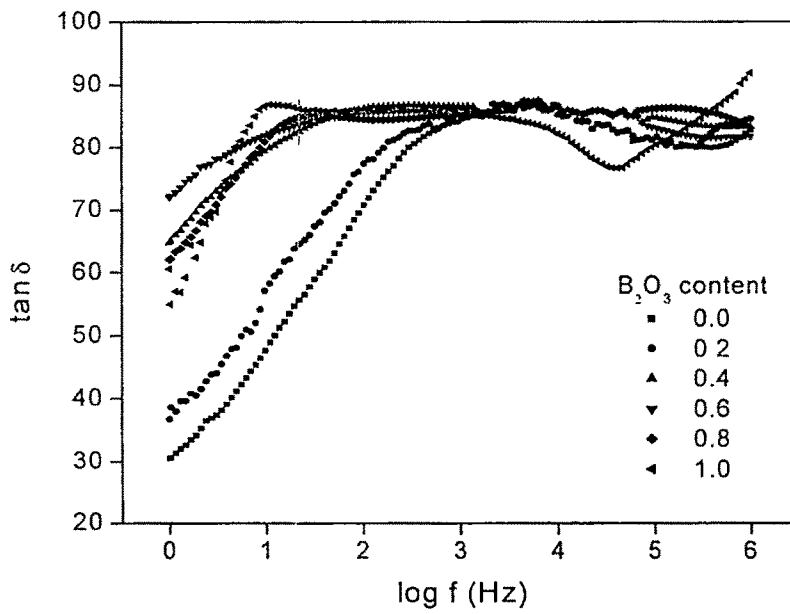


Fig.4.50 $\tan \delta$ versus frequency at different B_2O_3 content at room temperature.

beyond that. The dispersion in the $\tan \delta$ plot with frequency is found to shift towards higher frequencies with increase in temperature. Fig. 4.48 shows the plot of $\tan \delta$ versus frequency for different amount of dopant composition at room temperature. It can be seen from the figure that the dispersion region shifts to higher frequencies with increase in the dopant content. The rapid decrease in $\tan \delta$ and then attaining a constant value at higher frequencies clearly indicates that $\tan \delta$ is inversely proportional to some power of frequency. It is reported by Abdulkhadar et. al., [91] that the similar changes may be due to the presence of nano phase of AgI in which the rapid decrease in $\tan \delta$ is attributed to the energy absorption in nano particles. Therefore, the observed decrease in $\tan \delta$ with frequency and then tending to attain a frequency independent value at about 10^7 Hz can be ascribed due to the ionic jump and dipolar relaxation processes, but the reason for such a rapid decrease in dielectric loss may also be assigned to the presence of small size particles in the system [91]. However, no such confirmation for the presence of small particles has been done by us. According to Shastry et. al., [92] in phosphate glasses, there is a dispersion of $\tan \delta$ with frequency at all temperatures and the maximum of loss tangent increases as a function of temperature where as in systems containing AsO_4^{3-} and MoO_4^{2-} the maximum value of the loss tangent attained is almost independent of temperature. Fig.4.49 shows the $\tan \delta$ with frequency plot for x/y ratio 2.75 for the system $20\text{CdI}_2-80[x\text{Ag}_2\text{O}-y(0.7\text{V}_2\text{O}_5-0.3\text{B}_2\text{O}_3)]$. The value of loss tangent is found to increase with increase in frequency and then found to be constant if the measurement is taken from 1Hz to 10^6 Hz. Similarly Fig.4.50 shows the $\tan \delta$ plot for different amount of B_2O_3 content system of the series $20\text{CdI}_2-53.4\text{Ag}_2\text{O}-26.6[x\text{B}_2\text{O}_3-(1-x)\text{V}_2\text{O}_5]$. It also shows a decrease in the $\tan \delta$, if the measurement has been taken towards lower frequencies. It may

be noted that the loss increases significantly with frequency and a rather dielectric absorption spectrum (constant value of $\tan \delta$) is observed in the present systems studied instead of a peak, which has been observed in other systems [92,81,24] and then decreases with increase in frequency.

The plots of dielectric relaxation time against the inverse of temperature are observed to have an Arrhenius behavior. A typical plot has been shown in Fig. 4.51 for the 5 mole % of CdI_2 doped glass system $x\text{CdI}_2-(100-x)[2\text{Ag}_2\text{O}-(0.7\text{V}_2\text{O}_5-0.3\text{B}_2\text{O}_3)]$. The relaxation time is found out as suggested by Macedo et. al. [33] for a conducting dielectric,

$$\tau_\sigma = \frac{\epsilon_\infty \epsilon_0}{\sigma_0} \quad (4.41)$$

where ϵ_∞ is the high frequency dielectric constant and ϵ_0 is the permittivity of free space, σ_0 is the dielectric current conductivity. Similarly, Fig. 4.52 (a) shows the plot of dielectric relaxation time versus inverse of temperature for $20\text{CdI}_2-80[x\text{Ag}_2\text{O}-y(0.7\text{V}_2\text{O}_5-0.3\text{B}_2\text{O}_3)]$ system with x/y ratio 1.25 and Fig.4.52 (b) shows the plot for the system $20\text{CdI}_2-53.4\text{Ag}_2\text{O}-26.6[x\text{B}_2\text{O}_3-(1-x)\text{V}_2\text{O}_5]$ with $x= 0.8$. The activation energies obtained from the τ_σ plot are nearly the same as that obtained from the corresponding conductivity plots, which suggests that the relaxation time is determined by the flow of charge carriers. Thus, it is possible to say that the motion of mobile charge carriers, Ag^+ ions in the present case are responsible for both conductivity and relaxation effect.

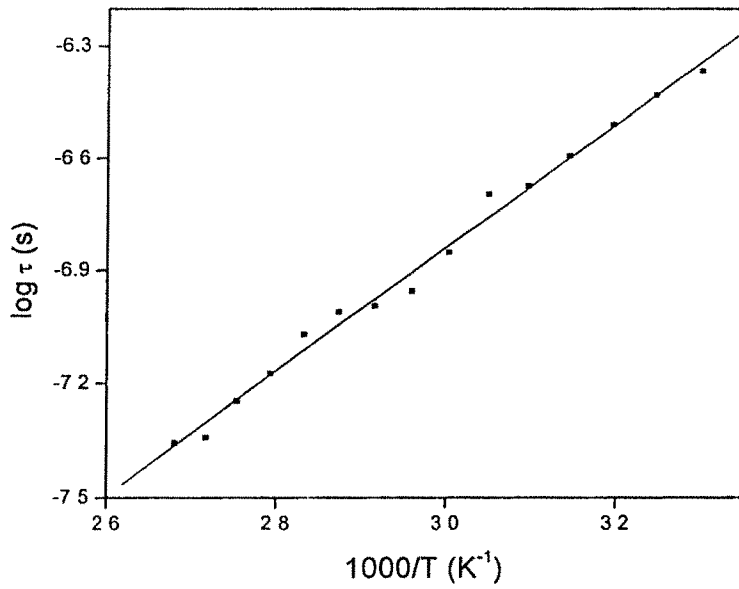


Fig.4.51. Dielectric relaxation time versus inverse of temperature for the 5 mole % of CdI₂ doped system.

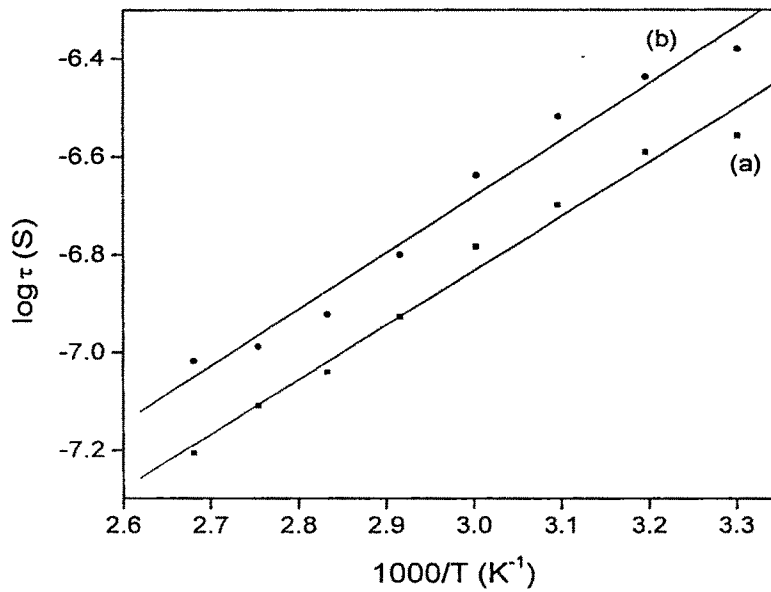


Fig.4.52. (a) and (b) Dielectric relaxation time versus inverse of temperature for the system with $x/y=1.25$ (second series) and $x=0.8$ (third series).

4.5. Modulus Analysis

The complex electrical modulus, M^* is related to complex dielectric constant, ϵ^* and complex impedance by the relation

$$M^* = 1/\epsilon^* = j\omega C_0 Z^* = M' + jM'' \quad (4.42)$$

$$M^* = M_\infty \left[1 - \int_0^\infty e^{-j\omega t} \left(-\frac{d\phi}{dt} \right) dt \right] \quad (4.43)$$

where M' and M'' are the real and imaginary part of the complex modulus M^* , $\omega=2\pi f$ is the angular frequency. $M_\infty=1/\epsilon_\infty$ is the inverse of high frequency dielectric constant, ϵ_∞ . C_0 is the vacuum capacitance of the cell without the sample and is equal to $\epsilon_0 A/l$, where ϵ_0 is the permittivity of free space, A is the area and l is the thickness of the space occupied by the sample and the function $\phi(t)$ gives the time evolution of the electric field within the material. The use of modulus formalism in presenting frequency depending dielectric or conductivity data has the advantage of eliminating any spurious effects due to contacts or interfaces (Maxwell-Wagner effects) [93,94]. The modulus formalism transforms a monotonically increasing function of frequency (the real part of ac conductivity $\sigma'(\omega)$) into one exhibiting a peak in $(M''(\omega))$ representation, scaling behavior of the data is more evident in the modulus representation. In a series of papers [33,95-99], it has been pointed out that for electrical relaxation in dielectrics containing substantial concentration of mobile charges it is generally useful to study the decay of electric field, E at constant displacement vector D . If surface charges of opposite sign are instantaneously placed on opposite faces of an ionic conductor at time zero and then maintained at a constant value,

there will arise inside the material an electric field which in time will decay to zero due to the migration of the mobile ions. The decay of the field can be represented as

$$E(t)=E(0)\phi(t) \quad (4.44)$$

where $E(0)$ denotes the electric field at time $t=0$ and $\phi(t)$ is a decay function of the general form

$$\phi(t) = \int_0^{\infty} d\tau_{\sigma} g(\tau_{\sigma}) \exp(-t/\tau_{\sigma}) \quad (4.45)$$

$$E(t) = E(0) \int_0^{\infty} g(\tau_{\sigma}) \exp(-t/\tau_{\sigma}) d\tau_{\sigma} \quad (4.46)$$

where τ_{σ} is the electric field or conductivity relaxation time and $g(\tau_{\sigma})$ is the normalized density function for relaxation times. Considering initially the frequency dependence of M^* for a conductor which exhibits a frequency independent relative permittivity ϵ_s and conductivity σ_0 , the complex permittivity of the system is given by

$$\epsilon^* = \epsilon_s - j\sigma_0 / \omega\epsilon_0 \quad (4.47)$$

Substituting eqn. (4.47) in eqn. (4.42) and introducing additional parameters

$$\tau_{\sigma} = \frac{\epsilon_0 \epsilon_s}{\sigma_0}, \quad M_s = \frac{1}{\epsilon_s} \quad (4.48)$$

$$M^* = M_s \left[\frac{(\omega\tau_{\sigma})^2}{1 + (\omega\tau_{\sigma})^2} + j \frac{\omega\tau_{\sigma}}{1 + (\omega\tau_{\sigma})^2} \right] \quad (4.49)$$

The real part of the modulus spectrum for 5 mole% of CdI_2 doped system at different temperatures is shown in fig.4.53. Similarly, all the other samples show the similar behavior as is shown for the system for $x/y=1.25$ in Fig.4.54 whereas the Fig. 4.55 shows the modulus spectrum for $x = 0.6$ B_2O_3 content in the system $20 CdI_2 - 53.4 Ag_2O - 26.6 [xB_2O_3 - (1-x) V_2O_5]$. From the figure we can see that at lower frequencies M'

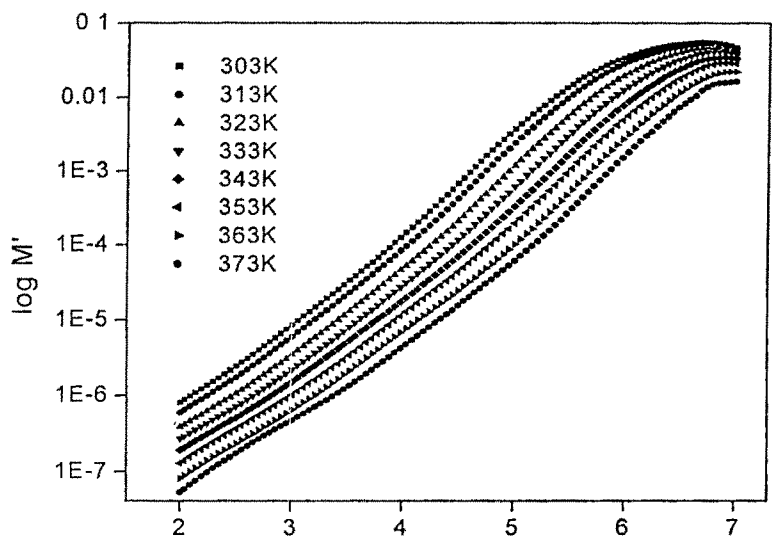


Fig.4.53. Real part of the modulus spectra versus frequency at different temperatures.

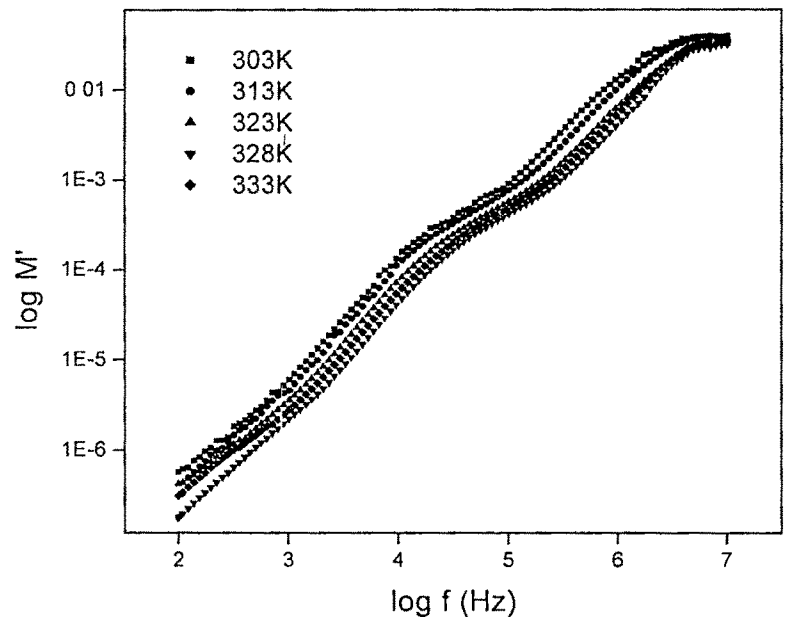


Fig.4.54. Real part of the modulus spectra versus frequency at different temperatures for the glass system with x/y ratio 1.25.

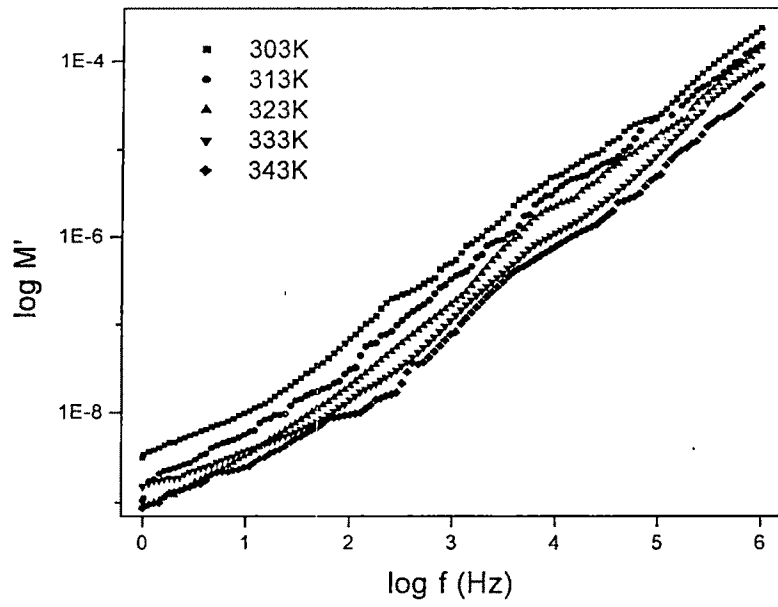


Fig.4.55. M' versus frequency plot at different temperatures for $x=0.6$ B_2O_3 content in the system $20CdI_2-53.4Ag_2O-26.6[xB_2O_3-(1-x)V_2O_5]$.

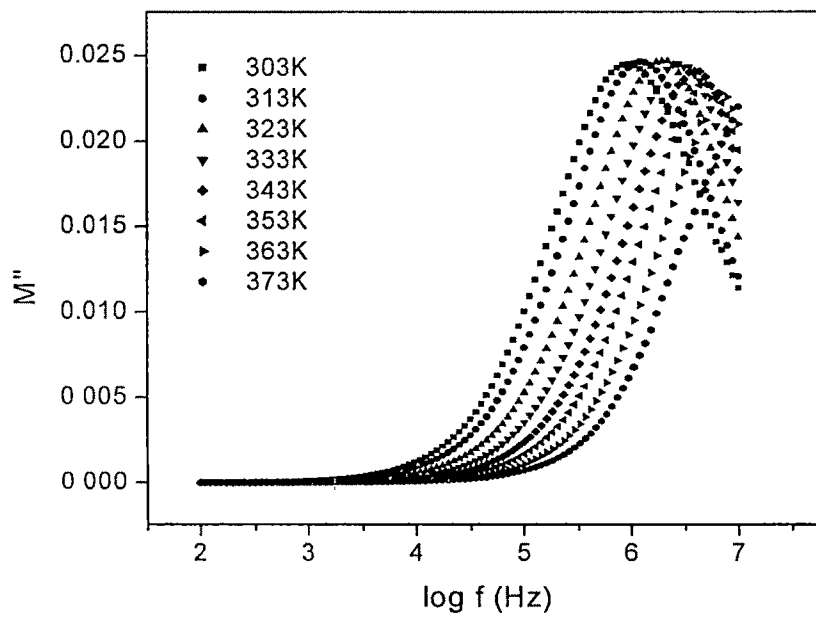


Fig.4.56. M'' spectrum for 5 mole% of CdI_2 doped system

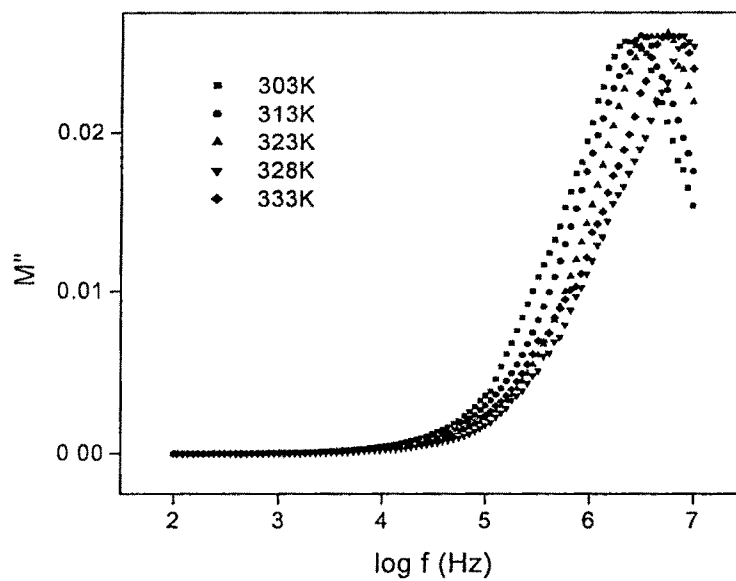


Fig.4.57. M'' spectrum against frequency for $x/y = 1.25$ at various temperatures

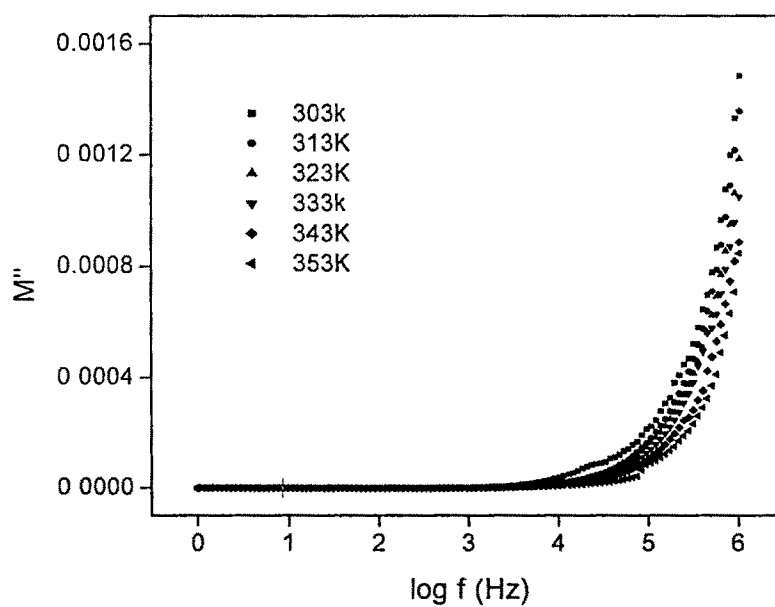


Fig.4.58. M'' spectra against frequency for the B_2O_3 content, $x=0.4$ in the system $20CdI_2-53.4Ag_2O-[xB_2O_3-(1-x) V_2O_5]$.

approaches to zero indicating that the electrode polarization makes a negligible contribution to M' and the dispersion is mainly due to conductivity relaxation. At higher frequencies, M' reaches a maximum constant value $M_{\infty}=1/\epsilon_{\infty}$. At higher temperatures, M' levels off at higher frequencies because the relaxation processes are spread over a range of frequencies.

Fig.4.56 shows the variation of the imaginary part of modulus M'' versus frequency at various temperatures for $x=5$ mole% CdI_2 content. Figure shows a long tail at low frequencies and is due to the large capacitance associated with the electrodes. The shape of the spectrum remains constant but the frequency of the modulus maximum, M''_{max} shifts to higher frequency side with increase in temperature. Fig.4.57 shows the modulus, M'' spectrum against frequency for $x/y = 1.25$ at various temperatures. Fig.4.58 shows the M'' spectra against frequency for the B_2O_3 content $x=0.4$ in the system $20\text{CdI}_2\text{-}53.4\text{Ag}_2\text{O-}26.6[x\text{B}_2\text{O}_3\text{-(}1\text{-}x)\text{V}_2\text{O}_5]$. All the other samples also show the similar behavior of M'' spectrum. The peaks are considerably broader and asymmetric on both sides of the maxima than predicted by ideal Debye behavior [73]. The full width half maximum (FWHM) is found to be constant with change in temperature. The constancy of the full width half maximum value and the height of the modulus plot suggest the invariance of the dielectric constant and distribution of relaxation time with temperature [101]. The region on the left of the peak where the charge carriers are mobile over long distance, while region to the right is where they are spatially confined to their potential wells. The frequency ω_c , where the maximum in M'' occurs is the indicative of the transition from a short range to long range mobility at decreasing frequency and is given by the condition $\omega_c\tau_c=1$, where τ_c is the conductivity relaxation time [58,100]. All these facts imply that

the present systems are also a practical solid electrolyte modeled by lumped RC circuits. Similar observations are reported in other silver conducting glasses [83,101]. The composition dependence of M'' spectra for the system $x\text{CdI}_2-(100-x)[2\text{Ag}_2\text{O}-(0.7\text{V}_2\text{O}_5-0.3\text{B}_2\text{O}_3)]$ at room temperature is given in Fig.4.59. It can be seen that M''_{max} shifts to higher frequencies as the increase in conductivity with the dopant content CdI_2 . However, the full width at half maxima increases with the dopant content which is quite visible for only two samples with $x=5$ and 10 mole% of CdI_2 doped system and similar increase in FWHM for other samples can be visualized at higher frequencies, as the observations are limited to 10^7 Hz only. Similar results have been observed by other workers [58,101,102] that the half width of the M'' peaks for all composition is independent of temperature but increases with increase in the AgI content. Fig.4.60 shows the M'' spectrum for different x/y ratios for the system $20\text{CdI}_2-80[x\text{Ag}_2\text{O}-y(0.7\text{V}_2\text{O}_5-0.3\text{B}_2\text{O}_3)]$. The variation of M' and M'' at low and high frequencies can be predicted by the following model proposed by Macedo et. al., [33].

$$\lim_{\omega\tau_\sigma \ll 1} M' = 0 \qquad \lim_{\omega\tau_\sigma \gg 1} M' = M_s \qquad (4.50)$$

$$\lim_{\omega\tau_\sigma \ll 1} M'' = 0 \qquad \lim_{\omega\tau_\sigma \gg 1} M'' = 0 \qquad (4.51)$$

and the result obtained in the present system is in good agreement with the above model.

The plot of frequency corresponding to M''_{max} , $\log f_{\text{max}}$ versus $1000/T$ for 5 and 10 mole% of CdI_2 doped system obeys the Arrhenius nature and is shown in Fig.4.61. The activation energy calculated from the modulus spectrum is also comparable to the value obtained from the impedance spectrum. The near value of the activation energy of both

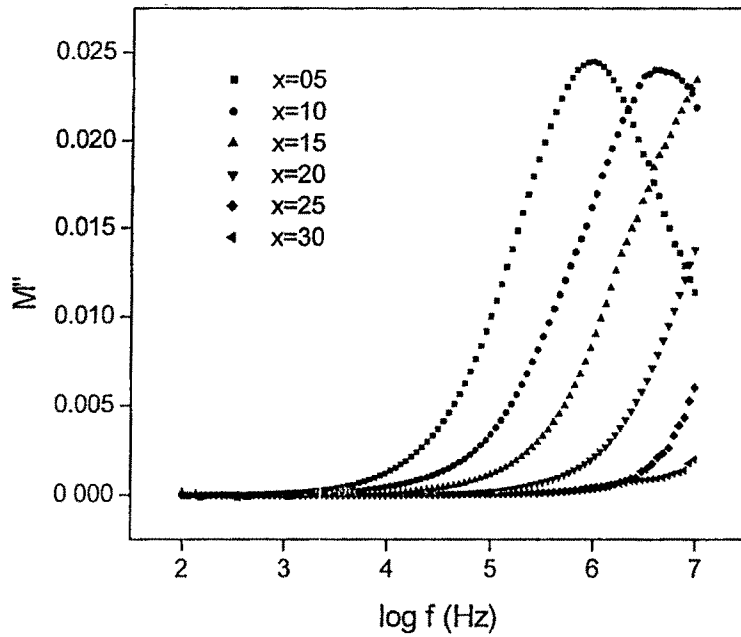


Fig.4.59. Composition dependence of M'' spectra for the system $x\text{CdI}_2$ -
 $(100-x)[2\text{Ag}_2\text{O}-(0.7\text{V}_2\text{O}_5-0.3\text{B}_2\text{O}_3)]$ at room temperature.

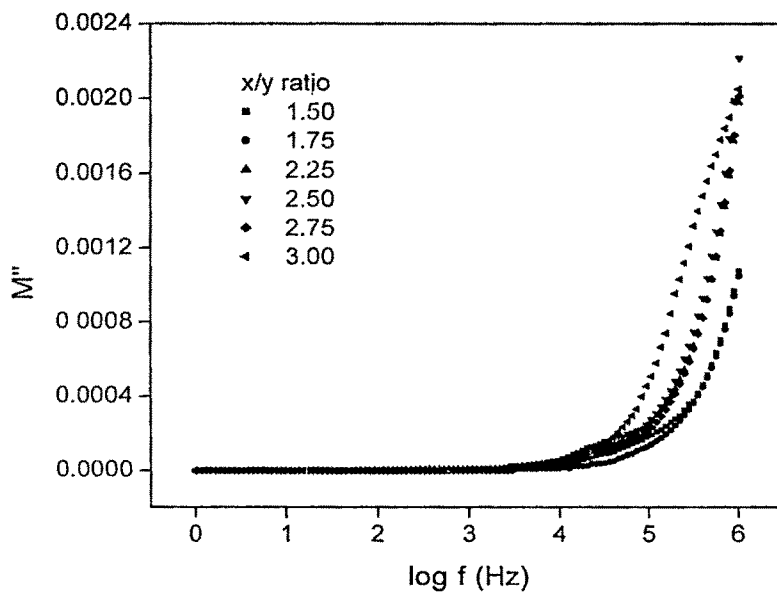


Fig.4.60. M'' spectrum for different x/y ratios for 20CdI_2 - $80 [x\text{Ag}_2\text{O}-$
 $y(0.7\text{V}_2\text{O}_5-0.3\text{B}_2\text{O}_3)]$ system at room temperature

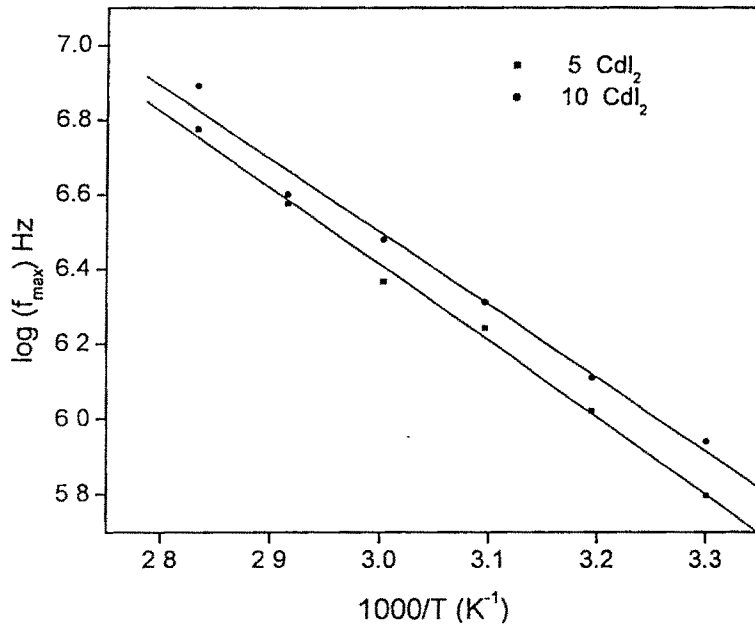


Fig.4.61. Frequency value of modulus maximum versus inverse of temperature for 5 and 10 mole% of CdI₂ doped system.

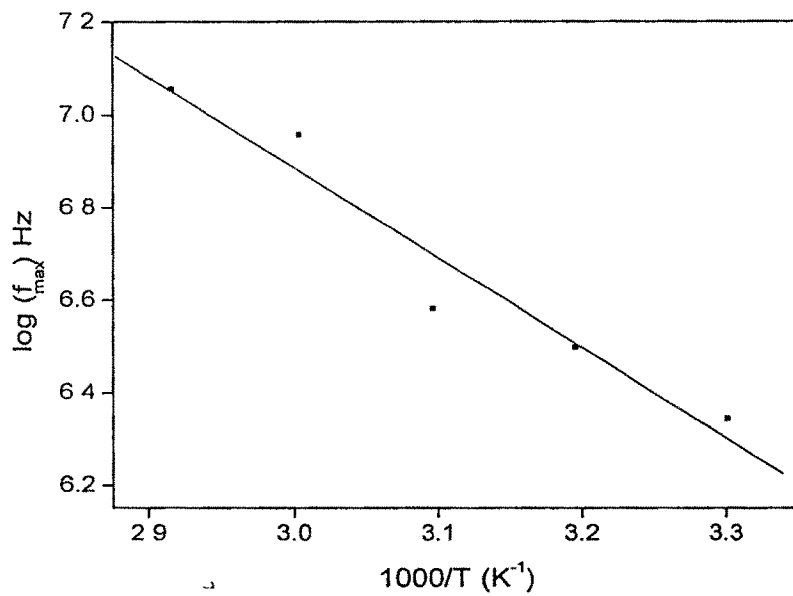


Fig.4.62. Frequency value of modulus maximum versus inverse of temperature for the system with x/y ratio 1.25.

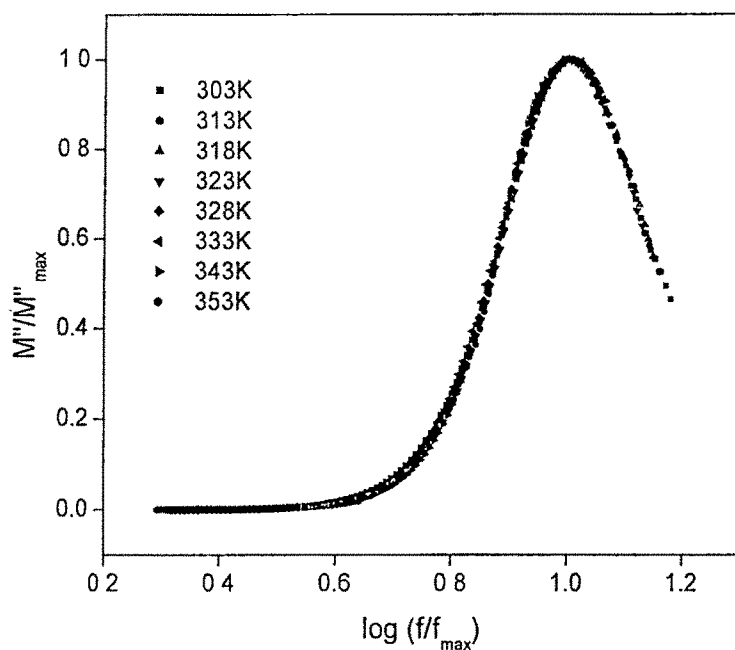


Fig.4.63. Normalized plot of modulus for 5 mole% of CdI_2 doped system at different temperatures.

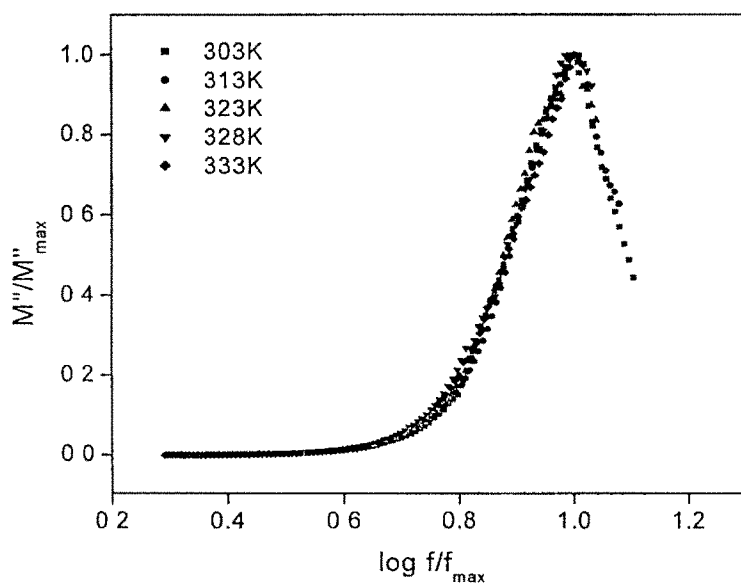


Fig.4.64. Normalized plot of modulus for the system with x/y ratio 1.25 at different temperatures.

impedance and modulus spectrum suggests that the transport of silver ions in the present system is by a hopping mechanism [83,101]. Similarly, Fig.4.62 shows the $\log f_{\max}$ versus $1000/T$ plot for the $x/y=1.25$ glass system of the series $20\text{CdI}_2-80[x\text{Ag}_2\text{O}-y(0.7\text{V}_2\text{O}_5-0.3\text{B}_2\text{O}_3)]$ also shows Arrhenius nature and its activation energy value is comparable with the impedance value. Fig.4.63 shows the normalized plot (M''/M''_{\max}) versus $\log(f/f_{\max})$ of the modulus for 5 mole% of CdI_2 doped composition at different temperatures. Fig.4.64 shows the normalized plot for the glass system with $x/y = 1.25$ (in second series). The normalized plot for the glass system $20\text{CdI}_2-53.4\text{Ag}_2\text{O}-26.6[x\text{B}_2\text{O}_3-(1-x)\text{V}_2\text{O}_5]$ with $x=0.4$ (in third series) is given in Fig.4.65. The approximate overlap of the modulus curves for all temperatures indicate the dynamical processes occurring at different frequencies are independent of temperatures. The full width half height (FWHH) obtained are clearly wider, has shown a value of ~ 1.8 and 2.0 decades for 5 and 10 mole% of CdI_2 doped system is greater than 1.14 decades which is the case for the ideal Debye behavior. This has usually been regarded as an indication of a distribution of relaxation times in the conduction process [103]. According to Hasz et. al., [104], the distribution of relaxation time is connected with a distribution of free energy barriers for ionic jumps, in which distribution is increased with increasing disorder whereas Grant et. al., [20] attributed that the distribution of relaxation times is not due to the disordered structure of glasses but is assumed to be the consequence of the cooperative nature of the conduction process. The normalized modulus plot is non-symmetric, in agreement with the non-exponential behavior of the electrical function, which is well described by the Kohlrausch-William-Watts exponential function [105,106].

$$\phi(t) = \exp(-t/\tau)^\beta \quad (0 < \beta < 1) \quad (4.52)$$

where τ and β are the conductivity relaxation time and Kohlrausch exponent respectively. The value of the Kohlrausch parameter β for most practical solid electrolyte is clearly smaller than one. The smaller is the value of β , the larger is the deviation of the relaxation with respect to Debye-type relaxation. The value of β can be evaluated by knowing the width at half height of the M''/M''_{\max} plot ($\beta=1.14/\text{FWHH}$ value). In the present system, β results in a value, 0.63 and 0.57 for 5 and 10 mole % of CdI_2 doped system. The width at half height of the modulus spectrum at different temperature is close to 1.8 decades, consequently β may be considered as independent of temperature in the temperature range studied. The β value obtained for the present glass composition are comparable with those of the other Ag^+ ion conducting glasses [58,101,102], where the β value decreases with the addition of the dopant amount. According to Nagai [99], the β parameter gives the extent to which the mobile ions couple during the conduction processes. The concept of the cooperative motions in a glass is issued from the Universal behavior discussed by Jonscher [53,101]. It means that jump of a mobile ion in a glass may not be treated as an isolated event i.e., when the ion jumps from one equilibrium position to another it causes a time dependent movement of other charge carriers in the surroundings, which leads to additional relaxation of the applied field. So it results the smaller value of β to a more extended co-operation between the charge carriers.

The ideal solid electrolytes can be represented by a single parallel RC element and is characterized by a single Maxwell time constant $\tau_{\sigma}=R_p C_p= \epsilon_0 \epsilon' / \sigma$ and is defined by Macedo et. al., [33] as the conductivity relaxation time. But in the case of practical solid electrolytes, a series array of RC elements needs to be considered [83]. In ideal solid electrolytes Z'' and M'' peak at the same frequency given by $\omega_{\max} RC=1$ [20, 107] and the

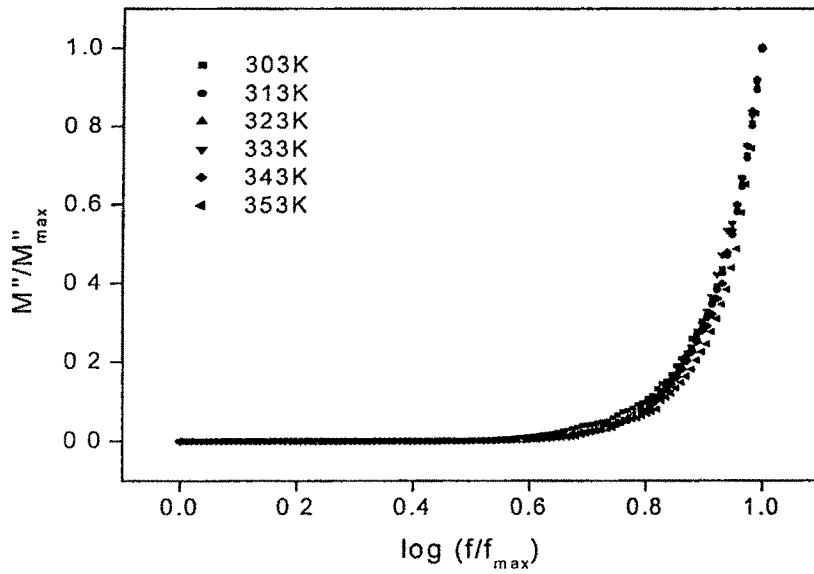


Fig.4.65. Normalized plot of modulus for $x=0.4$ B_2O_3 in the system $20CdI_2-53.4Ag_2O-[xB_2O_3-(1-x)V_2O_5]$ at different temperatures.

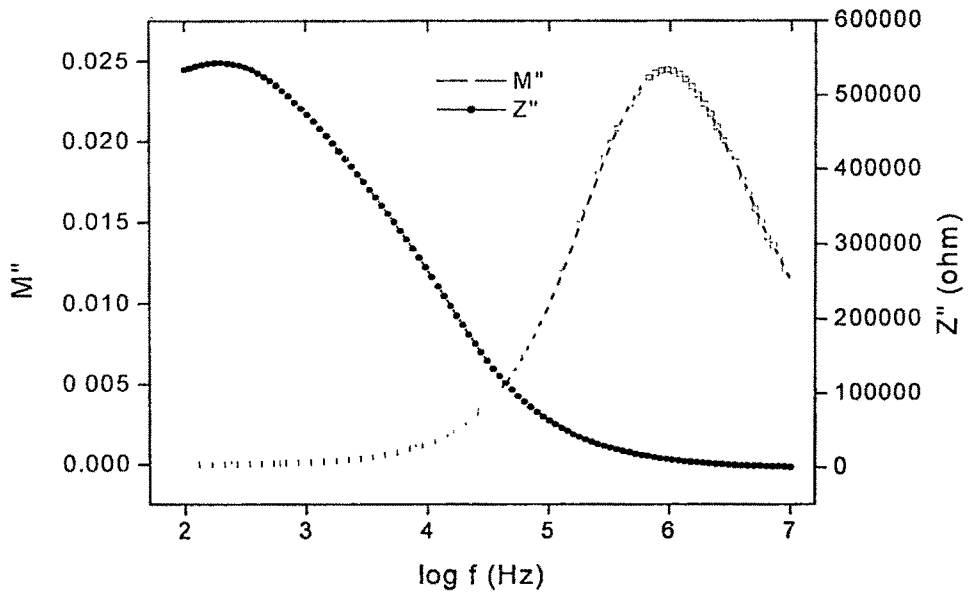


Fig.4.66. Z'' and M'' versus $\log f$ plot at room temperature for the system with $x=5$ mole % of CdI_2 system at room temperature.

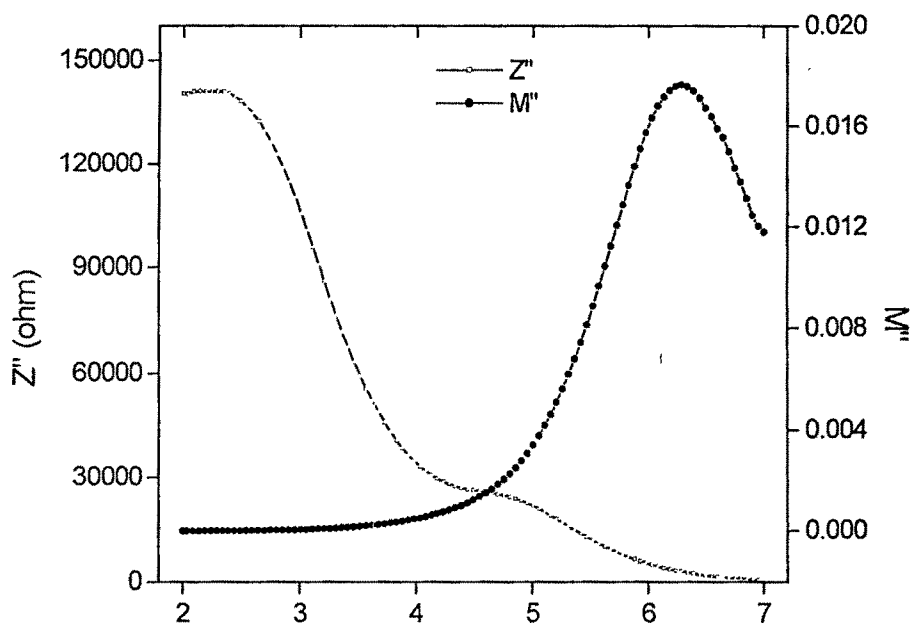


Fig.4.67. Z'' and M'' versus $\log f$ plot at room temperature for the system with x/y ratio 1.25.

shape of the peaks are identical with that predicted by Debye theory for dielectric loss. With the appropriate scaling, the normalized modulus and impedance spectra of the Debye curves are completely superposable and is given by the equations

$$Z'' = R \frac{\omega RC}{1 + (\omega RC)^2} \quad , \quad M'' = \frac{C_0}{C} \frac{\omega RC}{1 + (\omega RC)^2} \quad (4.53)$$

The term $\omega RC/[1 + (\omega RC)^2]$ in the imaginary parts of both Z'' and M'' is responsible for Debye-like peak shapes in the spectroscopic plots, i.e., in the Z'' , M'' versus $\log f$ plots, as can be seen. the Z'' peaks are scaled by R whereas the M'' peaks are scaled by C_0/C . To understand the non-Debye behavior of the present system, impedance and modulus spectrum at room temperature have been plotted. A typical plot for 5 mole% of CdI_2 doped system (first series) has been shown in Fig.4.66. It can be seen from this figure that the Z''_{max} and M''_{max} do not occur at the same frequency and a broadened modulus spectra is obtained which is an indication of the wide distribution of relaxation times. Similarly Fig.4.67 shows the Z'' , M'' versus $\log f$ plots for the system with x/y ratio 1.25 in the second series of glass system. West et al., [108,109] showed Z'' spectra are broadened on the low frequency side of the peak maximum and M'' spectra are broadened on the high frequency side. The large rise in Z'' occurring at low frequencies is caused mainly by electrode polarization.

Above results show that single relaxation time equation such as Eqn. 4.49 is not adequate to explain the dispersion effects over a broad range of frequencies. Hence, to describe the distribution of relaxation times, it is necessary to introduce a distribution function $g(\tau)$ to describe the phenomena [33]. Then eqn. becomes

$$M^* = M, \int_0^{\infty} g(\tau_{\sigma}) \left[\frac{(\omega\tau_{\sigma})^2 + j\omega\tau_{\sigma}}{1 + (\omega\tau_{\sigma})^2} \right] d\tau_{\sigma} \quad (4.54)$$

$$M^* = M, \left\langle \frac{(\omega\tau_{\sigma})^2 + j\omega\tau_{\sigma}}{1 + (\omega\tau_{\sigma})^2} \right\rangle \quad (4.55)$$

using the notation $\int_0^{\infty} g(\tau_{\sigma}) d\tau_{\sigma} x \equiv \langle x \rangle$. The low and high frequency limits of M' and M'' remain the same even after the introduction of the distribution of relaxation times and its only effect is to broaden the dispersion region for M' and broaden and depress the maximum of the M'' peak in the modulus plot as a function of frequency. The most significant effect of the introduction of a distribution of conductivity relaxation times is that it causes a frequency dependence of ε' and σ [33]

$$\varepsilon' = \frac{M'}{M'^2 + M''^2} \quad (4.56)$$

$$\varepsilon' = \frac{1}{M,} \left[\frac{\left\langle \frac{(\omega\tau_{\sigma})^2}{1 + (\omega\tau_{\sigma})^2} \right\rangle}{\left\langle \frac{(\omega\tau_{\sigma})^2}{1 + (\omega\tau_{\sigma})^2} \right\rangle^2 + \left\langle \frac{\omega\tau_{\sigma}}{1 + (\omega\tau_{\sigma})^2} \right\rangle^2} \right] \quad (4.57)$$

Taking the low and high frequency limits

$$\lim_{\omega\tau_{\sigma} \ll 1} \varepsilon' \equiv \varepsilon_0 = \frac{1}{M,} \frac{\langle \tau_{\sigma}^2 \rangle}{\langle \tau_{\sigma} \rangle^2} = \frac{\varepsilon, \langle \tau_{\sigma}^2 \rangle}{\langle \tau_{\sigma} \rangle^2} \quad (4.58)$$

$$\lim_{\omega\tau_{\sigma} \gg 1} \varepsilon' = \varepsilon, = \frac{1}{M,} \quad (4.59)$$

The introduction of the distribution of conductivity relaxation times leads to a dispersion in ε' arising from the long range ionic diffusion process of magnitude

$$\varepsilon_0 - \varepsilon_s = \varepsilon_s \left(\frac{\langle \tau_\sigma^2 \rangle - \langle \tau_\sigma \rangle^2}{\langle \tau_\sigma \rangle^2} \right) \quad (4.60)$$

When there is only single relaxation time, $\langle \tau_\sigma^2 \rangle = \langle \tau_\sigma \rangle^2$ and $\varepsilon_0 - \varepsilon_s = 0$. When there is a distribution of relaxation times, $\langle \tau_\sigma^2 \rangle > \langle \tau_\sigma \rangle^2$ and $\varepsilon_0 - \varepsilon_s > 0$. The actual magnitude of the dispersion $\varepsilon_0 - \varepsilon_s$ depends on the nature of the distribution function for the conductivity relaxation time and hence on the kinetic parameters controlling the ionic diffusion process. For explaining the dispersion in the conductivity

$$\sigma = \omega \varepsilon_0 \varepsilon'' = \omega \varepsilon_0 \left(\frac{M''}{M'^2 + M''^2} \right) \quad (4.61)$$

$$\sigma = \omega \varepsilon_0 \varepsilon_s \left[\frac{\left\langle \frac{\omega \tau_\sigma}{1 + (\omega \tau_\sigma)^2} \right\rangle}{\left\langle \frac{(\omega \tau_\sigma)^2}{1 + (\omega \tau_\sigma)^2} \right\rangle^2 + \left\langle \frac{\omega \tau_\sigma}{1 + (\omega \tau_\sigma)^2} \right\rangle^2} \right] \quad (4.62)$$

The low and high frequency value of σ are given by

$$\lim_{\omega \tau_\sigma \ll 1} \sigma \equiv \sigma_0 = \frac{\varepsilon_0 \varepsilon_s}{\langle \tau_\sigma \rangle} = \frac{\varepsilon_0}{M \langle \tau_\sigma \rangle} \quad (4.63)$$

$$\lim_{\omega \tau_\sigma \gg 1} \sigma \equiv \sigma_s = \varepsilon_0 \varepsilon_s \left\langle \frac{1}{\tau_\sigma} \right\rangle \quad (4.64)$$

For a single relaxation time, $1/\langle \tau_\sigma \rangle = \langle 1/\tau_\sigma \rangle$ and $\sigma_0 = \sigma_s$ and for a distribution of relaxation times $1/\langle \tau_\sigma \rangle < \langle 1/\tau_\sigma \rangle$ and $\sigma_0 < \sigma_s$, and the observed value of σ will exhibit an increase with increasing frequency in the conductivity relaxation region and it can be explained as follows. At low frequencies of the applied field, the probability is that a series of many jumps can occur and the probability is proportional to $1/\langle \tau_\sigma \rangle$. At high frequencies only a

few ions perform more than one jump in a given cycle of the electric field and the probability that a single jump will occur is now proportional to $\langle 1/\tau_\sigma \rangle$. The frequency depended conductivity and permittivity observed in the presently studied systems is due to the distribution of relaxation times [33]. Distribution of relaxation time arises from the distribution of activation energies which represent the random distribution of potential barrier heights between the allowed positions for Ag^+ ions [33].

It is worth to mention that some authors do not agree with the basis of modulus formalism [94, 110,111]. They are of the opinion that modulus is not a directly measurable quantity and is not directly related to the microscopic physical processes etc., however many other authors believe in the electric modulus analysis [112-115].

The knowledge of the conductivity relaxation time τ_σ could allow to calculate the glass decoupling index, $R_\tau(T_g)$, which describes how well the ion conductivity relaxation process is decoupled from the glassy matrix. The glass decoupling index $R_\tau(T_g)$ of a system is given by Angell [118,119] as the ratio of $(\tau_s(T_g)) / (\tau_\sigma(T_g))$ where $(\tau_s(T_g))$ and $(\tau_\sigma(T_g))$ are the average structural and conductivity relaxation times respectively at the glass transition temperature T_g . $R_\tau(T_g)$ determines the extent to which the motion of the conducting ions decoupled from the viscous motion of the glassy network and is related to the ability of the mobile ions to migrate in the glassy electrolyte at T_g . The conductivity relaxation time $\tau_\sigma (=1/f_p)$ determined from the frequencies at the modulus (M'') peak maxima. The decoupling index, R_τ is obtained by extrapolating the $\log f_p$ versus $1000/T$ curve to T_g and assuming the structural relaxation time τ_s equal to 200s [101,103]. It may be noted that the values of $R_\tau(T_g)$ increases with the increase in the dopant content CdI_2 , here it could be taken only for 5 and 10 mole% of CdI_2 and the values obtained are

1.66×10^9 and 1.93×10^9 . This observation is in agreement with the variation of the conductivity with the dopant content. The increase in the calculated value of $R_1(T_g)$ with the increase in the dopant content suggests that the motion of Ag^+ ions is decoupled less and less from the viscous motion of the glass network suggesting an increase in the conductivity with the increase in the dopant content. The composition effect on the glass system can be discussed mainly with the movement of ions [102] and this movement may depend upon the ion \leftrightarrow ion pair equilibrium and the effect of temperature. The AgI clusters formed in the present system due to the exchange reaction between Ag_2O and CdI_2 , become localized in the glassy network. An increasing amount of AgI content increases the contribution of mobile Ag^+ ions with the increasing addition of dopant salt CdI_2 , to the silver oxysalt system causes a greater variation in the electrostatic field of the environments in which the ion pairs move and that increases the distribution of relaxation times [102].

The above frequency dependent electrical conductivity study on CdI_2 doped $Ag_2O-V_2O_5-B_2O_3$ shows that migration of the Ag^+ ions from the AgI clusters formed due to the exchange reaction between CdI_2 and Ag_2O are responsible for dispersion and the broad relaxational losses in the frequency range studied. The observed dispersion behavior and the relaxation phenomena in the presently investigated systems can be explained on the basis of the Diffusion Controlled Relaxation (DCR) model proposed by Elliott [120]. The DCR model is in consistent with the Glarum model; it assumes that relaxation preferentially takes place by means of correlated or co-operative motion of ions. The AgI molecule formed after the exchange mechanism is assumed to be separated by a distance λ .

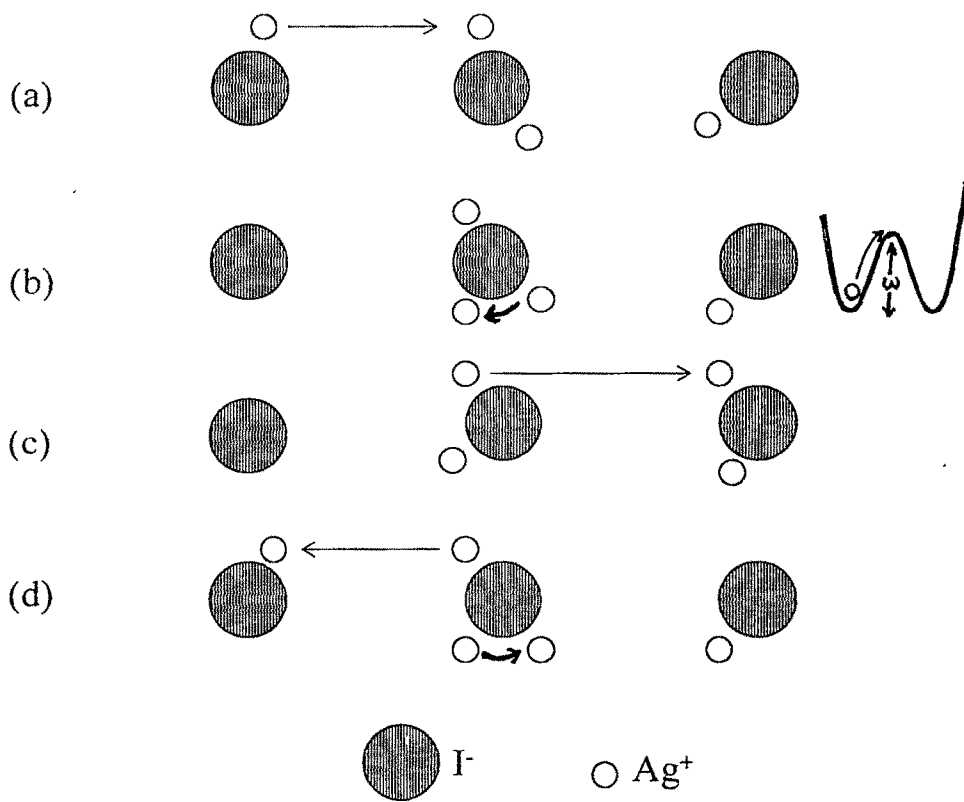


Fig.4.68. Schematic diagram to represent DCR model

First the Ag^+ ion near I^- ion diffuses to another I^- ion Fig.4.68 (a) making the latter an interstitial (defect) pair. In the second step, it is assumed that the arrival of the incoming ion at the defect site causes the ion which was originally present to move position, in a rotational sense with respect to the non-bridging oxygen with which it is associated. In other words, this ion moves from a position associated with a potential minimum to another potential minimum position, due to an interaction with the other ion. Fig.4.68(b). This change in energy configuration due to ionic motion is similar to that describe by Funke [121]. This step is on the basis of the Glarum-type approach, [122] that the relaxation and consequent polarization of an ion at a site preferentially occurs when another ion diffuses to the same non bridging oxygen site. The diffusion independent relaxation can occur at a given site by the thermally activated motion between positions 1 and 2, fig.4.68 (b). Following that one of the two Ag^+ ion at the defect site can diffuse to a third site and thereby repeating the relaxation process and contributing to dc conductivity, Fig.4.68(c). Alternatively, the ion, whose arrival caused the formation of a doubly occupied non bridging oxygen defect, can hop back to the site where it originally came from, and this consequent back and forth motion between the neighboring sites will contribute to ac conductivity, Fig.4.68 (d). After the second ion has gone, it is presumed that the other ion can relax back to the potential minimum position it originally occupied, thereby also contributing to the overall polarization. Thus, this mechanism gives rise to a combination of ac and dc conductivities. Hence, through this model two contributions to ac conductivity can be observed as inter site hopping motion of ions and the intra site motion of ions.

4.6. Summary

Ac dependent electrical conductivity studies on CdI_2 doped $\text{Ag}_2\text{O-V}_2\text{O}_5\text{-B}_2\text{O}_3$ solid electrolyte system has been studied over a range of frequencies and temperature, first by changing the dopant concentration, then by varying the glass modifier (Ag_2O) to glass former ratio ($\text{V}_2\text{O}_5\text{-B}_2\text{O}_3$) by keeping the dopant content constant and last is the study of the mixed former effect, i.e., substitution of one former by another by keeping the dopant and glass modifier amount constant. The dc conductivity of the bulk samples were found out from the resistance value obtained from the impedance plot or from the frequency independent plateau region of the conductivity spectra. In the first series, by the addition of CdI_2 to the silver oxysalt system increases the conductivity and a maximum value is obtained for the 30 mole% CdI_2 doped system. In the second series, with the x/y ratio the conductivity shows a non-linear behavior gives the idea that the glass modifier Ag_2O content affects the ionic conductivity. In the third series, substitution of B_2O_3 to the $\text{CdI}_2\text{-Ag}_2\text{O-V}_2\text{O}_5$ system increases the conductivity and has been explained in terms of the structural changes in the glass, but of a non-linear nature and there is no change in the order of conductivity values, it shows that the enhancement of conductivity in the system mainly depends on the concentration of mobile ions, which is constant in the present series. The conduction mechanism in this system has been explained by the diffusion path model. The frequency dependence of electrical conductivity for the presently studied systems has been analyzed by Jonschers power law. These type of systems show three regions in the conductivity spectrum; the high frequency dispersion at low temperatures, the low frequency dispersion at high temperatures and a frequency independent plateau region. The high frequency dispersion is found to shift to higher frequencies with increase in

temperature and this dispersive nature is due to the many body effects commonly found in disordered materials. The hopping frequency, ω_p and mobile ion concentration factor K have been evaluated and ω_p is found to be thermally activated in the same way as that of dc conductivity. In the Dielectric analysis, the dielectric constant is found to decrease with increase of frequency and saturate at higher frequencies. The dielectric loss, ϵ'' is found to vary inversely with frequency due to the presence of dc conductivity. Dielectric relaxation in these glasses has been explained using Stevels model. The frequency dispersion in $\tan \delta$ manifests the persistence of Ag^+ mobility and dipolar relaxation losses are attributed for the dielectric loss. The activation energy obtained from the dielectric relaxation time is comparable with that of conductivity suggesting that the motions of the mobile charge carriers are responsible for conductivity and relaxation effect. In the modulus analysis, the M'' plot obtained is asymmetric and broader on both side of the maxima than would be predicted by the ideal Debye behavior and is attributed due to the distribution of relaxation times. The relaxation frequency obtained from the modulus peak is also thermally activated as that of dc conductivity, suggests the transport of silver ions in the system and is probably due to hopping mechanism. The normalized modulus plot is non-symmetric, in agreement with the Kohlrausch-William-Watts exponential function, $\phi(t)=\exp(-t/\tau)^\beta$, giving a β value ~ 0.6 . The glass-decoupling index obtained increases with increase in the dopant content and is in consistent with the increase in conductivity with the dopant. The behavior of ac conductivity and relaxation phenomenon has been explained by the Diffusion Controlled Relaxation model. The migration of mobile ions is responsible for the dispersion effects and relaxational spectra in these studied systems.

References

1. Warburg G, *Ann. Phys.* 21 (1884) 622.
2. Ravaine D, Ionic conductive Glass, in *Glass Current Issues*, (ed.) Wright A.F and Dupuy J (1985) Martinus Nijhoff Publishers, 439.
3. Tuller H. L, Button D.P and Uhlmann D.R, *J. Non-Cryst. Solids* 40 (1980) 93.
4. Ingram M.D, *Current Opinion in Solid State and Material Science* 2 (1997) 399.
5. Tomozawa M in *Treatise on Material Science*, ed. Hannay. H, Academic Press, New York (1977) 283.
6. Hagenmuller P and Van Gool W (ed.) *Solid Electrolytes*, Academic Press, New York (1978).
7. Hughes K and Isard J.O. The Ionic transport in Glasses, in *Physics of Electrolytes*, (ed.) Hladik. J, Academic Publishers, New York (1972).
8. Grant R.J, Hodge I.M, Ingram M.D and West A.R, *Nature* 266 (1977) 42.
9. Ingram M.D, Ionic conductivity in Glass, *Phys. Chem. Glass.* 28 6 (1987) 215.
10. Minami T, *J. Non-Cryst. Solids* 73 (1985) 273
11. Kawamura J, Frequency Response of Glasses in *Recent Advances in Fast Ion Conducting Materials and Devices* (ed.) Chowdari B.V.R, Lin Q.G and Chen L.-Q, World Scientific Publishing Company, Singapore (1990) 47.
12. Grant R.J, Ingram M.D and West A.R, *J. Electroanal. Chem.* 80 (1977) 239.
13. Badwal S.P.S, *Solid State Ionic Devices*, World Scientific Singapore (ed.) Chowdari B.V.R (1988) 165
14. Macdonald J.R in *Super Ionic conductors* (ed.) Mahan G.D and Roth W.L, Plenum Press, New York (1976) 81.
15. Kulkarni A.R, Maiti H.S and Paul A, *Bull. Mater. Sci.* 6. 2 (1984) 201.
16. Kulkarni A.R and Maiti H.S, *Solid State Ionics* 9/10 (1984) 605.
17. Hodge I.M, Ingram M.D and West A.R, *J. Electroanal. Chem.* 74 (1976) 125.
18. Bauerle J.F. *J. Phys. Chem. Solids* 30 (1969) 2657.
19. Mellander B.-E, Lunden A, *Materials for Solid State Batteries* (ed.) by Chowdari B.V.R and RadhaKrishna S. World Scientific Publishing Company. Singapore (1986) 161.
20. Grant R.J, Ingram M.D, Turner I.D.S and Vincent C.A. *J. Phys. Chem.* 82 (1978) 2838.
21. Kawamura J and Shimoji M. *J. Non-Cryst. Solids* 79 (1986) 367.
22. Chiodelli G and Magistris A, *Mater. Res. Bull.* 17 (1982) 1.
23. Shastry M.C.R and Rao K.J. *Solid State Ionics* 44 (1991) 187.

24. Pathmanathan K, Hope S.R and Johari G.P. J. Non-Cryst. Solids 94 (1987) 186.
25. Sebastian K and Frischat G. H, Physics Chem. Glasses 33, 5 (1992) 199.
26. Hariharan K and Kaushik R, J. Mate. Sci. 22(1987) 3335.
27. Singh K, Chiodelli G and Magistris A, J. Power Sources 58 (1996) 103.
28. Arof A.K. J. Power Sources 52 (1994) 129.
29. Malugani J.P, Mercier R and Techez M, Solid State Ionics 21 (1986) 131.
30. Hariharan K and Suresh Kumar R in: Solid State Ionics: Materials and Applications, eds. Chowdari B.V.R et al, World Scientific, Singapore (1992) 533.
31. Chandrasekhar V.G and Suthanthiraraj S.A, Solid State Ionics 62 (1993) 61.
32. Hariharan K and Suresh Kumar R, Solid State Ionics 104 (1997) 227.
33. Macedo P.B, Moynihan C.T and Bose R, Physics Chem. Glasses 13,6 (1972) 171.
34. Jonscher A.K, Dielectric Relaxation in Solids, Chelsea Dielectric Press, London,1983
35. Macdonald J.R (ed.) Impedance Spectroscopy, Wiley, New York (1987).
36. Viswanathan A, Suthanthiraraj S.A. Solid state Ionics: Materials and Applications (ed.) Chowdari B.V.R et.al. World Scientific Publishing Company, Singapore (1992) 379.
37. Jonscher A.K, J. Mate. Sci. 13 (1978) 553.
38. Satyanarayana N, Karthikeyan A and Venkateswarlu M, J. Mate. Sci. 31 (1996) 5471.
39. Satyasainath Prasad P and Radhakrishna S, Solid State Ionics, 28-30 (1998) 814.
40. Sarma R.V.G.K and Radhakrishna S, J. Solid State Chem. 91 (1991) 204.
41. Sarma R.V.G.K and Radhakrishna S, Solid State Ionics 28-30 (1998) 808.
42. Chiodelli G, Magistris A and Villa M, Solid State Ionics 18/19 (1986) 356.
43. Hariharan K and Kaushik R, Solid State Commun. 63 (1987) 925.
44. Magistris A, Chiodelli G and Duclot M, Solid State Ionics 9/10 (1983) 611.
45. Deshpande V.K, Pradel A and Ribes M, Mat.Res. Bull. 23 (1988) 379.
46. Satyasainath Prasad P and Radhakrishna S. J. Mat. Sci. Lett. 7 (1988) 113.
47. Pollak M and Geballe T.H, Phys. Rev 122 (1961) 1745.
48. Jonscher A.K, J. Phys. C, Solid State Physics 6 (1973) L235.
49. Austin I.G and Mott N.F, Adv. Phys. 18 (1969) 41.
50. Richards P.M, in: Fast Ion Transport in Solids, eds. Vashishta P, Mundy J.N and Shenoy G.K (North Holland, NewYork,1979).
51. Funke K, Z. Phys. Chem. (NF) 154 (1987) 251.
52. Elliott S.R and Owens A.P, Philos. Mag. B 60 (1989) 777.
53. Jonscher A.K, Nature 267 (1977) 673.
54. Ngai K.L and White C.T, Phys. Rev. B20 (1979) 2475.

55. Dissado L.A and Hill R.M, *Nature* 279 (1979) 685.
56. Verof A.H and den Hartog H.W, *Solid State Ionics* 68 (1994) 305.
57. Maass P, Petersen J, Bunde A, Dietrich W and Roman H.E, *Phys. Rev. Lett* 66 (1991) 52.
58. Chowdari B.V.R and Gopalakrishnan R, *Solid State Ionics* 23 (1987) 225.
59. Jonscher A.K, *J. Mate. Sci.* 13 (1978) 553.
60. Ingram M.D, *Phys. Chem. Glasses* 128 (1987) 215.
61. Jain H and Mundy J.N, *J. Non-Cryst. Solids* 91 (1987) 315.
62. Jonscher A.K, *J. Mate. Sci.* 16 (1981) 2037.
63. Cramer C and Funke K, *Ber. Bunsenges. Physik. Chem.* 96 (1992) 1725.
64. Pradel A and Ribes M, *J. Non-Cryst. Solids* 131-133 (1991) 1063.
65. Le Staguennec M. Elliott S.R, *Solid State Ionics* 73 (1994) 199.
66. Funke K, *Progr. Solid State Chem.* 22 (1993) 111.
67. Peterson J and Dietrich W, *Philos. Msg.* B65 (1992) 231.
68. Viswanathan A, Suthanthiraraj S.A., *Solid State Ionics* 62 (1993) 79.
69. Bruce P.G, West A.R and Almond D.P, *Solid State Ionics* 7 (1982) 57.
70. Almond D.P, West A.R and Grant R.J, *Solid State Commun.* 44 (1982) 1277.
71. Almond D.P, Duncan G.K West A.R, *Solid State Ionics*, 8 (1983) 159.
72. Almond D.P and West A.R, *Solid State Ionics*, 9/10 (1983) 277.
73. Almond D.P and West A.R, *Solid State Ionics*, 11 (1983) 57.
74. Huggins R.A, in, *Diffusion in Solids: Recent Development*, Eds. Nowick A.S and Burton J.J, Academic Press (1975) 445.
75. Haque N.U, Hashmi R.A and Anis M.K, *J. Non-Cryst. Solids* 175 (1994) 244.
76. Hashmi R.A. , Noor-Ul Haque, N. Bano, M.K. Anis, *J. Mat. Sci.* 29 (1994) 6615.
77. Davidovic M. Cajkovski T, Cajkovski D, Likar-Smiljanic V, Biljic R, Mioc V.B, Nedic Z, *Solid State Ionics* 147 (2002) 123.
78. Verhoef A.H., den Hartog H.W, *Solid State Ionics* 68 (1994) 305.
79. Colomban Ph., Badot J.C., *Solid State Ionics* 61 (1993) 55.
80. Yadav A and Seth V.P, *Ind.J. Pure & Appl. Phys.* 33 (1995) 746.
81. Kaushik R, Hariharan K, Radhakrishna S, *J. Appl. Electrochem.* 17 (1987) 813.
82. Chowdari B.V.R., Radhakrishnan K., *J. Non-Cryst. Solids* 110 (1989) 101.
83. Chowdari B.V.R and Gopalakrishnan R., *Solid State Ionics* 18&19 (1986) 483..
84. Armstrong R.D, Taylor K, *Electroanal. Chem. Interface Electrochem.* 63 (1975) 9.
85. Cohrane G and Fletcher N.H, *J. Phys. Chem. Solids* 32 (1971) 2557.
86. Susic M.V and Mentus S.V, *Electrochim. Acta.* 28 (1983) 35.

87. Suthanthiraraj S.A and Radhakrishna S, *Cryst. Latt. Def. Amorph. Mat.* 11(1985) 185.
88. Magistris A, Chiodelli G, *electrochem. Acta* 26 (1984) 1241.
89. Venkateswarlu M, Reddy K.N, Rambabu B, Satyanarayana N, *Solid State Ionics* 127 (2000) 177.
90. Haque N.U, Hashmi R.A and Anis M.K, *Phys. Stat. Solidi (a)* 142 (1994) 429.
91. Abdulkhadar M, Thomas B, *Bull. Mater. Sci.* 19, 4 (1996) 631.
92. Shastry M.C.R, Rao K.J, *Solid State Ionics* 44 (1991) 187.
93. Elliott S.R, *Physics of Amorphous Materials* (Longman, London, 1984).
94. Elliott S.R, *J. Non-Cryst. Solids*, 170 (1994) 97.
95. Moynihan C.T, Boesch L.P, Laberge N.L, *Phys. Chem. Glasses*, 14, 6 (1974) 639.
96. Howell F.S, Bose R.A, Macedo P.B, Moynihan C.T, *J. Phys. Chem.* 78, 6 (1974) 639.
97. Ambrus J.H, Moynihan C.T, Macedo P.B, *J. Phys. Chem.* 76, 22 (1972) 3287.
98. Ngai K.L, Martin S.W, *Phys. Rev. B* 40 (1989) 10550.
99. Ngai K L., Mundy J.N, Jain H, Balzer-Jollenbeck G, Kanert O, *Phys. Rev. B* 39 (1989) 6169.
100. Sural M, Ghosh A, *Solid State Ionics* 120 (1999) 27.
101. Reau J.M, Rossignol S, Tanguy B, Rojo J.M, Herrero P, Rojas R.M, Sanz J, *Solid State Ionics* 74 (1994) 65.
102. Mangion M.B.M, Johari G.P, *Phys. Chem. Glasses* 29 6 (1988) 225.
103. Sural M, Gosh A, *Solid State Ionics* 130 (2000) 259.
104. Hasz W.C, Moynihan C.T, Tick P.A, *J. Non-Cryst. Solids* 172-174 (1994) 1363.
105. Kohlrausch R, *Progg. Ann.* 12 3 (1847) 393.
106. Williams G and Watts D.C, *Trans. Faraday Soc.* 66 (1970) 80.
107. Grant R.J. Ingram M.D and West A.R, *Electrochimica Acta* 22 (1977) 729.
108. West A.R, Sinclair D.C , Hirose N, *J. Electroceram*, 1:1(1997) 65.
109. Andres- Verges M, West A.R. *J. Electroceram*, 1:2 (1997) 125.
110. Roling B. *Solid State Ionics* 105 (1998) 185.
111. Dyre J.C. *J. Non-Cryst. Solids* 135 (1991) 219.
112. Moynihan C.T, *J. Non-Cryst. Solids*, 203 (1996) 359.
113. Fontanella J.J. Wilson J.J. Smith M.K, Wintersgill M.C, Coughlin C.S. Mazaud P. Greenbaum S.G. *Solid State Ionics* 50 (1992) 259.
114. Carini G, Federico M, Trpodo G, *Philosophical Magazine B*, 62, 2 (1992) 153.
115. Funke K. *Philos.Mag. A*, 64, 5 (1991) 1025.
116. Subramony J.A and Kulkarni A.R. *Solid State Ionics* 67 (1994) 235.

117. Gosh S and Gosh A, Solid State Ionics 149 (2002) 67.
118. Angell C.A, Solid State Ionics 9/10 (1983) 3.
119. Angell C.A, Solid State Ionics 18/19 (1896)72.
120. Elliott S.R. Solid State Ionics 27 (1988) 131.
121. Funke K. Solid State Ionics 18/19 (1986) 183.
122. Glarum S.H, J. Chem. Phys. 33 (1960) 369.